Experimental Testing of a Rotational Friction Connection for Use with Precast Concrete Cladding Panels in Metal Building Systems

by

Vincent Antonio Sellers

A thesis submitted to the Graduate Faculty of
Auburn University
in partial fulfillment of the requirements for the Degree of
Master of Science in Civil Engineering

Auburn, Alabama
December 16th, 2017

Keywords: Earthquake Engineering, Metal Building Systems, Hard Walls, Energy Dissipation, Cladding, Rotational Friction

Approved by

Justin D. Marshall, P.E., Chair, Associate Professor of Civil Engineering
Robert Barnes, P.E., Associate Professor of Civil Engineering
Mary L. Hughes, Lecturer of Civil Engineering

Abstract

Lightweight clad metal building systems have been shown to exhibit excellent performance in seismic events; however, metal building systems clad in masonry or precast concrete panels (hard walls) have been shown through analytical studies, shake table tests, and post-earthquake reconnaissance to be susceptible to significant damage and potential panel collapse. There exists a stiffness incompatibility between the stiff wall cladding and the flexible steel frame. Improper connection design between the hard walls and steel frame have resulted in premature failure of the connections, leading to a loss of a critical load path and the wall system falling away from the structure.

To improve the seismic performance of metal building systems, clad with hard walls, it is necessary to develop a new seismic force resisting system in the longitudinal direction (parallel to the ridgeline). A new rotational friction connection (RFC) between the hard wall and steel frame has been developed to act as the ductile fuse element in the new system. Emphasis was placed on the connection being economic, easy to construct, minimize the need for repairs after seismic events, and have a high energy dissipating capacity. Energy dissipation is geared in the in-plane horizontal direction while maintaining out-of-plane capacity.

This thesis reports the experimental component testing of the new rotational friction connection for various bolt sizes. The testing included a monotonic pushover test, unidirectional cyclic testing in the in-plane horizontal direction, a biaxial test, pullout test, and extended uniaxial test. Hysteretic behavior of the connection is discussed. The results of the testing show that the

connection can withstand large displacements as well as dissipate energy in a stable manner without damaging the surrounding components. The rotational friction connection is suitable for use as the ductile fuse component in metal building systems with hard walls.

Acknowledgements

I'd like to thank my advisor Dr. Justin Marshall for his guidance and patience throughout this research. He has been a major influence on me during my time at Auburn, including sparking an interest in structural dynamics in me. I'd also like to thank the other professors who have taught me at Auburn, Dr. Barnes, Dr. Davidson, and Dr. Stallings, each of your classes expanded not only my academic knowledge, but my creative problem solving as well. I'd like to thank the other members of my committee, Dr. Barnes and Dr. Hughes for their assistance in completing this thesis. I'd like to thank the NSF for the funds provided on this project, I truly hope that this research aids future endeavors.

I'd like to give a huge thank you to Michael Langley, who has been instrumental in my academic growth during my time at Auburn. Your inquisitive mind truly influenced me to seek the bigger picture. Your help, that has been constant throughout my entire research, is greatly appreciated. I'd like to thank Andy Weldon for all his help and practical advice throughout the experimental testing. His practical insight was truly invaluable and helped me to grow as a graduate student.

The importance of the friendships I've made and the support those friendships have provided cannot be overstated. Particularly, I'd like to thank my friends Jordan Nemiroff, Eric Gross, Todd Deason, Hongyang Wu, Lester Lee, Daniel Richey and Kelsey Doan for their support during my time at Auburn.

I'd like to thank my family for their continued love and support throughout my research, especially my parents who have helped me in ways that are immeasurable. Finally, I'd like to thank my girlfriend, Maddie Malone, for her amazing love and support, for always encouraging me and keeping my spirits up. I couldn't have done this without you by my side.

Table of Contents

List of Tables

List of Figures

Chapter 1. Introduction

1.1 Defining the Problem

Metal building systems are commonly used in low-rise non-residential structures due to their optimized design, quick construction, and low cost. The failure of these structures can result in the loss of lives, or revenue streams in addition to the associated cost of repairs, therefore, the proper design of these structures is critical. Metal building systems often include concrete or masonry wall panels (hard walls) that act as nonstructural elements to clad the building.

The combination of the flexible, metal building system and the stiff hard wall have displayed poor seismic response through numerous studies and post-earthquake reconnaissance earthquake assessments. Most recently, the post-earthquake reconnaissance work performed in Haiti and New Zealand has highlighted the failure of the connections between the metal building system and the hard wall, resulting in severe structural damage to the system (Marshall and Gould 2012).

The post-earthquake reconnaissance performed by Marshall and Gould (2012) discovered many brittle failures of the connections between the metal building system and the hard walls of these structures. During seismic events, these systems undergo large force and displacement demands; therefore, the elements in these structures should also be designed appropriately. The stiffness incompatibility between light, flexible metal building system and the heavy, stiff hard walls can

result in failure of these brittle connections. The failures of these connections disrupt the load path and can result in critical failures.

1.2 Proposed Solution

The brittle nature of the connections displayed in the Haiti and New Zealand seismic events poses a serious problem. As such, a resilient connection that can undergo large displacements while remaining minimally damaged is desirable for the connection of the hard walls to the metal building system. The connections will be designed to dissipate energy in the longitudinal direction of the metal building frame while maintaining strength in the transverse direction.

The rotational friction connection is a new method of connecting the incompatible hard walls and metal building systems and aims to provide the capability for large displacements and minimal damage to the structural system. The rotational friction connection is located between the external concrete cladding panel and the spandrel beam of the metal building frame. Figure 1-1 shows a typical metal building frame with an external hard wall and highlights the location of the connection. Figure 1-2 shows an elevation and plan view of the connection between the hard wall and the metal building system.

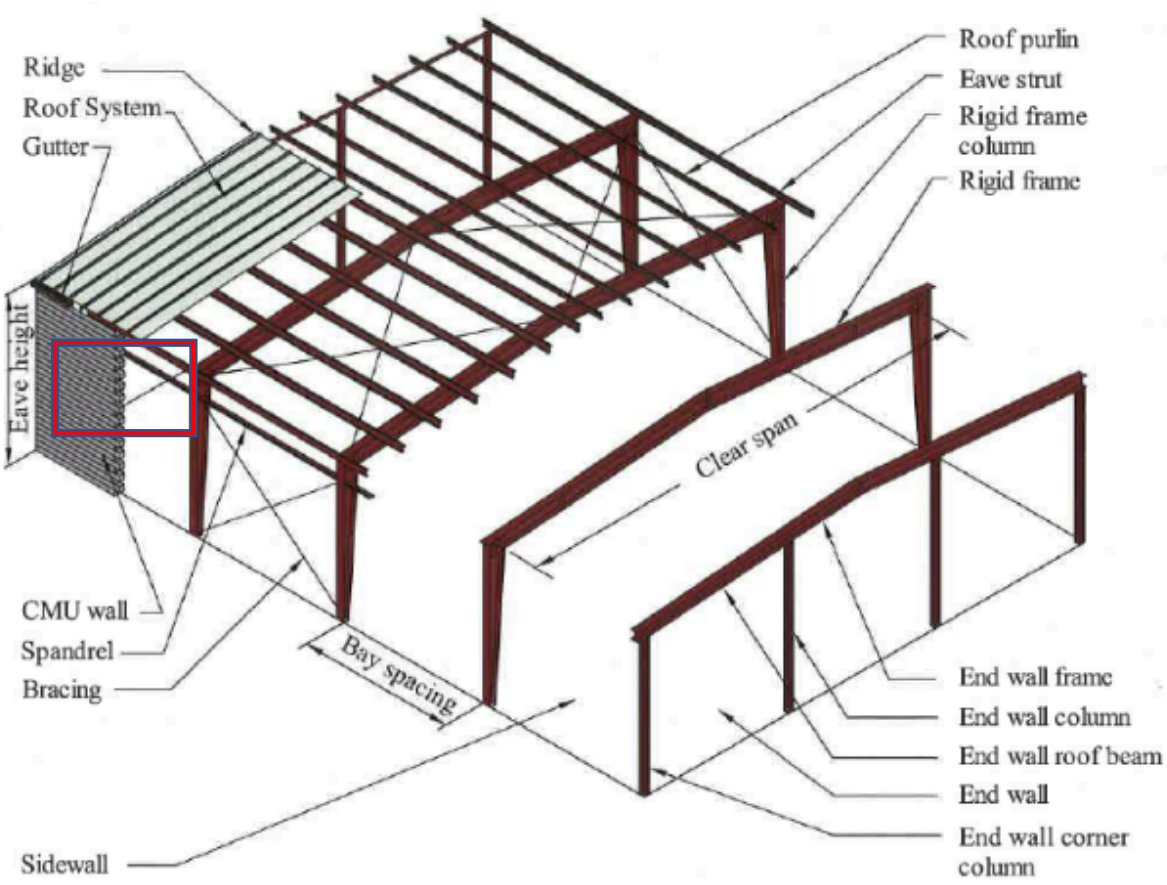

Figure 1-1: Typical Metal Building Frame with Hard Wall (NCMA 2011)

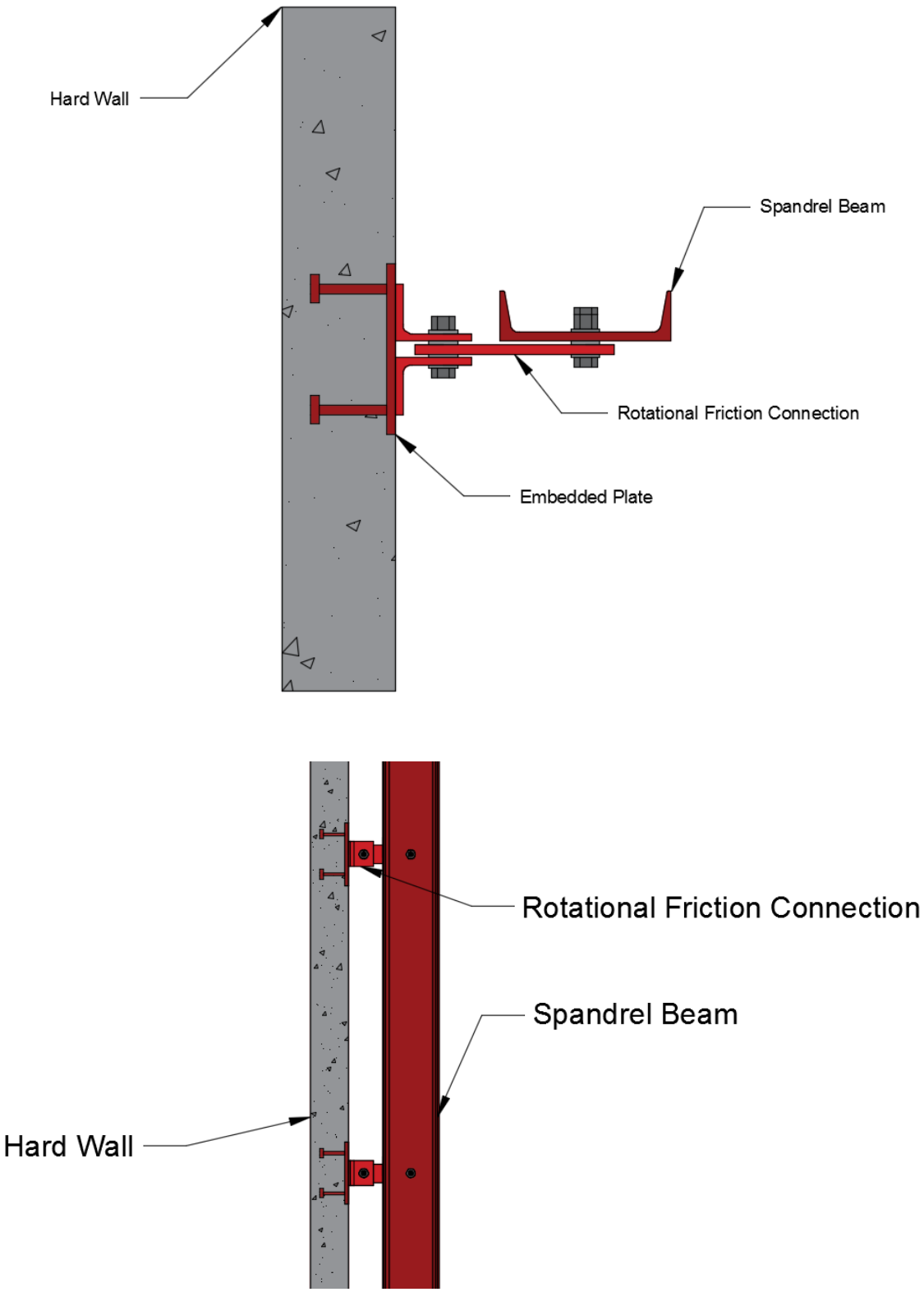

Figure 1-2: Elevation (top) and Plan (bottom) View of Connection Location

The connection presented in this thesis focuses damage primarily on the washers, bolts, and friction surfaces of the connection. This allows for the structural system to remain undamaged throughout the seismic event.

1.3 Scope of Work

The objective of the research was to develop a connection between the metal building system and a concrete hard wall that resolved compatibility issues by allowing for large displacements in one direction of the wall-to-frame connection to reduce damage that could compromise the strength of the structural system. Additionally, this connection should provide support for the nonstructural hard walls. This thesis focuses on the testing and evaluation of the rotational friction connection. Results are primarily discussed in terms of the connection's capability to dissipate energy and damage resulting to the structural system. The testing consists of pushover, uniaxial, biaxial, and pullout tests. Testing with many cycles was also performed to test the resiliency of the connection over repeated loading.

1.4 Organization of Thesis

Chapter 2 discusses previous testing of energy dissipation methods for resilient connections for these systems. The results of sliding friction and plastic deformation energy dissipation methods are shown.

Chapter 3 explains the experimental test set up used during testing and provides a description of the connection. The testing plan, materials, setup, loading protocol, relevant equipment, and instrumentation are explained in detail.

Chapter 4 presents and discusses the results of the experimental testing that was performed.

Chapter 5 provides a summary of the research performed, conclusions from the testing, and recommendations for future work to be performed

Chapter 2. Literature Review

2.1 Background and Motivation

Metal building systems are commonly used for low-rise commercial building construction due to their efficiency, low construction cost, and flexibility for expansion (Hong and Uang 2011). Metal building systems are generally designed as an Ordinary Moment Frame (OMF) with R=3.5. This design results in low redundancy and ductility. In metal building systems without tilt-up concrete wall panels or masonry walls (i.e. hard walls) this low ductility is acceptable because of the low seismic weight of the structure. In most of these frames the controlling load case is governed by the gravity loads (Uang, Smith and Shoemaker 2011). However, the presence of these concrete or masonry walls causes an increase in seismic weight, increasing the risk for earthquake damage to these structures. The combination of these metal building systems with tilt-up concrete wall panels gained popularity in the 1950s due to their favorable cost and ease of construction (Thurston 1990). Buildings with this type of construction have experienced damage from seismic events dating back to the 1971 San Fernando earthquake and most recently the Haiti earthquake in 2010 and the Canterbury sequence in 2012 in New Zealand. As noted by Thurston (1990) and Marshall and Gould (2012) the element that experienced critical damage was the connection between the building frame and the relatively stiff concrete wall panel. Examples of the damage of these connections can be seen in Figure 2-1 and Figure 2-2. These compatibility issues typically cause failures in other elements that may have otherwise performed adequately had it not been for the connection failure (Thurston 1990).

Figure 2-1: Concrete Anchor Connection Failure (Marshall 2012)

Figure 2-2: Damaged Connection at the Beam-to-Panel Interface (Marshall 2012)

2.2 Energy Dissipation in Cladding

A cladding system is defined as the exterior panels, attachment points, connection elements, and building attachment points (Craig, Leistikow and Fennell 1988). Previous testing indicates that the concrete inserts are not adequate to provide the necessary ductility and damping to prevent element or system failure. For the concrete panel and connection anchor to remain linear elastic, the connecting body must be the yielding component (Pinelli, Craig and Goodno 1995). The addition of tilt-up concrete wall panels to metal building systems increases the seismic weight of the system approximately 20-30% (Baird, Palermo and Pampanin 2013). The addition of these panels also correlates to an increase in maximum base shear and initial stiffness of 41% and 47%, respectively (Baird, Palermo and Pampanin 2013). Due to the poor seismic performance of these concrete wall panels, the need for research arose to better understand the impacts of these panels and how to mitigate the additional damage caused by the inclusion of the panels into the structural system.

2.3 Plastic Deformation Mechanisms

Plastic deformation mechanisms rely on steel's ability to absorb energy when deformed beyond the elastic limit (Pinelli, Moor, et al. 1996). Additionally, steel is commonly commercially available and easy to fabricate into custom shapes. Several methods have been tested in the past to utilize this method of energy dissipation including ductile or flexing rods, advanced tapered connections, and flexural U-plates.

2.3.1 Ductile Rods

Ductile rod connections were designed with the philosophy of providing isolation for the in-plane motion while also providing out-of-plane resistance (Craig, Leistikow and Fennell 1988). A typical configuration for this type of connection is shown in Figure 2-3. When displaced, the connecting rod will bend and deform, using the plastification of steel as the energy dissipation method. Experimental testing performed by Craig (1988) included 8 cases of in-plane action and 2 specimens of out-of-plane action. The testing showed that although these connections exhibit ductile behavior, they are prone to failure within the range of cycles to be expected by moderate earthquakes. In all 8 cases the rods cracked at interstory drifts less than the UBC drift limit at anywhere from 47 to 90 cycles. In half of the specimens, complete fracture occurred within 25 displacement cycles.

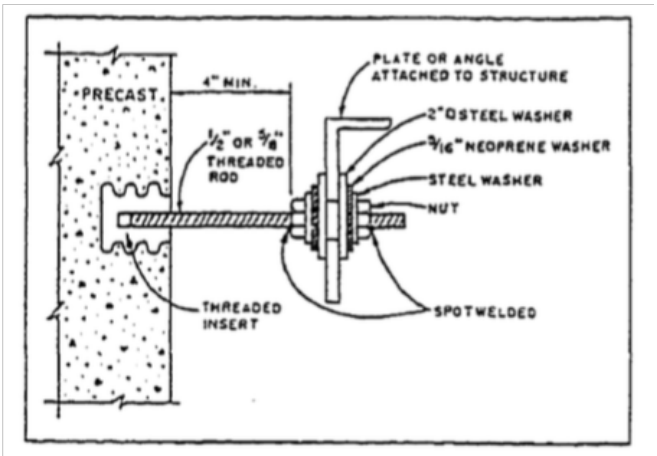

Figure 2-3: Ductile Rod Configuration (Craig 1988)

The pullout tests performed by Craig (1988) included only two specimens. The two specimens showed out-of-plane strength up to 4 times the specified working load. The failure mechanisms observed were shear cones in the concrete for both specimens tested.

Pantoli (2015) performed a series of 16 experiments using the setup shown in Figure 2-4. Experiments were performed at several universities in collaboration. The coil rods used were ASTM A36 steel and used a diameter (d) of either ¾" or 1". The free rod length (L_f) varied from 10.9" to 18.9". The variable D_{pl} refers to the imposed drift during testing. Testing was stopped when the rod could no longer support an out-of-plane load of 300 pounds.

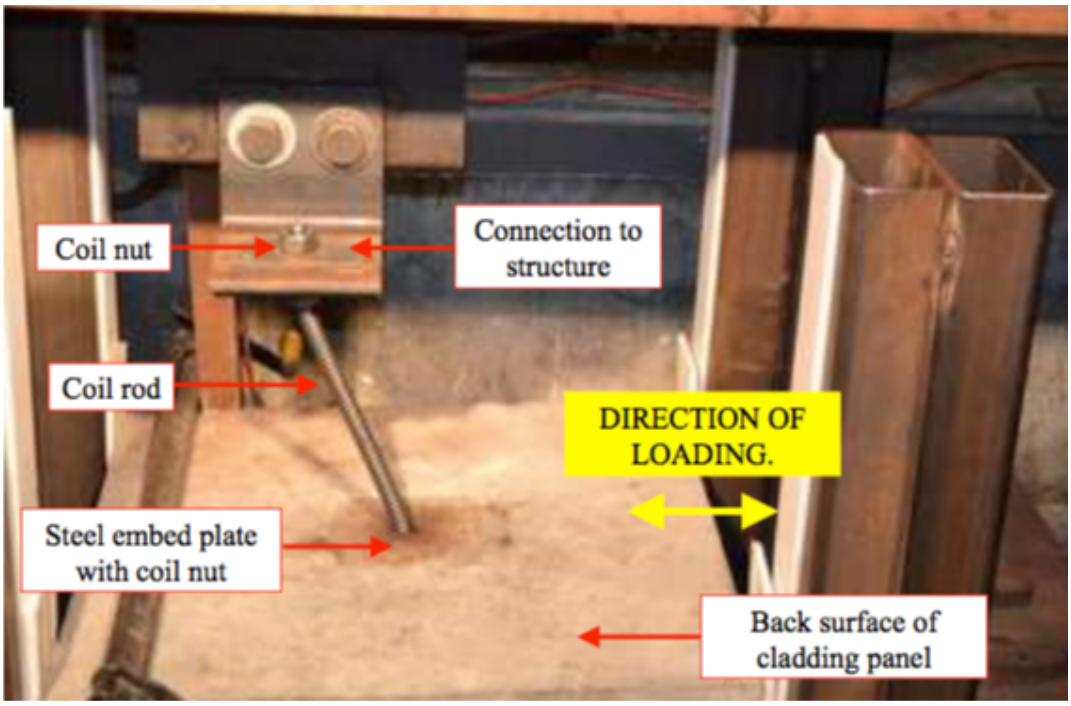

Figure 2-4: Experimental Setup Used by Pantoli (2015)

Like Craig (1988) the testing yielded results that displayed increased ductility when compared to a bearing connection; however, low-cycle fatigue was still apparent in the results, as seen in Figure 2-5. The results of Figure 2-5 are provided by the experimental testing done at San Jose State University. It was observed that the ductile rods had inelastic regions equal to approximately one

to two rod diameters. Despite this, the rods still resisted displacements much greater than the yield displacement.

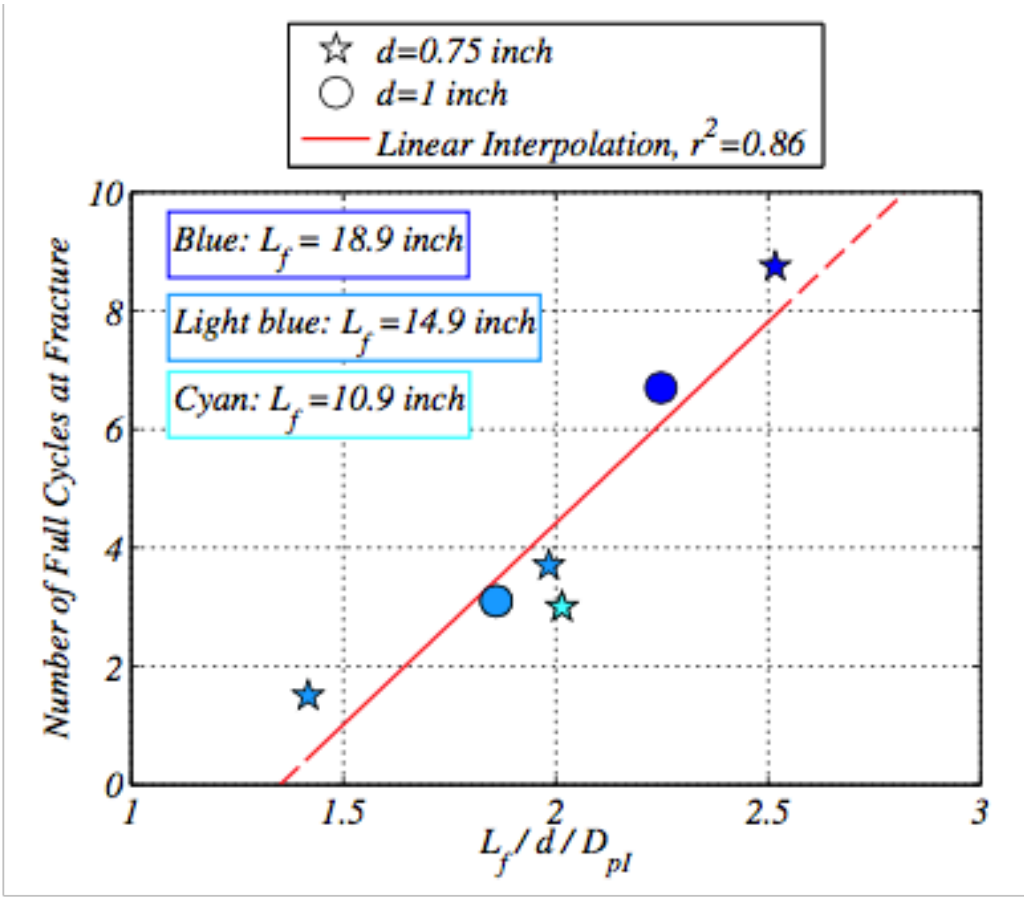

Figure 2-5: Number of Cycles to Fracture for Experimental Testing at SJSU (Pantoli 2015)

2.3.2 Advanced Tapered Connections

The advanced tapered connection consists of a square flexural tube with cutouts to create a taper that will cause plastification over a significant portion of the connection (Pinelli, Craig and Goodno 1995). A conceptual model of the advanced tapered connection is shown in Figure 2-6.

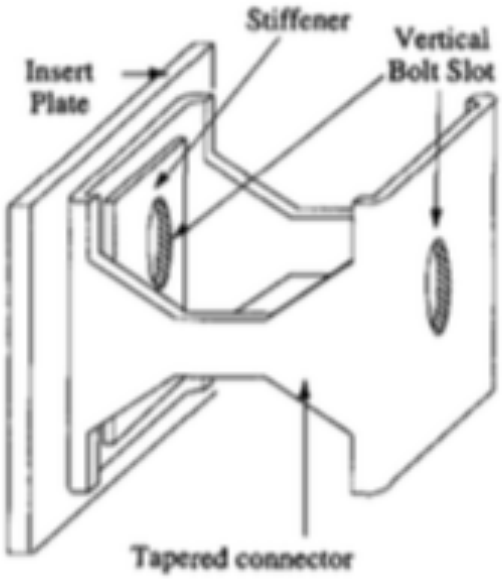

Figure 2-6: Advanced Tapered Connection (Pinelli, Craig, Goodno 1995)

The parameters varying in this connection were the thickness, method of attachment and the type of test performed. A summary of the results is seen in Table 2-1. The experimental testing yielded large, stable hysteresis loops, uniformly distributed plastic deformation, and favorable low-cycle fatigue behavior.

Table 2-1: Results of Pinelli (1996) Testing of Advanced Tapered Connections

Specimen ID	Thickness	Attachment	Type of test	Maximum displacement (mm)	Maximum strain (%)	Cycles to failure
TT375	9·5 mm (3/8″)	Welded	Cycles of increasing amplitude to failure	70	10·2	24
TT500	12·7 mm (1/2″)	Welded	Cyc. increasing ampl. fatigue	38 31	9·4 7·5	10 16*
TB375	9·5 mm (3/8″)	Bolted	Cyc. increasing ampl. fatigue	71 25	10·2 3·5	21 24*
TF375	9·5 mm (3/8″)	Bolted	Fatigue	25	3·5	42
TW375	9·5 mm (3/8″)	Bolted	Fatigue w/increasing gravity load	25	3·5	37
TB250	6·4 mm (1/4″)	Bolted	Cyc. increasing ampl. fatigue	74 58	4·4 3·5	20 9*

*Fatigue cycles are in addition to cycles of increasing amplitude

2.3.3 Flexural U-Plates

The concept of the flexural U-plate dates to (Kelly, Skinner and Heine 1972). The setup for a flexural U-plate energy dissipator is shown in Figure 2-7. As the ground motion displaces the wall panels, the connecting U-plate will plastically deform and dissipate energy.

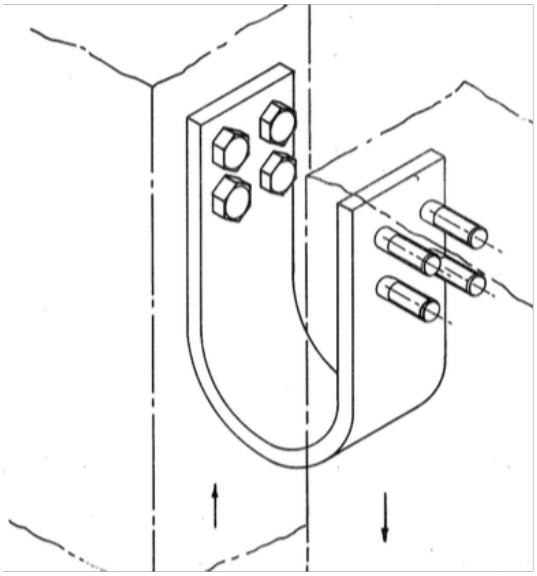

Figure 2-7: Flexural U-Plate Setup (Kelly, Skinner, Heine 1972)

Testing was performed using a controlled displacement cyclic loading procedure. The experimental results for Kelly (1972) are presented in Table 2-2. The predominant mode of failure that occurred was kinking of the strip and then transverse fracture. This device was also tested by Schultz (1994) and yielded similarly promising results. Per the results, the device was approximately 8 times more ductile and dissipated approximately 3 times as much energy when compared to a notched shear plate.

Table 2-2: Results of Flexural U-Plate Connection Testing (Kelly 1972)

	Span in	Stroke cm	Peak Load kg	En/cycle Joules	En/vol/cycle 10^6 N/M^2	Cycles life	Cumul. Ener.Abs	P1/bt^2 N/M^{2}x10^6	$\frac{100st}{\ell^2}$
805	4	4	490	257	3.9	300	1170	480	2.46
806	4	6	580	465	7.1	125	890	570	3.70
803	3	3	725	223	4.5	255	1150	530	3.28
802	3	4	880	357	7.2	135	970	647	4.36
801	3	6	1050	645	13.1	55	720	770	6.56
807	2	3	1550	380	11.5	142	1630	760	7.4
808	2	4	1850	710	21.5	72	1550	905	9.80

Baird (2013) utilized full-scale, single story test frames to test the U-shaped plates at the University of Canterbury. The device tested was different from Kelly (1972) and Schultz (1994) by adding a square tube as a housing unit and including slotted holes for sliding friction to dissipate energy as well. The housing unit was shown to ensure uniform bending and provide out-of-plane support. The device tested is shown in Figure 2-8.

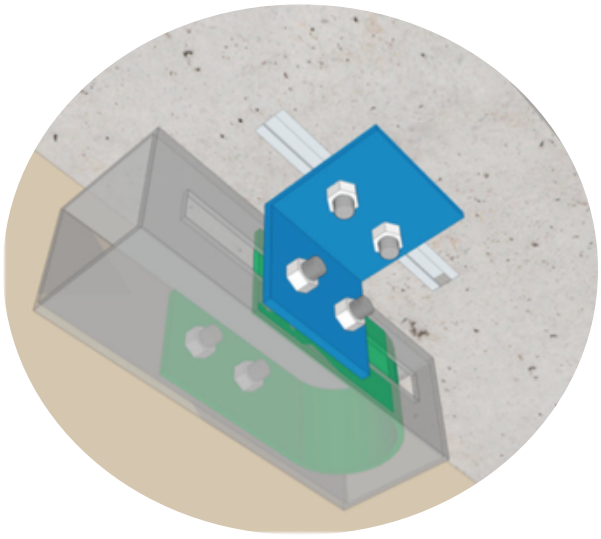

Figure 2-8: UFP Device Tested by Baird (2013)

The frame was displaced by using a hydraulic actuator placed at the top of the test assembly, seen in Figure 2-9. The hysteresis loop for Baird's experiment is shown in Figure 2-10. The hysteresis loop shown in Figure 2-10 displays no strength or stiffness degradation even through a high number of cycles. The concrete panels remained uncracked and the connection maintained the original shape. Additionally, the amount of energy dissipated by the structure dropped by 48% and the maximum displacement at the top of the structure was reduced by 42%.

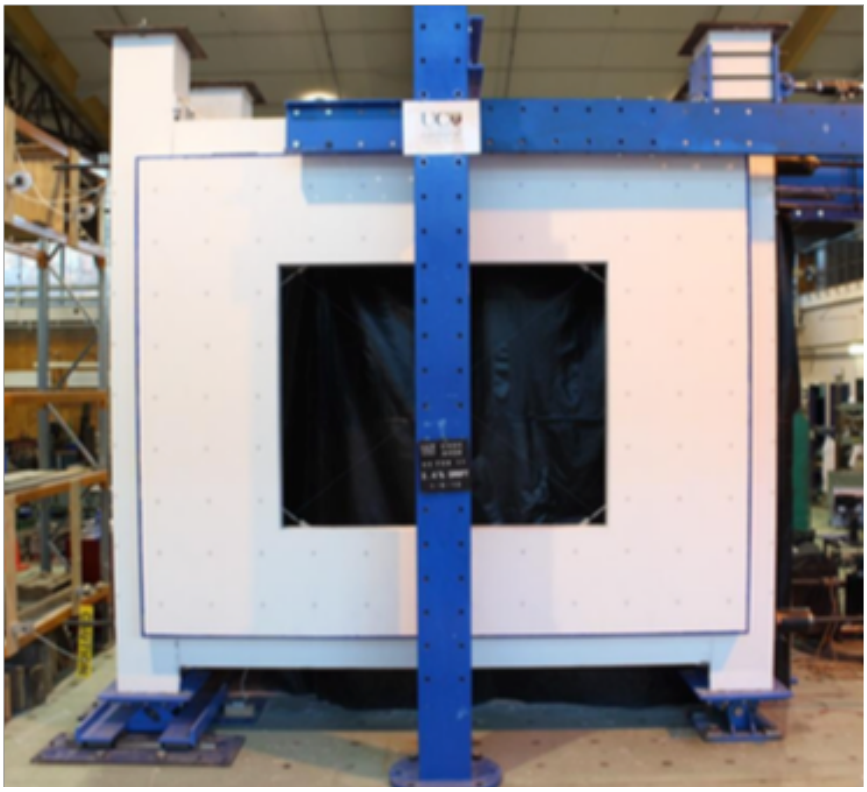

Figure 2-9: Testing Setup Used by (Baird 2013)

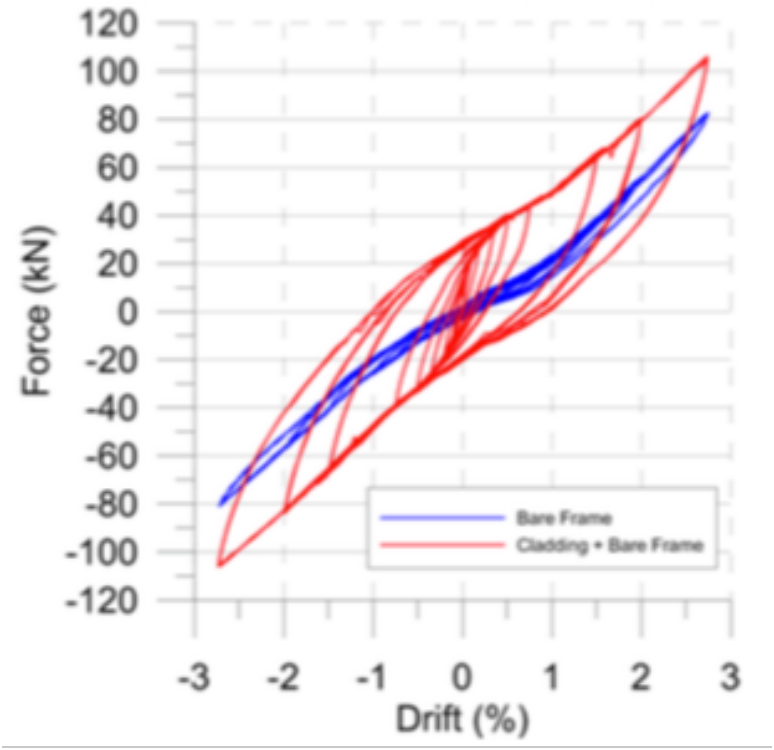

Figure 2-10: Hysteresis Loops for a Clad and Unclad Frame (Baird 2013)

2.4 Friction Mechanisms

Energy dissipation by friction is a favorable option due to the ability to dissipate large amounts of energy with negligible degradation over many reversal cycles (Pinelli, Moor, et al. 1996). Positive results in studies such as reported by Grigorian et al. (1993) show stable hysteresis loops with promise for using the mechanism as an energy dissipater in a cladding application.

2.4.1 Sliding Friction Connection

Brass friction devices (BFD) in cladding were greatly influenced by the work of Grigorian et al. (1993) who tested similar devices, although not in a cladding application. Schultz (1994) experimentally tested a brass friction device used in a cladding application, seen in Figure 2-11.

Per the results of the study, the BFD is approximately 8 times as ductile and dissipates approximately 5 times as much energy when compared to a notched shear connection.

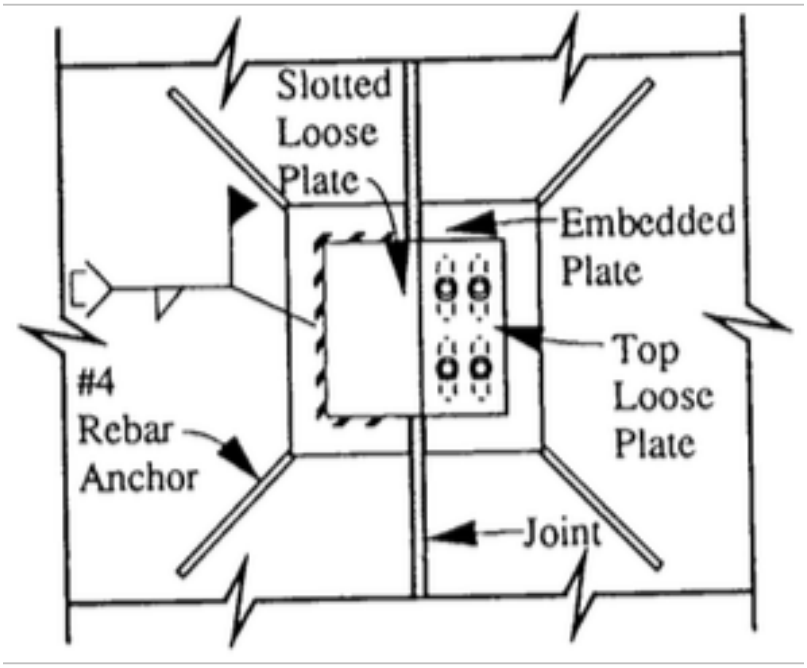

Figure 2-11: Brass Friction Device Tested by Schultz (1994)

Pantoli (2015) tested a sliding connection using the setup shown in Figure 2-12. A summary of Pantoli's results can be seen in Figure 2-13.

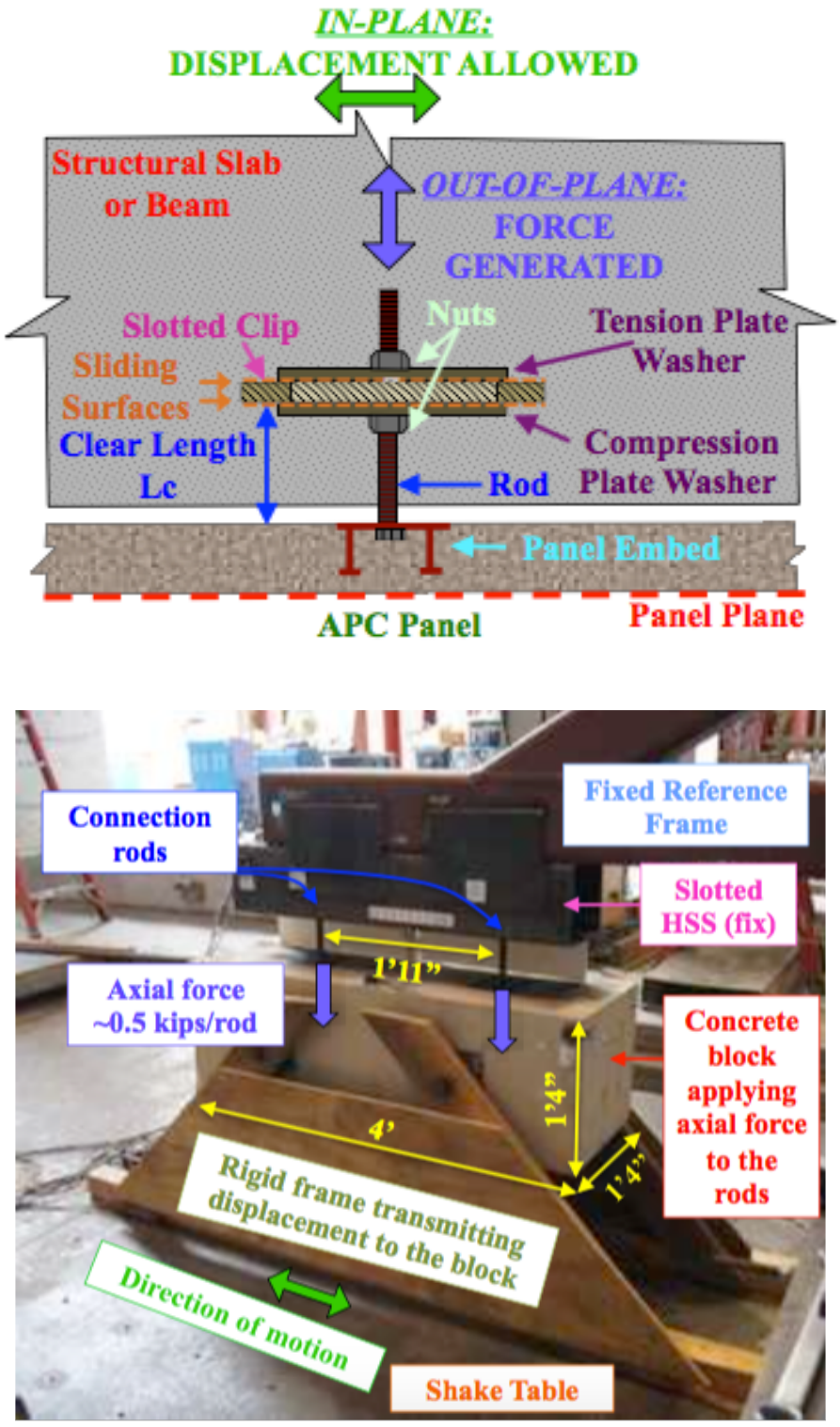

Figure 2-12: Sliding Connection Setup Utilized by Pantoli (2015)

Some observations from the experiment were that, due to the flexibility of the connection, the connection rods often bent before achieving the intended sliding motion. These bending induced rotations can cause a clamping force that increase the normal force, thereby, reducing the likelihood of sliding. As such, short, stiff rods were recommended due to the connection exhibiting less rotations, therefore causing less clamping force. Even with shorter, stiffer, rods, the connection exhibited a ratcheting effect, accumulating deformations in one direction and sliding in the other direction. Due to this, it is possible that severe damage, such as fracture of the connection rods, could occur under large displacements. As shown in Figure 2-13, due to the greater flexibility of the longer rods, damage is more likely to occur. However, as stated earlier, due to the binding mode of the connection, even configurations with shorter rods have the possibility of fracture. It was recommended to eliminate the free length of the connection rod by using a bolt instead. Connections using this configuration consistently displayed good performance. Alternatively, the compression washer can be removed, which makes it impossible for the binding force to develop; however, removal of this component makes the connection a tension-only connection.

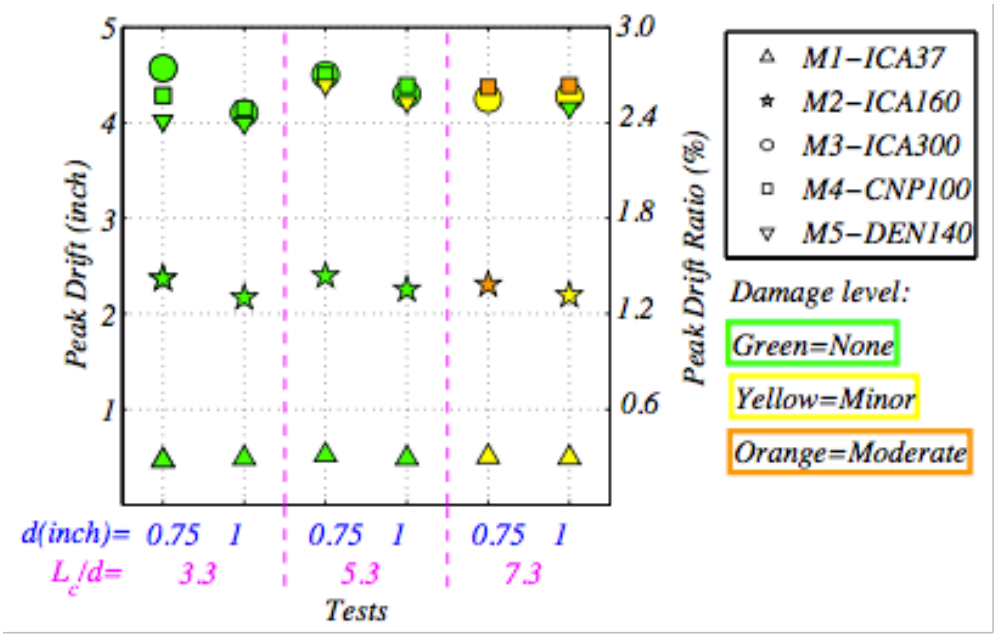

Figure 2-13: Experimental Results for Pantoli (2015) Sliding Connection

2.5 Summary

The purpose of this literature review was to provide background into previously tested energy dissipation methods. The need for these energy dissipative connections arose when the addition of concrete hard walls to metal building frames caused unforeseen collapses due to the increase in seismic weight as well as compatibility and ductility issues as well.

The two primary methods that have been tested involve either a plastic deformation mechanism or a frictional mechanism. Concepts involving plastification of the connection material have existed since Kelly (1972) tested flexural U-plates. The plastic deformation of a connection is desirable; however, it still involves the post-earthquake replacement of some elements such as connecting rods or entire connections. Concepts involving a frictional mechanism have stemmed from the initial research by Grigorian et al. (1993). The sliding friction mechanism allows for less damage

and replacement than the plastic deformation concept; however, Pantoli (2015) showed that such connections can display a ratcheting effect of accumulating deformations in one direction.

The research presented in this thesis includes the testing of a friction device using rotational friction as the energy dissipation method. The goal of this new connection is to require minimal replacement of the elements in the connection. Furthermore, the goal of the connection is to have the replaced elements be inexpensive, such as washers and bolts as compared to the entire connection.

Chapter 3. Experimental Evaluation of Rotational Friction Connection

3.1 Introduction

Chapter 3 introduces the design philosophy, practical application, and testing setup of the rotational friction connection. The rotational friction connection was developed to offer a low-damage method of energy dissipation for use in metal building systems with hard walls. A final design for the RFC prototype was selected based on analytical models that simulated typical loads experienced by these connections. The prototype was then tested in the Auburn University Structural Research Laboratory to verify its performance. This chapter also discusses the laboratory setup used to perform the tests as well as the testing protocol used.

3.2 Design Philosophy

The research presented in this thesis tested a friction device using rotational friction as the energy dissipation method. The goal of this new connection is to have minimal replacement of the elements in the connection. Furthermore, the goal of the connection is to have the replaced elements be inexpensive, such as washers and bolts as compared to the entire connection.

The design philosophy used to develop this connection was to use rotational friction as a method

to allow for large displacements with minimal damage. The use of rotational friction as a mechanism for dissipating energy has returned promising results in applications such as braces (Mualla and Belev 2002). The results reported by Mualla and Belev (2002) matched the performance objectives of this experiment: a system that allows for large displacements and results in minimal damage. As discussed in Chapter 2, plastic deformation energy dissipation methods require replacement of elements (Mirzabagheri, et al. 2015) and sliding friction connections can display ratcheting effects that can cause fracture if large displacements are experienced by the connection (Pantoli and Hutchinson 2015). The rotational friction connection discussed in the following chapters attempts to remedy both issues of the plastic deformation connection and sliding friction connection by using rotational friction as a method of minimally destructive energy dissipation. Numerical modeling was performed in ABAQUS on different connection types to determine a viable prototype. A sliding friction connection and a rotational friction connection were modeled. The sliding friction connection displayed "ratcheting" effects of accumulating deformations in one direction and inducing bolt bearing on the slotted hole, causing an increase in force. The rotational friction connection displayed a constant force throughout the analysis; therefore, the rotational friction connection was selected to use in experimental testing. The damage in this connection is designed to be concentrated on relatively inexpensive elements such as bolts and nuts so that cost of replacement, if it is needed, will be minimal.

3.3 Connection Design and Detailing

The connection consists of two steel angles welded to an embedded plate in the hard wall, a steel strut with two interior washers, and a top bolt to connect to the spandrel beam of the structural

system as seen in Figure 3-1. The size of the angles was specific to testing and could vary in the actual structure. The list of structural elements used for testing are as follows:

- *L4"x3"x0.375", 4 inches in length, A572 Gr. 50 Steel*
- *PL12"x10"x5/8" A36 Embedded Plate (Not shown)*
- *C9x20, 9'2" in length, A572 Gr. 50 Steel*
- *A325 Bolts, 5/8" and 3/4" diameter*
- *A563 Structural Nuts*
- *F436 Circular Washers*
- *PL10.5"x3.5"x0.5" A572 Gr. 50 Steel*
- *Jamb Nuts, Grade 8*

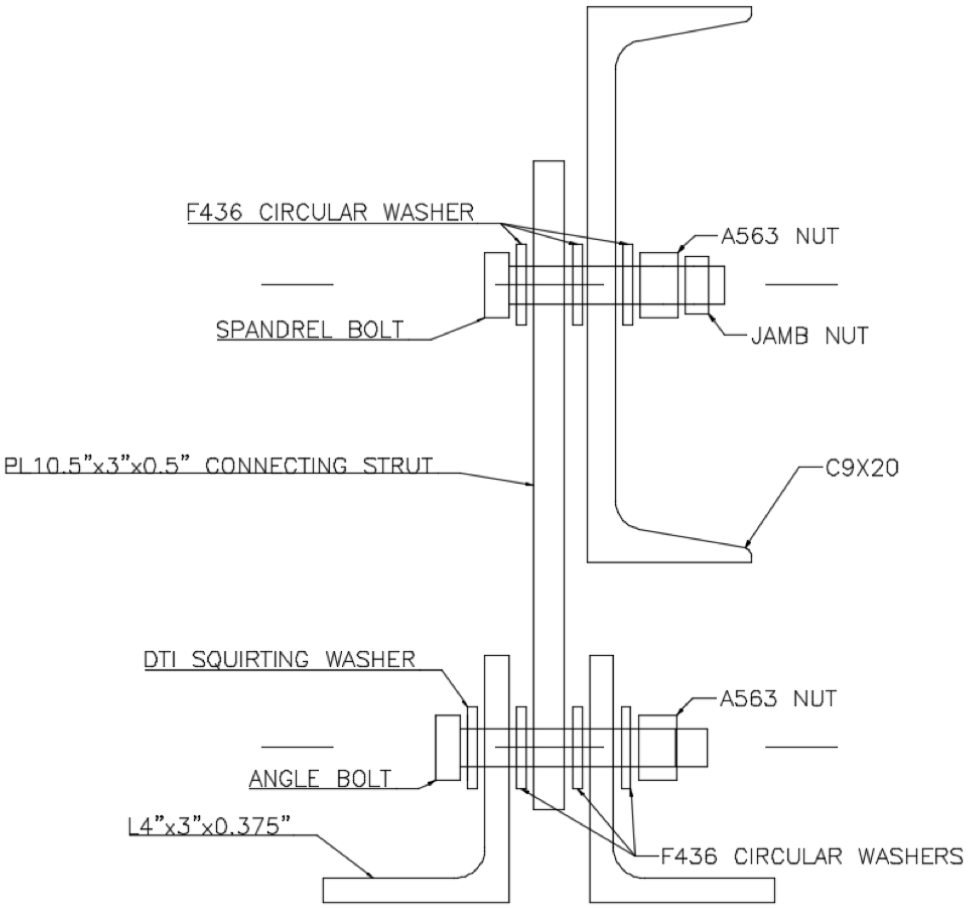

Figure 3-1: Assembly Drawing of Rotational Friction Connection

Component drawings of the listed structural elements can be seen in Appendix B. The connection shown in Figure 3-1, is representative of the orientation used in experimental testing, however the connection will be installed into a real structure as seen in Figure 1-2.

In the case of a seismic event, the connection will slip at the slip force, and then rotate about the angle bolt for the duration of the event. This rotational freedom results in limiting damage to the structural system. The connection functions as a method of resolving compatibility issues by allowing rotational movement to limit forces within the connection. This limitation of forces will prevent catastrophic failures seen in the New Zealand and Haiti earthquakes discussed in Chapter 2.

The connection is simple to install and allows for easy assembly and disassembly. The angle bolt requires full pretension. Tolerances in bolt holes and angle placement may have an impact on aspects such as exact bolt tension and the resulting friction coefficient. Full pretension was indicated by direct tension indicating squirting washers as well as a calibrated value from the strain gauge installed in the bolt. The spandrel bolt should be installed in a snug-tight fashion, loosened a quarter of a turn, then install a jamb nut behind the structural nut as stated in AISC Specification Commentary J3.1 (AISC 2011). This method was used to prevent the nuts from loosening in the spandrel bolt during testing. Both bolts have the threads excluded from the shear planes.

During uniaxial testing, it is expected that the linear displacement of the spandrel channel will cause the connecting strut to rotate about the fully pretensioned angle bolt. This rotation will be

the primary method of energy dissipation in this connection. Due to the release of tension in the spandrel bolt, the spandrel bolt acts as a pin connection that freely rotates. The embedded plates were sized to permit testing of multiple connections on one panel so that more samples could be tested. The strut was designed to be wide enough to preclude bolt bearing failure and long enough to extend from the center of the angle to the center of the spandrel beam plus additional edge requirements. The bolt sizes were selected to target frequently used bolt sizes in the industry. Multiple sizes were required for the calibration of numerical models and to determine any sizing effects. The limit state of bolt shear during the pullout test was the most important. Due to the low force present in the connection during all other testing, structural failures of the system were unlikely.

3.4 Experimental Setup and Testing Sequence

The experimental testing was performed in the Auburn University Structural Research Laboratory. Testing was performed on two separate concrete panels, Panel A and Panel B. Panels A and B were identical in construction. The panels consisted of 4000 psi specified compressive strength concrete. The panels had dimensions of 90”x42”x6” as well as three embedded plates. The embedded plates were 10”x12”x5/8” made of A36 steel. These dimensions were used to allow for two samples per embedded plate to be tested rather than just one. The thickness of the plate was determined using principles of plate bending. The embedment system was designed using Hilti PROFIS Anchor software (Hilti 2017). The panels were fabricated and delivered by Oldcastle Precast. Panel A used angle sections that were compatible with the 5/8” diameter angle bolts; Panel B used angle sections that were compatible with 3/4” diameter angle bolts. Two bolt sizes

were utilized to test for possible sizing effects as well as provide more data for validation of numerical models of the connection. Panel A was installed, a full array of tests was run on it, it was uninstalled, and then Panel B was installed and tested. Due to the need for anchoring to the strong floor and other geometric constraints the experimental setup was modeled using SketchUp (SketchUp 2017) prior to installation. Figure 3-2 shows a rendering of the experimental test setup as well as the setup as it was in the lab.

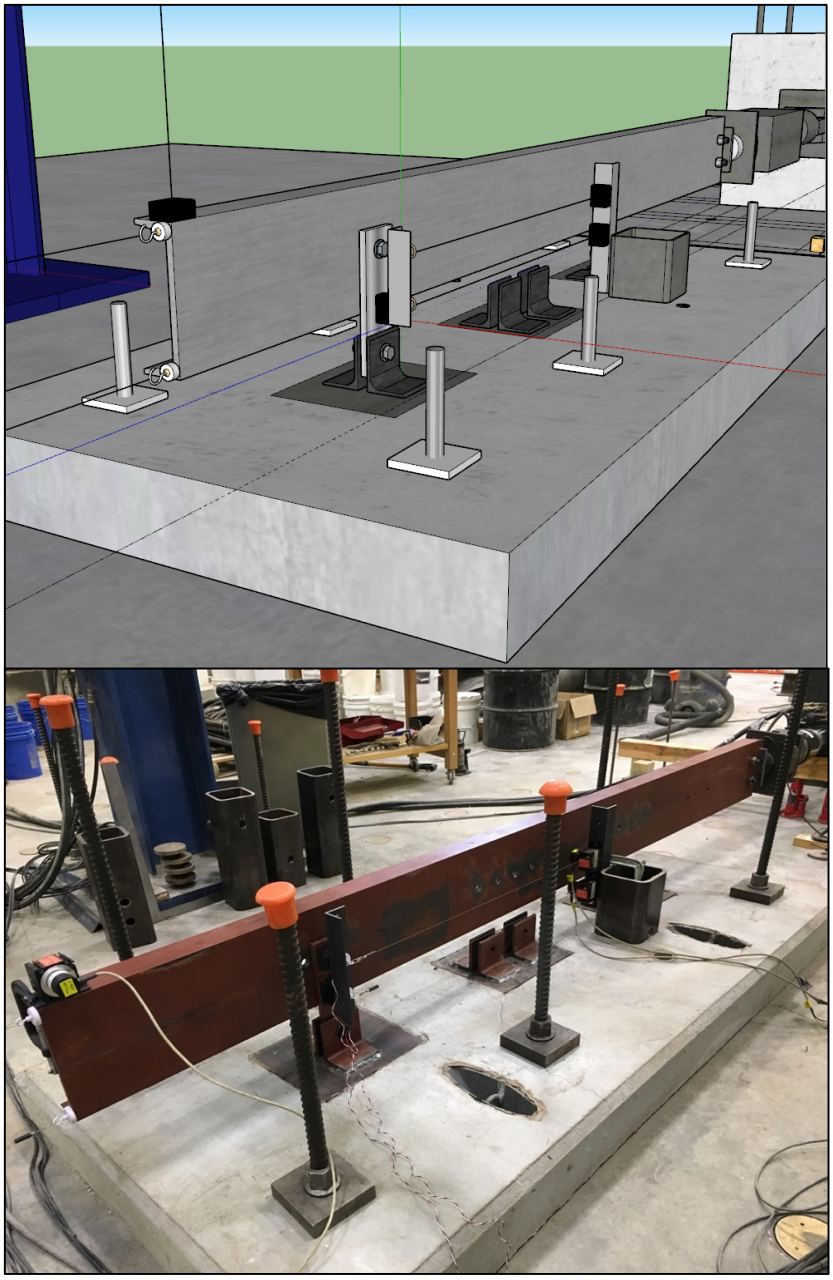

Figure 3-2: Rendering and Actual Experimental Setup

There were five connections of identical setup tested on each panel. The connection locations are noted in Figure 3-3.

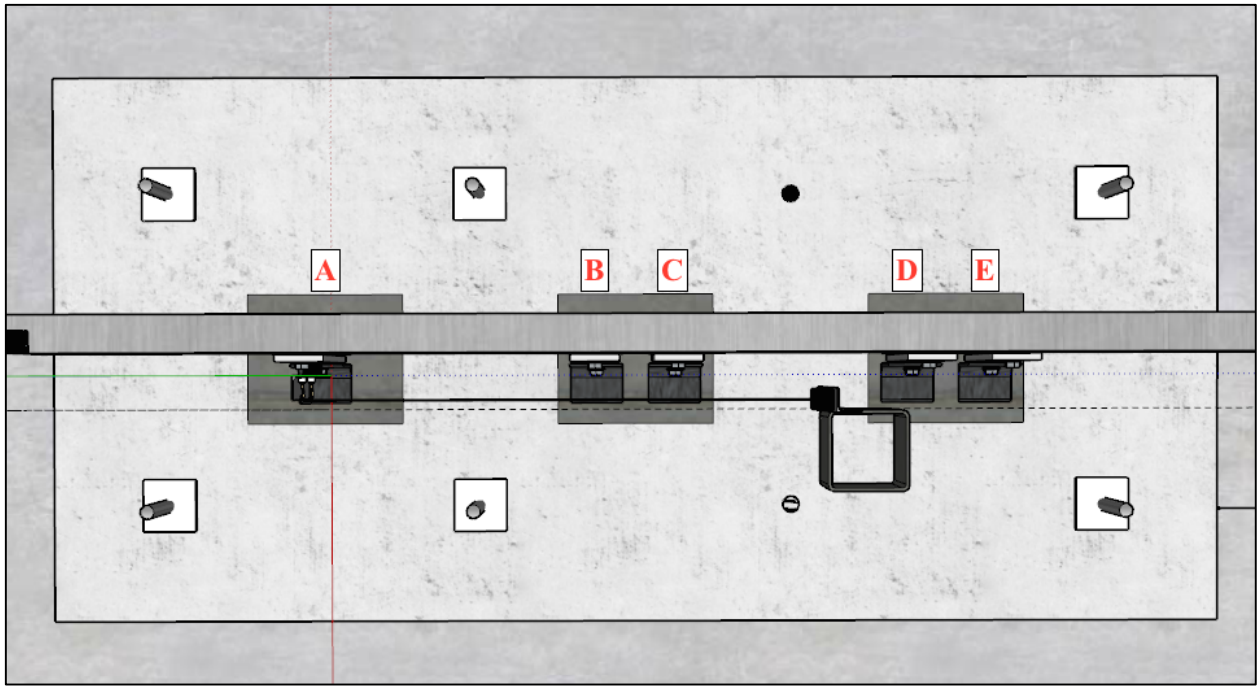

Figure 3-3:Plan View of Test Panel with Locations of Connections Tested

The channel section, angles, tension tab, bolts and washers were donated by American Buildings Corporation in Eufaula, Alabama. Before testing, the friction surfaces of the angles, struts, and channels were prepared by sanding off all paint and smoothing the surface with an angle grinder. Dwyidag post-tensioning rods were used to tension the panels and the reaction block to the strong floor. Tensioning was performed using a manual hydraulic pump. The concrete panels were tensioned to the strong floor in a similar fashion as the reaction block. The reaction block, concrete panel, and C9x20 channel section were all put into place using the crane.

The testing utilized a horizontal and vertical actuator. The horizontal actuator was used to apply displacements in the direction of the longitudinal axis of the spandrel beam. The vertical actuator was used to apply displacements in the direction normal to the plane of the wall panel. Uniaxial

testing used only the horizontal actuator while biaxial testing used the horizontal and vertical actuator. The pullout test required only a vertical actuator. The horizontal actuator was connected to a reaction block that was tensioned to the strong floor and the vertical actuator was connected to a reaction frame in the Auburn Structural Laboratory. Due to the experimental testing setup being 90 degrees from the building application, it should be noted that the horizontal actuator applies displacements in what would be the longitudinal direction of the metal building system while the vertical actuator applies displacements in what would be the transverse direction of the metal building system.

Testing consisted of a pushover, uniaxial, biaxial, pullout, and 100-cycle testing. The sequence of this testing is shown in Figure 3-4. On Panel B, a first and second test was performed per connection location for the uniaxial testing. This was to collect additional data as well as observe the performance of the connection in the case of a second seismic event with no adjustment after the first seismic event. The 100-cycle testing was only performed on Panel B.

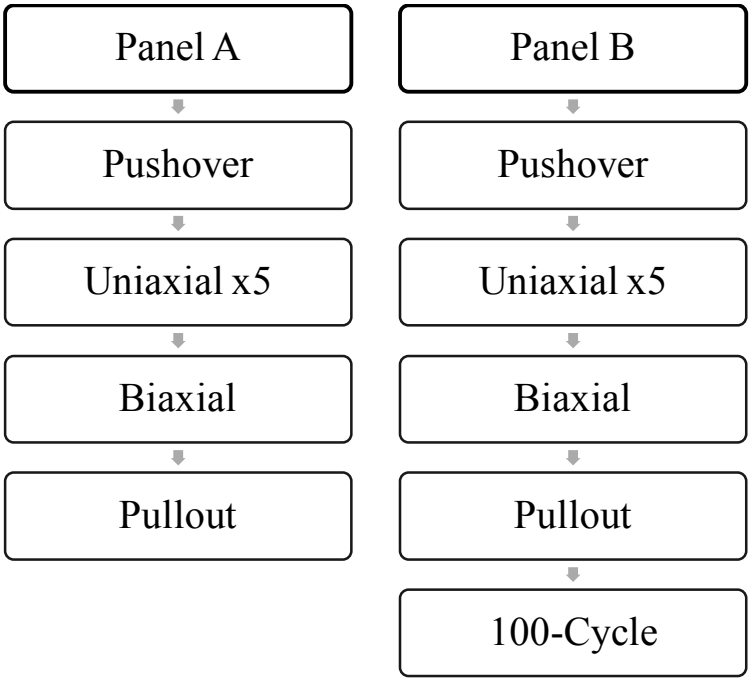

Figure 3-4: Experimental Testing Sequence

Testing began with a monotonic pushover test to determine the damage limit states as defined by FEMA 461, *Interim Testing Protocols for Determining the Seismic Performance Characteristics of Structural and Nonstructural Components* (Applied Technology Council 2007). The monotonic pushover protocol consisted of a forced displacement in the longitudinal direction of 4.5 in from the neutral position. This displacement limit was based on the geometry of the connection. After 4.5 in, the channel will begin to bear onto the angle section causing damage to the connection. Following the monotonic pushover test, a full uniaxial test was performed on each of the five connection locations on the panel seen in Figure 3-3. Uniaxial testing consisted of using just the horizontal actuator to cycle the connection. The maximum displacement for the uniaxial testing was 3 inches in each direction. The biaxial and pullout test were then performed on Location A

on both panels due to its location under the vertical actuator. The biaxial test consisted of a static tension force of approximately 3.5 kips being applied using the vertical actuator while the horizontal actuator cycled between a maximum amplitude of 2 inches in either direction. The pullout test used only the vertical actuator to increase the out-of-plane force in the connection to measure the response and observe possible damage in the out-of-plane direction. Following the pullout testing on Panel B, testing was performed that consisted of a 100-cycle protocol at a certain displacement, followed by 10 cycles at a higher displacement to confirm effects of surface roughening that were identified during uniaxial testing and to determine the behavior of the connection under many load cycles.

A small capacity load cell was attached by placing it between two fabricated plates and using countersunk screws to maintain its position between the plates. A tension tab was then welded to the base plate of the tension tab and used to connect the actuator to the channel section as seen in Figure 3-5. The tension tab bolts were then aligned and installed. Connections were installed and tested one at a time.

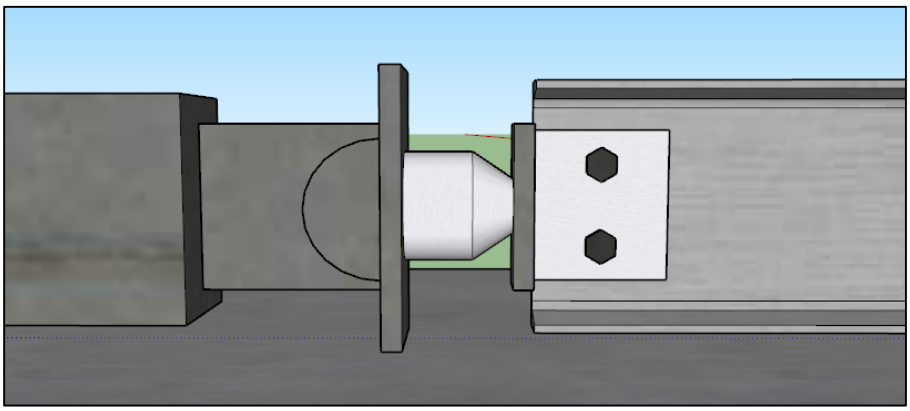

Figure 3-5: System Used to Connect Actuator to Channel

For biaxial and pullout testing, 1/2 in diameter holes were drilled near the top of the channel web, 6 inches in either direction of the hole being tested. Steel wire rope with a diameter of 7/16 in was placed through these holes and then connected to the vertical actuator to allow for the application of vertical force. The appropriate size wire rope clamps were then installed. Figure 3-6 shows the experimental setup for biaxial and pullout testing.

Figure 3-6: Experimental Setup for Application of Out-of-Plane Force

3.4.1 Loading Protocol

For the monotonic pushover testing of the connection the system was displaced to 4.5" at a rate of 0.02 in/sec. At 4.5" the channel begins bearing on the top of the angle sections and testing was terminated.

For uniaxial testing the loading protocol was the interim protocol I-quasi-static cyclic testing from the FEMA 461 (Applied Technology Council 2007) standard. The load rate was the same as the monotonic pushover test. The load rate input to the actuator was required to be slow enough to disregard dynamic effects but fast enough so that the length of the test is not excessive. Loading was specified as displacement based. The input displacement protocol specified by FEMA 461 is shown in Figure 3-7.

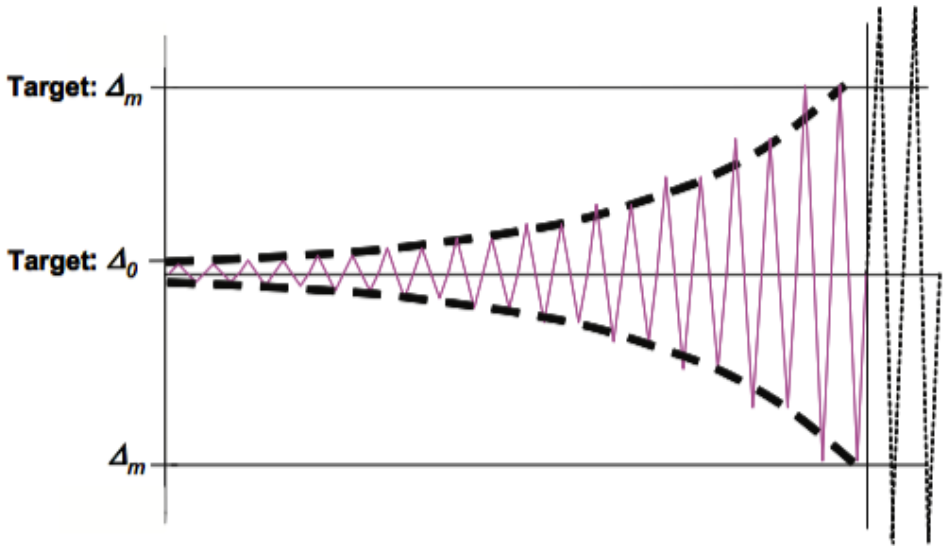

Figure 3-7: FEMA 461 Displacement Protocol (Applied Technology Council 2007)

The initial amplitude, Δ_0, was defined as the smallest deformation amplitude of the loading history. After two cycles, the amplitude increased by 40% until the final target amplitude, Δ_m, is achieved.

The Δ_0 and Δ_m for the uniaxial testing were 0.05 in and 3 in, respectively. The full displacement protocol used for uniaxial testing can be seen in Appendix A.

The biaxial testing protocol consisted of a constant tension force using the vertical actuator, followed by 2 cycles with an amplitude of 2 in using the horizontal actuator. The magnitude of out-of-plane force was determined using AISC 7-10 for a nonstructural attachment. To test how the connection would behave under large in-plane amplitudes 2 inches was selected. The purpose of the minimal cyclic action was that large out-of-plane forces are not sustained loads during seismic events, therefore, the biaxial testing was used to capture the behavior of the connection in reaction to pulses of out-of-plane forces using a sustained out-of-plane load.

The load rate for the pullout test was decreased to 0.005 in/sec. Due to the high out-of-plane stiffness, force accumulated quickly once testing began. A lower load rate was desirable to observe and capture any observable failures. Safety was also a consideration in decreasing the load rate. Loading continued until the design capacity of the wire ropes was exceeded, then testing was terminated due to safety reasons.

The 100-cycle testing used a load rate of 0.1 in/sec and consisted of three levels, a low displacement protocol, a medium displacement protocol, and a high displacement protocol. The low displacement protocol began at a displacement of 0.28 in for 100 cycles and then increased to 0.56 in for 10 cycles. The medium displacement protocol began at a displacement of 0.56 in for

100 cycles and then increased to 1.10 in for 10 cycles. The high displacement protocol began at a displacement of 1.10 inches for 100 cycles and then increased to 2.20 in for 10 cycles.

3.5 Instrumentation

Notable equipment used in the experiment is as follows:

- *MTS Systems Corporation (MTS) 243.35 Single Ended Actuator*
- *MTS 506 Hydraulic Power Supply*
- *MTS 292.14 Hydraulic Service Manifold Model*
- *MTS 111.12C-06 Piston Accumulator*
- *Pacific Instruments 6000 Data Acquisition System*
- *Micro-Epsilon WDS-1000-P60-CR-P Drawstring Gauges (Stringpots)*
- *Load Cell Central LPSW-B-10K Load Cell*
- *32"x32"x32" Reinforced Concrete Reaction Block with 1.5" PVC holes at 24" o.c. for anchorage to strong floor*
- *Tokyo Sokki Kenkyujo Co., LTD BTM-6C Bolt Strain Gages*

To accurately evaluate the effectiveness of the connection the displacement of the channel section as well as the system forces were required to be accurately measured. The bolt tension was also measured to determine if bolt tension was lost throughout the experiment. The readings from the linear variable displacement transducers (LVDT) as well as the load cells in the actuators were recorded. String potentiometers (stringpots) were used to measure the longitudinal displacement of the channel in two places, the longitudinal displacement of the strut in two places, the vertical displacement at the end of the channel, the displacement of the reaction block, and the displacement of the concrete panel. Due to the low magnitude of the expected force in this experiment, an additional, small-capacity load cell was utilized in line with the actuator to more

accurately measure the force occurring. Finally, strain gages were installed into both bolts to measure the bolt tension throughout the experiment. Holes 2 mm in diameter were drilled into the center of the bolt heads, strain gages were placed inside, then epoxied. To ensure this was done properly, bolt calibration tests were performed using a *Tinius-Olsen Super "L" Hydraulic Universal Testing Machine* to incrementally load the bolts up to 35% of the yield stress in three separate trials and force versus strain plots were generated. A direct relationship between strain and tension was established and used to determine when bolts were fully pretensioned during installation in addition to the use of DTI squirting washers. The test setup for this calibration process and a representative sample of the results are shown in Figure 3-8 and Figure 3-9, respectively.

Figure 3-8: Experimental Setup for Bolt Calibration

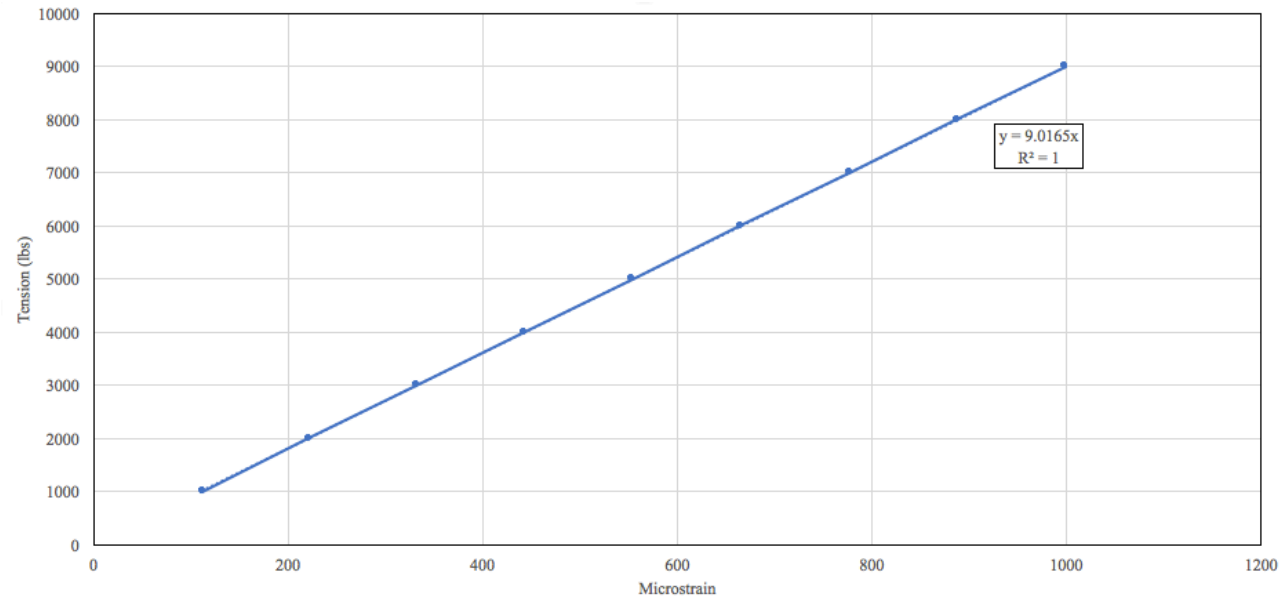

Figure 3-9: Bolt Calibration Results for 5/8" Diameter Bolt

The instrumentation plan for the connection is summarized in Table 3-1. The labels in the table correspond with the placement of the sensors shown in Figure 3-10,Figure 3-11, and Figure 3-12. The load cell and LVDT (1,2,3,4) in the actuators were already operational and calibrated before the experiment. The string potentiometers for the longitudinal displacement of the channel (7,8), the reaction block (5), the panel (6), and the longitudinal displacement of the strut (9,10) were attached using magnetic hooks. The string potentiometers for the reaction block and panel were clamped to a block of wood that was then secured to the strong floor using a post tensioned rod. The magnetic hooks were placed on the reaction block and to a small plate of steel epoxied to the panel, respectively. The string potentiometers for the longitudinal displacement of the channel were bolted to an instrumentation post consisting of a W-section clamped to an angle section, which were available in the lab. The magnetic hooks were placed at the top and bottom of the channel section. The string potentiometers for the struts were bolted to an instrumentation post consisting of an angle section clamped to an HSS section. The magnetic hooks were on a piece of

angle that was magnetically attached to the strut. The vertical string potentiometer (11) was clamped using C-clamps to the end of the channel section. For the vertical stringpot it was necessary to add an extension to reach to the magnetic hook where it was connected. Due to the range of the stringpots and the tolerance of the angle at which the strings can still be effective, the stringpots were pulled to a maximum allowable length to allow for small angles. The load cell (12) was fixed in between two plates. The strain gages were epoxied into the bolts prior to testing (13,14).

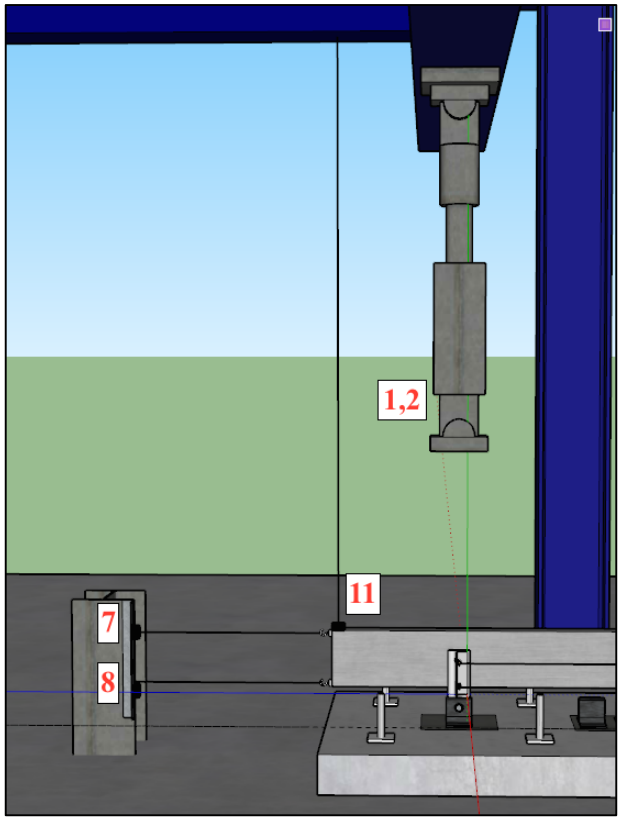

Figure 3-10: Sensor Positions of NE Actuator, Longitudinal Wires and Vertical Wire

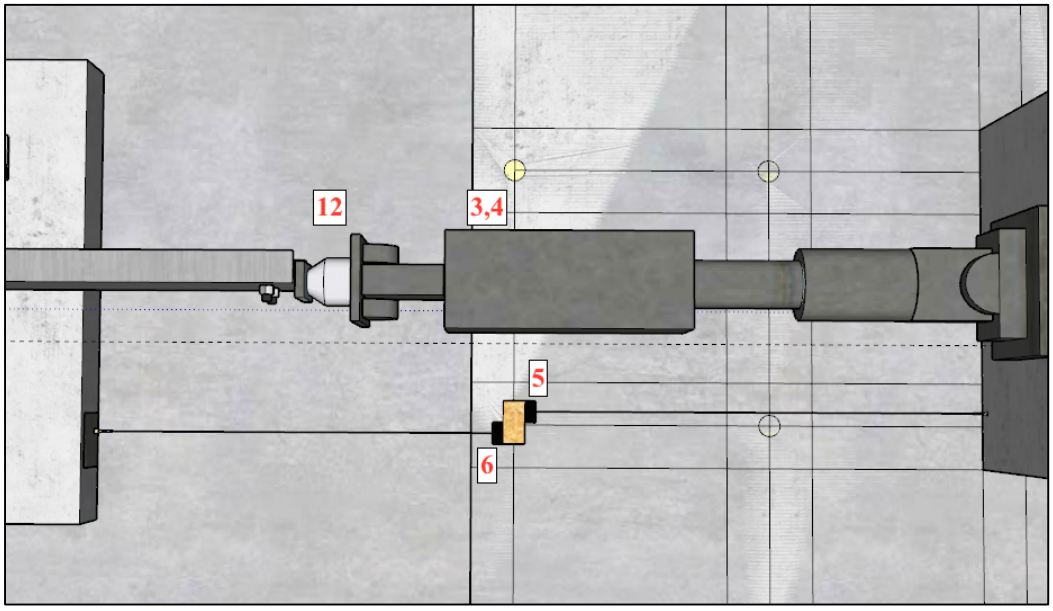

Figure 3-11: Sensor Positions of NW Actuator, Reaction Block and Slab Wires, and Load Cell

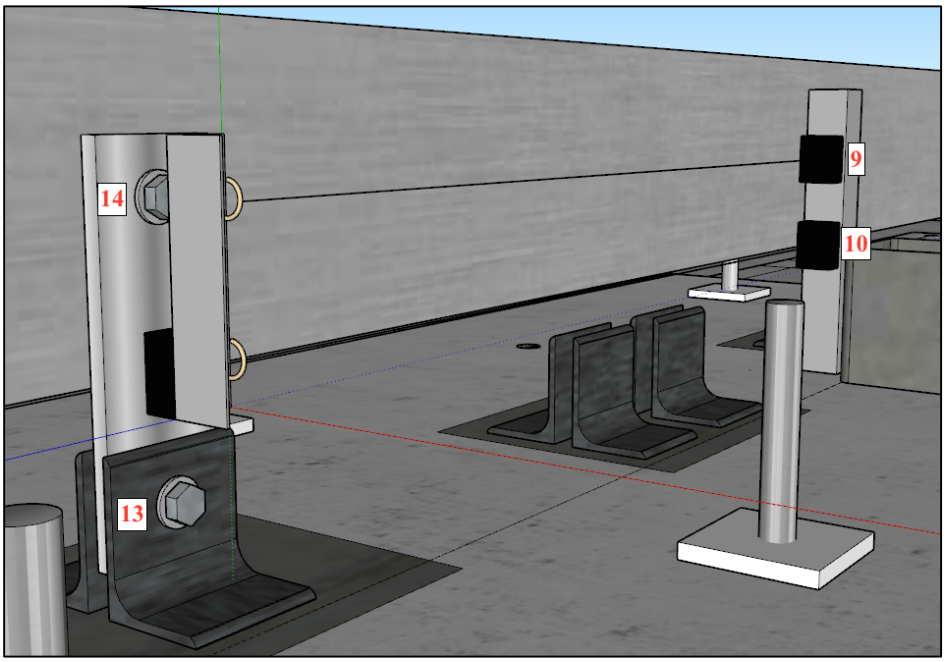

Figure 3-12: Sensor Positions of Strut Wires and Strain Gaged Bolts

Table 3-1:Instrumentation Used in Experimentation

Label	Sensor Label	Sensor	Purpose	Manufacturer Calibration Constant		Excitation Voltage (V)
				Value	Units	
1	NE ACT DIS	LVDT	Actuator Displacement	2000	mV/in	10
2	NE ACT FOR	Load Cell	Actuator Force	0.1	mV/lb	10
3	NW ACT DIS	LVDT	Actuator Displacement	2000	mV/in	10
4	NW ACT FOR	Load Cell	Actuator Force	0.1	mV/lb	10
5	RXNB WIRE	Stringpot	Displacement of Reaction Block	0.968	mV/V/mm	10
6	SLAB WIRE	Stringpot	Displacement of Panel	0.968	mV/V/mm	10
7	LONGWIRET	Stringpot	Longitudinal Displacement of Channel	0.968	mV/V/mm	10
8	LONGWIREB	Stringpot	Longitudinal Displacement of Channel	0.968	mV/V/mm	10
9	STRUTTOP	Stringpot	Longitudinal Displacement of Strut	0.969	mV/V/mm	10
10	STRUTBOT	Stringpot	Longitudinal Displacement of Strut	0.969	mV/V/mm	10
11	SPAN_VERT	Stringpot	Vertical Displacement at the End of Channel	0.967	mV/V/mm	10
12	LC	Load Cell	Force Applied	3.9795	mV/V/mm	10
13	ANGLEBOLT	Bolt Strain Gage	Strain in Angle Bolt	Gage Factor	2.10	1
				Resistance	120	
14	SPAN_BOLT	Bolt Strain Gage	Strain in Spandrel Bolt	Gage Factor	2.10	1
				Resistance	120	

3.6 Conclusions

The rotational friction connection is a connection that will allow for large displacements while experiencing minimum damage. The connection is designed to use common, readily available materials to achieve an economic, reliable solution to the connection of concrete hard walls to flexible metal building system steel frames. All testing was performed in the Auburn Structural Research Laboratory. The testing matrix for a single panel consisted of a monotonic pushover test, five uniaxial tests according to the guidelines FEMA 461 interim protocol I-quasi-static cyclic, a biaxial test, a pullout test, and 100-cycle testing performed on Panel B. Panel A utilized the angle sections compatible with 5/8" diameter bolts and Panel B utilized angle sections compatible with 3/4" diameter bolts. Instrumentation consisted of stringpots, load cells, and bolt strain gages. The test setup was designed to allow for quick exchange of specimens and allow for significant amounts of testing per day. The next step in this experiment was to analyze the data collected from these tests to demonstrate that the connection exhibited desirable behavior.

Chapter 4. Results and Discussion

4.1 Introduction

This chapter will discuss the experimental data collected from the experimentation discussed in Chapter 3. Due to having many samples of data for the testing performed, representative samples will be selected to be displayed. Relevant figures of all trial runs are in Appendix A. Monotonic pushover test results will be briefly discussed to give background on how damage limit states were defined. Uniaxial testing results will focus on the hysteresis loops generated by testing, free rotation forces, tabulated energy dissipated per amplitude values, bolt tension over time graphs, and pictures of the wearing surface before and after the test. Biaxial testing results will focus on the hysteretic behavior of the connection. Pullout tests will be discussed in terms of damage to the connection and approximate out-of-plane stiffness. The 100-cycle connection test results will be discussed in terms of confirming surface roughening behavior on the connection, normalized energy dissipation, normalized free rotation force, and stiffness over the course of testing, as well as damage from a larger number of load cycles.

4.2 Monotonic Pushover Testing

Monotonic pushover testing was used to identify the damage limit states as defined in FEMA 461. The two damage limit states in this experiment were the initial slip of the connection and the bearing of the channel onto the angle sections. The pushover curve in Figure 4-1 shows the

behavior of the connection when pushed 4.5 inches in one direction. The connection exhibits a growing force until the slip force is reached, then free rotation can occur until the channel begins bearing on the angle, after which the force dramatically increases. The results of the pushover tests for both panels are summarized in Table 4-1. It should be noted that the high stiffness and free rotation values for Panel A were under the conditions of full pretension for both the spandrel and angle bolt. Panel B was tested under the "jamb nut" conditions as described in Chapter 3, where the spandrel bolt was not pretensioned which provided minimal rotational resistance.

Table 4-1: Results of Monotonic Pushover Tests

	Initial Stiffness (k/in)	Free Rotation Force (lb)
Panel A	38.2	985
Panel B	7.54	527

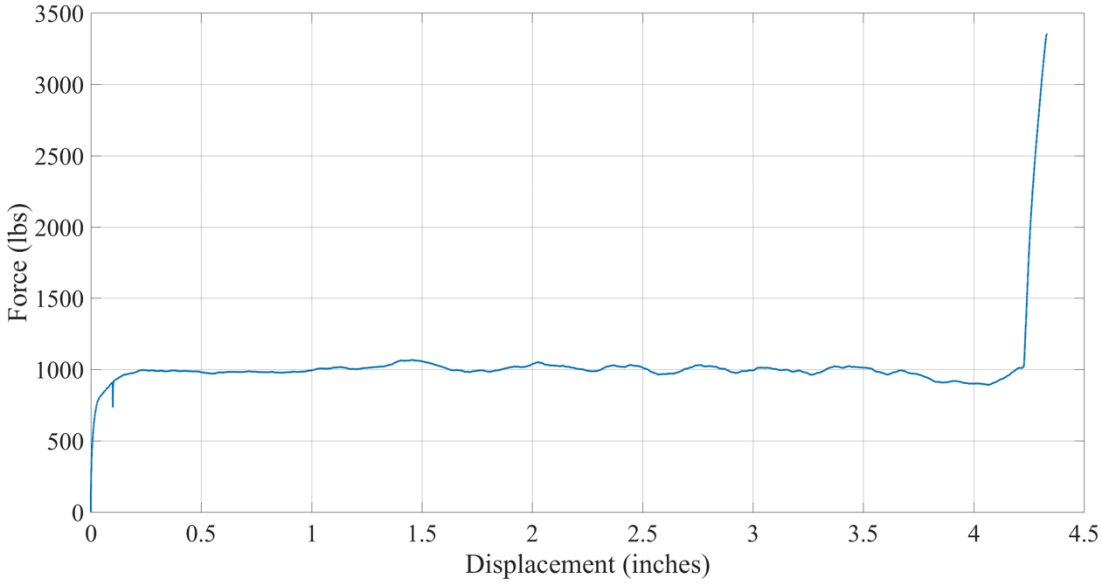

Figure 4-1: Pushover Curve for Connection A on Panel A

4.3 Uniaxial Testing

The primary results in this section of testing were the hysteretic behavior of the connection over repeated load reversals and relatively large displacements. Due to bolt tolerances and signal noise, initial stiffness values were inconclusive. Energy dissipated per amplitude for each panel is also presented and discussed. Friction connections often exhibit loss of pretension in bolts; therefore, bolt tension versus time is discussed as well. Finally, visual observations of the system are discussed to ascertain whether the connection can be classified as a low-damage connection.

The initial connection configuration consisted of a fully pretensioned bolt in both the angle and the spandrel beam. However, as seen in Figure 4-2, the variability of the force in the spandrel bolt posed an issue. The tension in the spandrel bolt began at approximately 22 kips but ended at approximately zero kips due to loosening of the bolts. The angle bolt lost approximately 10% of the original pretension. Due to the symmetric nature of the angle bolt connection, the slip surfaces were confined within the angles, keeping the slip away from the nut. However, with the asymmetric spandrel bolt connection, the slip occurred directly adjacent to the nut, causing it to loosen and result in significant loss of pretension in the spandrel bolt. The tension in the spandrel bolt began around 20 kips and reduced to approximately 2.5 kips, an 88% loss of pretension.

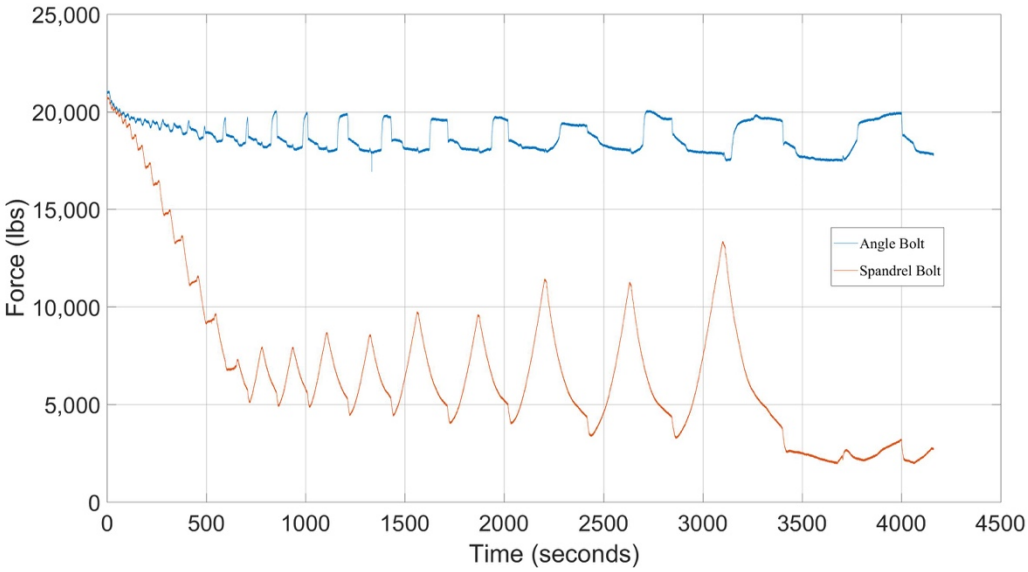

Figure 4-2: Bolt Tension versus Time for a Pretension-Pretension Connection

The next configuration to be tested included a fully pretensioned angle bolt and a snug-tight spandrel bolt. This configuration posed the same issue as the first configuration in that the spandrel bolt saw a complete loss of any initial pretension as seen in Figure 4-3. The tension in the spandrel bolt began around 10 kips and reduced to approximately zero kips, a 100% loss of pretension.

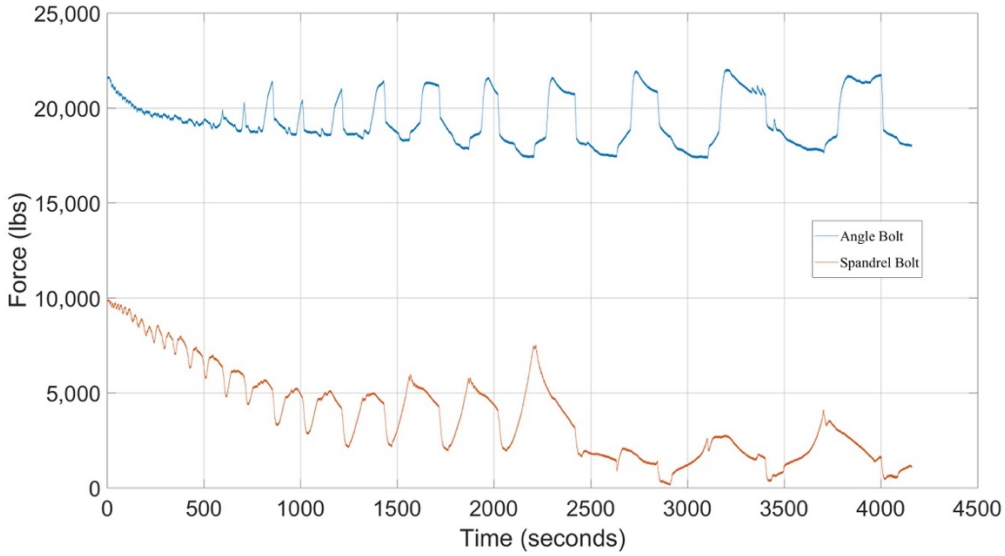

Figure 4-3: Bolt Tension versus Time for Pretension-Snug-Tight Connection

The method that proved most effective involved installing the spandrel bolt to the snug-tight condition, loosening the bolt a quarter turn, then placing a jamb nut behind the structural nut to prevent any further movement of the structural nut (AISC 2011). The results from this test, shown in Figure 4-4, provided for an average constant force in the spandrel bolt. The tension in the spandrel bolt began at approximately zero and remained at approximately this level for most the testing. This is the installation method recommended due to the predictable nature of the force in the spandrel bolt.

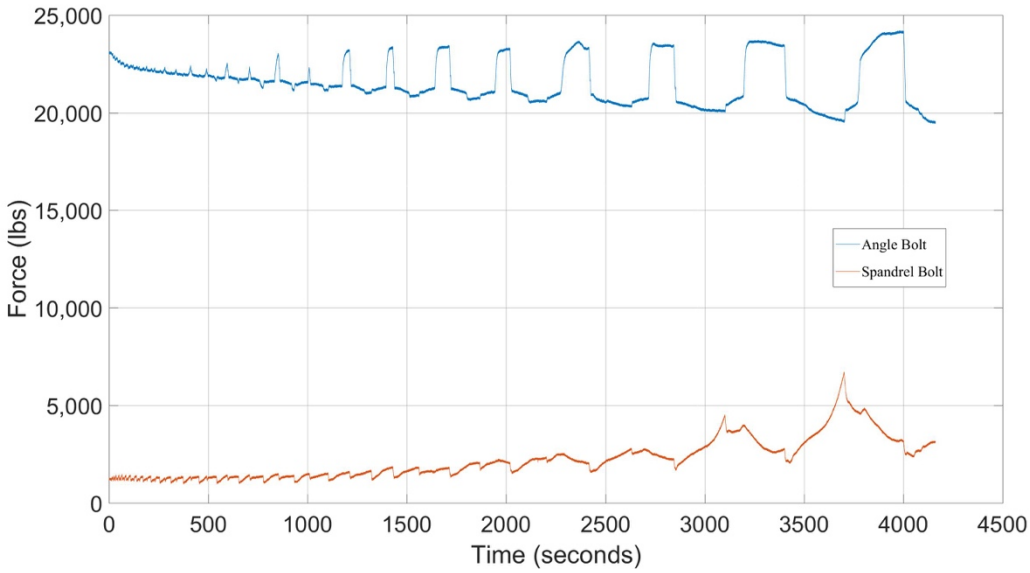

Figure 4-4: Bolt Tension versus Time for Pretension-Jamb Nut Connection

The connection using jamb nut installation was then used for all further testing. In all configurations, it was typical for a loss of approximately 10% bolt tension to occur in the angle bolt. Bolt tension for both bolts underwent a pattern of increasing and decreasing, although the net losses or gains should ideally be minimal to produce a constant force demand in the connection.

This is due to the changing direction of the displacement causing a “tightening” and then “loosening” effect on the bolts.

The hysteretic results of the uniaxial testing for Location A on Panel A and Panel B are shown in Figure 4-5.

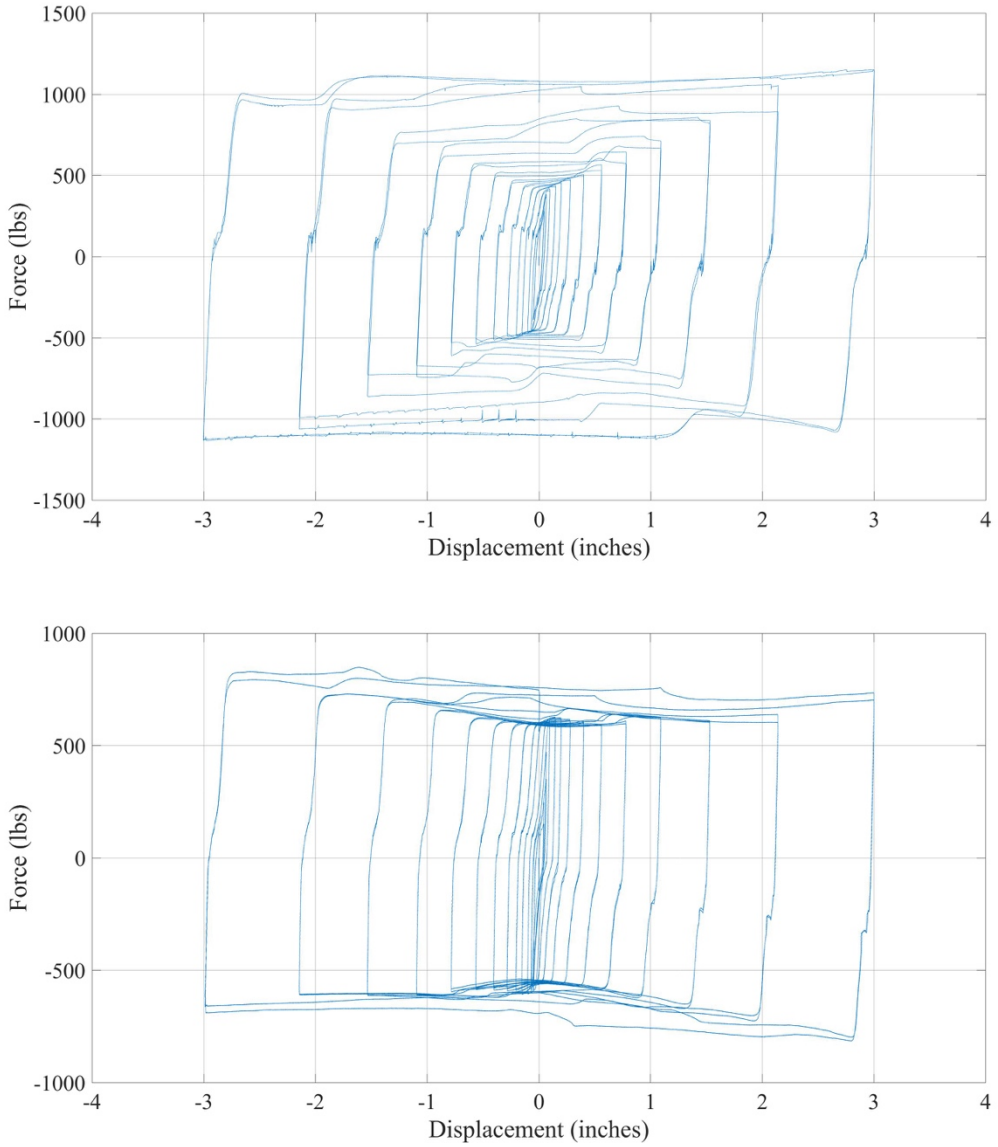

Figure 4-5: Hysteresis loops for Panel A testing (top) and Panel B testing (bottom)

The overall pattern of the hysteresis loops can be described as rectangular; however, the area of the rectangle increases over additional deformation cycles. The initial average slip force for the 5/8" diameter bolts and the 3/4" diameter bolts was 600 lb and 750 lb, respectively. The connection exhibited a growing hysteretic behavior rather than a degrading effect, as evidenced by the increasing slip force and free rotation force. It is believed that this growth can be attributed partially to the roughening of the slip surface, causing an increase in the amount of energy dissipated over time, as opposed to a degradation behavior. During testing, the connection would gradually increase in force until the slip force is reached followed by periods of free displacement with minor additional force. This was the designed intention of the connection, to create a system that allowed for large displacements while keeping force values relatively constant.

The energy dissipated per amplitude for Panel A is shown in Table 4-2 and Figure 4-6. It can be seen during the larger amplitudes that more energy is dissipated. This is due to the larger displacements over which these amplitudes take place. The results of the first test run is shown in Table 4-3 and Figure 4-7. The second test runs on Panel B are shown in Table 4-4 and Figure 4-8. The second test run generally shows a pattern of more energy dissipated at the same amplitudes, possibly due to a rougher slip surface. The smaller amplitudes tend not to comply with this pattern; however, the amplitudes in these cycles were potentially too small to make any meaningful assumptions about a trend in data.

Table 4-2: Energy Dissipated in (kip-in) per Amplitude for Panel A

Amplitude Number	Location A	Location B	Location C	Location D	Location E
1	0.05	0.06	0.05	0.07	0.08
2	0.09	0.12	0.09	0.11	0.15
3	0.19	0.22	0.19	0.18	0.24
4	0.37	0.37	0.51	0.30	0.41
5	0.56	0.50	0.90	0.42	0.59
6	0.87	0.73	1.57	0.62	0.90
7	1.35	1.07	2.53	0.92	1.33
8	2.04	1.54	3.83	1.37	2.04
9	3.23	2.28	5.69	2.02	3.16
10	5.33	3.53	8.32	3.12	4.91
11	8.90	5.90	12.11	5.02	7.72
12	15.59	9.98	17.74	8.28	12.73
13	24.70	19.24	25.66	13.42	20.94

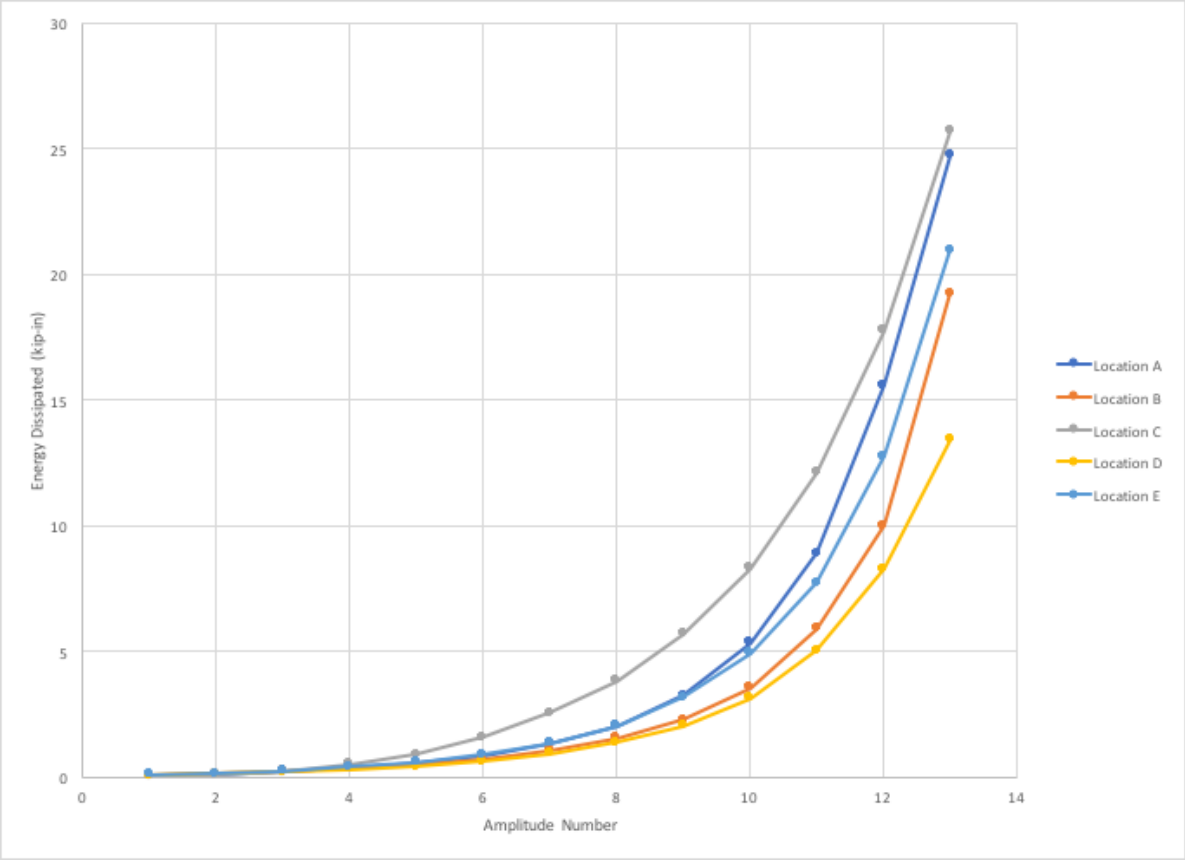

Figure 4-6: Energy Dissipated per Amplitude for Panel A

Table 4-3: Energy Dissipated in (kip-in) per Amplitude for Panel B on First Test Run

1st Test Run					
Amplitude Number	Location A	Location B	Location C	Location D	Location E
1	0.06	0.07	0.08	0.11	0.09
2	0.08	0.14	0.15	0.19	0.18
3	0.19	0.26	0.28	0.32	0.31
4	0.43	0.47	0.50	0.54	0.53
5	0.68	0.69	0.71	0.74	0.75
6	1.04	1.04	1.06	1.05	1.13
7	1.60	1.57	1.59	1.52	1.72
8	2.34	2.27	2.32	2.17	2.53
9	3.36	3.23	3.35	2.82	3.69
10	4.98	4.58	4.77	3.94	5.45
11	7.44	6.41	6.22	5.65	7.49
12	10.89	8.88	8.68	8.28	11.01
13	16.91	13.40	13.29	13.56	17.61

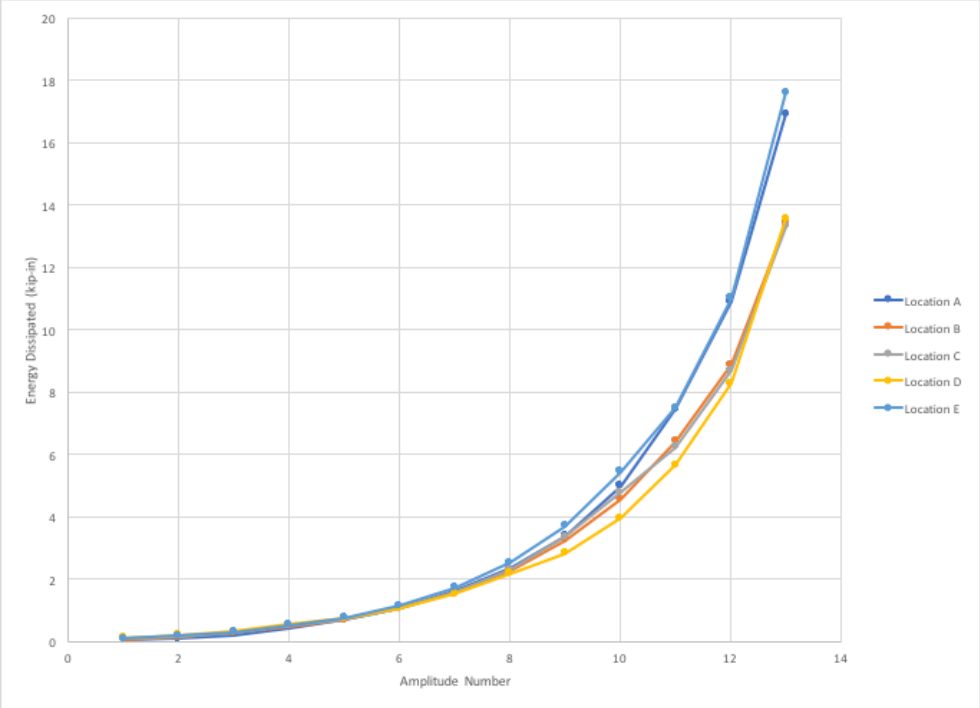

Figure 4-7: Energy Dissipated per Amplitude for Panel B on First Test Run

Table 4-4: Energy Dissipated in (kip-in) per Amplitude for Panel B on Second Test Run

2nd Test Run					
Amplitude Number	Location A	Location B	Location C	Location D	Location E
1	0.07	0.06	0.03	0.07	0.03
2	0.13	0.10	0.05	0.11	0.06
3	0.26	0.21	0.04	0.22	0.11
4	0.54	0.42	0.28	0.43	0.34
5	0.84	0.63	0.51	0.66	0.62
6	1.32	0.97	0.85	1.04	1.09
7	2.02	1.50	1.35	1.57	1.82
8	2.87	2.18	2.04	2.31	2.82
9	4.51	3.18	3.03	3.49	4.05
10	6.68	4.70	4.57	5.54	6.62
11	10.00	7.20	7.20	8.78	10.50
12	16.12	10.50	10.76	13.49	15.62
13	25.44	17.15	17.72	21.51	26.58

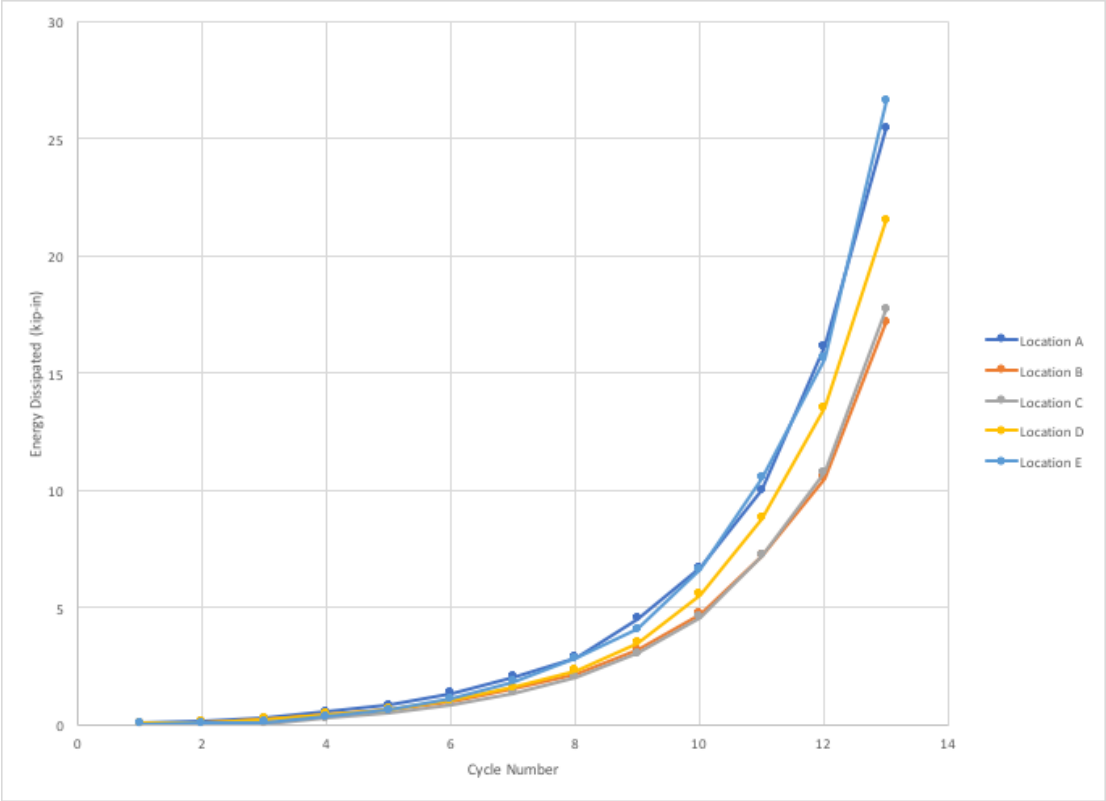

Figure 4-8: Energy Dissipated per Amplitude for Panel B on Second Test Run

The total energy dissipated for Panel A is shown in Table 4-5. The average energy dissipated for connections on Panel A was 56 kip-in. The total energy dissipated for Panel B in the first and second test runs is shown in Table 4-6. The average energy dissipated for the first and second test runs were 46 kip-in and 60 kip-in, respectively. It is important to note that the total energy dissipated increased during the second test run by approximately 30%.

Table 4-5: Total Energy Dissipated for Connections on Panel A

Test	Hysteretic Energy (kip-in)
Location A	63.3
Location B	45.5
Location C	79.2
Location D	35.9
Location E	55.2

Table 4-6: Total Energy Dissipated for Connections on Panel B

Test	Hysteretic Energy (kip-in)	
	Run 1	Run 2
Location A	50.0	70.8
Location B	43.0	48.8
Location C	43.0	48.5
Location D	40.9	59.2
Location E	52.5	70.3

The free rotation forces for both panels are summarized in Table 4-7 and Table 4-8. The average initial free rotation force for Panel A was 400 lb, excluding connection location C. However, connection location C had undergone several dummy tests prior to the measured testing. The connection was also installed with full pretension on the angle bolt and spandrel bolt and the washers were not replaced from the previous dummy tests. Due to these reasons, the initial free rotation force is likely inflated due to surface roughening and the presence of fully pretensioned angle and spandrel bolts.

Table 4-7: Free Rotation Forces for Panel A

Test	Initial Free Rotation Force (lb)
Location A	428
Location B	414
Location C	1154
Location D	390
Location E	368

Table 4-8: Free Rotation Forces for Panel B

Test	Initial Free Rotation Force (lb)	
	Run 1	Run 2
Location A	626	671
Location B	554	555
Location C	561	580
Location D	584	665
Location E	554	775

The average initial free rotation force for Panel B connections on the first run was 575 lb. The average initial free rotation force for Panel B connections on the second run was 650 lb. For the second runs of the testing protocol, no replacement of washers was performed. The increased initial free rotation force can be attributed to slight surface roughening effects.

To better define the damage in the connection, photographs were taken before and after testing. Figure 4-9 shows the damage state of the connecting elements before and after testing. After the test was completed, the observable damage was minor surface polishing of the washers, and minor surface damage to the bolt hole surface around the area where the pretensioned bolt was. The bolt holes remained undamaged. The bolts showed minor damage on the shank of the bolt.

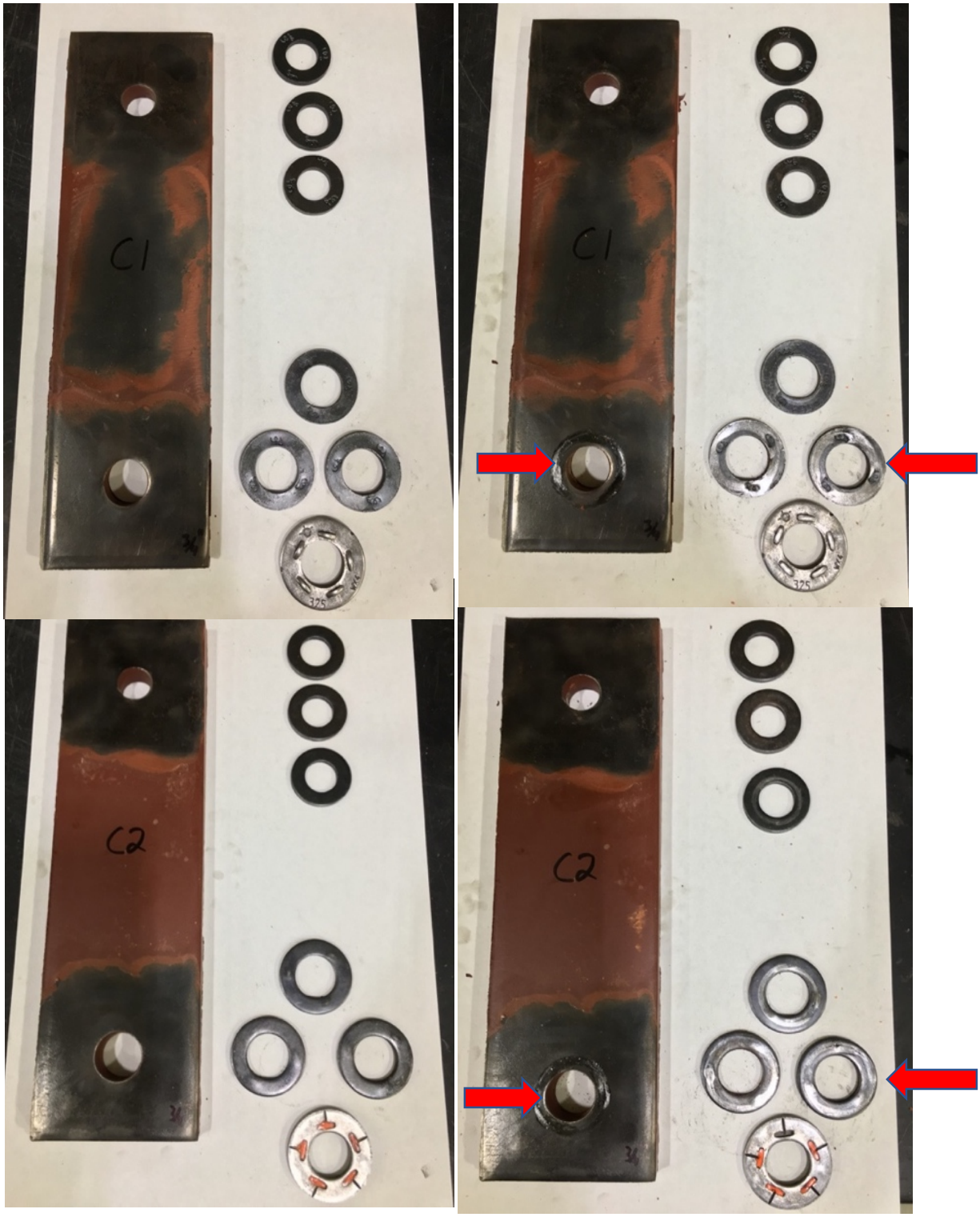

Figure 4-9: Connection Elements Before (Left) and After (Right) Uniaxial Testing

4.4 Biaxial Testing

The biaxial testing was applied to connection A of the experimental setup on panels A and B. The result for a biaxial test on Panel A is shown in Figure 4-10.

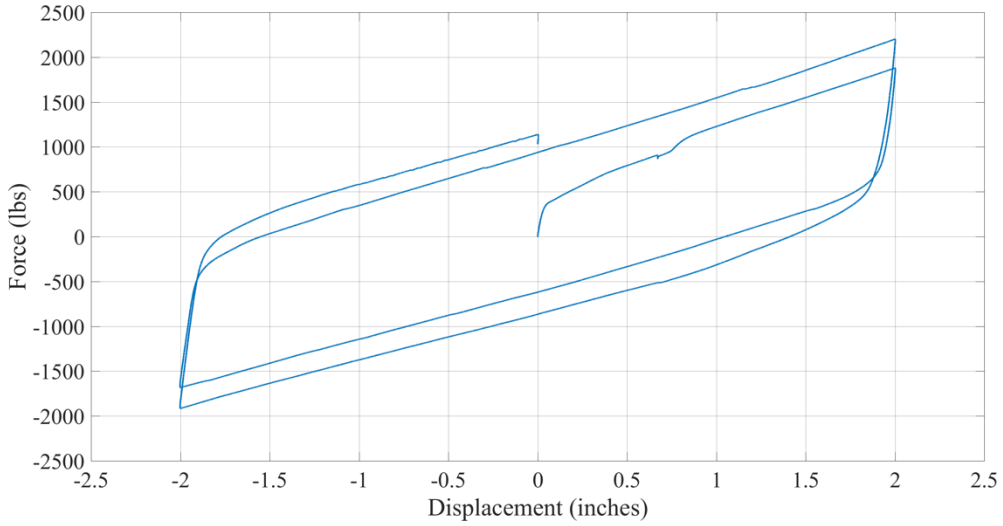

Figure 4-10: Biaxial Testing of Connection on Panel A

The biaxial testing results confirm the geometric effects of the connection. As the connection moves farther from the neutral position P-Δ effects magnify and increase the force in the connection. The post-slip stiffness can be attributed to a positive geometric stiffness in the connection. This results in a large, growing hysteresis. Under a compression force, the same connection would result in a degrading secondary stiffness. Table 4-9 summarizes the results of biaxial testing.

Table 4-9: Results of Biaxial Testing

	Initial Stiffness	Secondary Stiffness	Free Rotation Force	Energy Dissipated	Maximum Force	Minimum Force
	k/in	k/in	lb	k-in	lb	lb
Panel A	8.27	0.76	380	12.4	2228	-1892
Panel B	16.47	0.79	543	15.1	2430	-2040

In general, initial stiffness, secondary stiffness, free rotation force, and energy dissipated values were larger for Panel B. This is an expected outcome due to the larger bolt size used on Panel B.

4.5 Pullout Testing

The pullout testing was applied to connection A of the experimental setup on panels A and B. The force-displacement plot is shown in Figure 4-11.

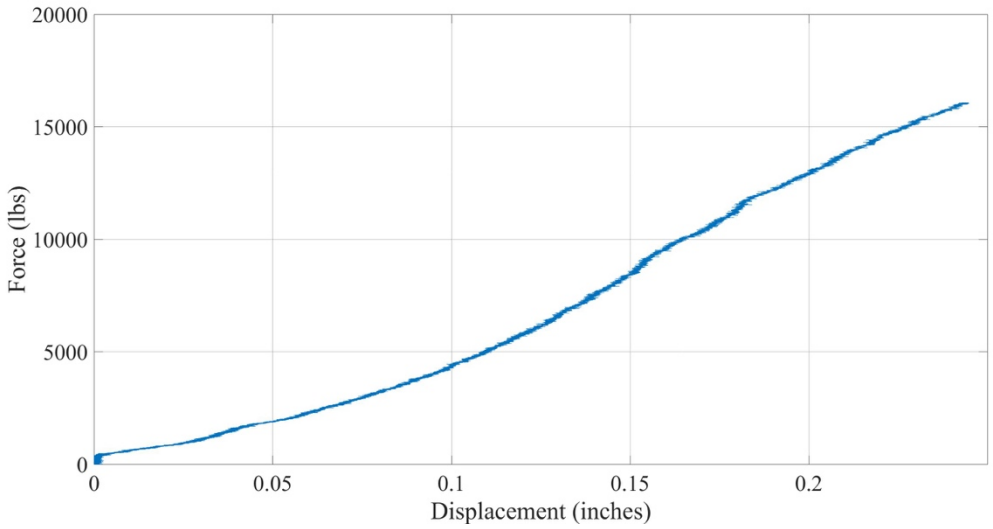

Figure 4-11: Vertical Pullout Test Results for Connection on Panel A

Pullout testing was terminated after reaching 16 kips to not exceed the safe working load of the wire ropes. The primary goal of the pullout testing was to provide more data for the numerical

models to be calibrated using this data. Recorded data was used to calculate out-of-plane stiffness values which will be compared to numerical models in future work. The calculated out-of-plane stiffness is approximately 63 k/in and 67 k/in for Panel A and Panel B, respectively.

The out-of-plane stiffness is generally linear throughout the test, with an R^2 value of 0.97 for Panel A and B. After the test, there was no observable damage to the connection in the steel or concrete. The behavior and stiffness for both sizes of bolts were similar, implying that the out-of-plane behavior is not dependent on the bolt size.

4.6 100-Cycle Testing

The 100-cycle testing was performed to confirm that surface roughening was a contributing factor in the growing hysteresis loops and to determine how long it would persist in a longer duration loading event. This was initially suspected when an increase in the slip and free rotation force was observed during the uniaxial testing. On Panel B, an additional second run was performed to provide more data on this pattern. The 100-cycle testing was performed to exaggerate and definitively confirm the pattern of increasing slip and free rotation force during the uniaxial testing. Initially, the free rotation force was approximately 600 lb, however, by the end of the test it was approximately twice that. The results of the 100-cycle testing using the high displacement protocol are shown in Figure 4-12. Results from the low and medium displacement protocols were similar in behavior, however the high displacement protocol shows the most noticeable behavior change throughout testing.

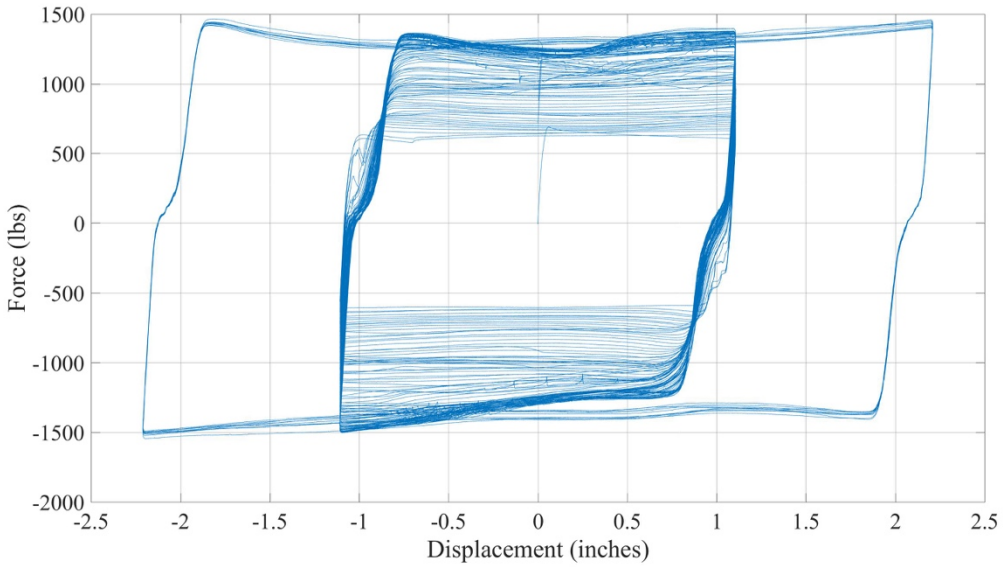

Figure 4-12: Hysteresis for 100-Cycle High Displacement Testing Protocol

The stiffness of the connection at different points during the testing is shown in Table 4-10. In general, the connection starts out very stiff and shows a degrading stiffness pattern throughout the course of testing. This is likely due to the pattern of decreasing bolt tension, shown in Figure 4-13. The angle bolt loses approximately half of the pretension during testing and the stiffness degrades to less than half of its original value.

Table 4-10: Stiffness Values at Different Cycle Numbers

	Low	Medium	High
Initial Stiffness (kip/in)	23.2	23.6	21.0
Cycle 2	16.3	6.8	9.0
Cycle 25	16.5	6.0	6.1
Cycle 50	15.0	7.7	7.3
Cycle 75	13.1	6.0	7.8
Cycle 100	11.3	7.5	6.9
Cycle 101	6.5	10.3	6.2
Cycle 110	8.1	10.2	8.5

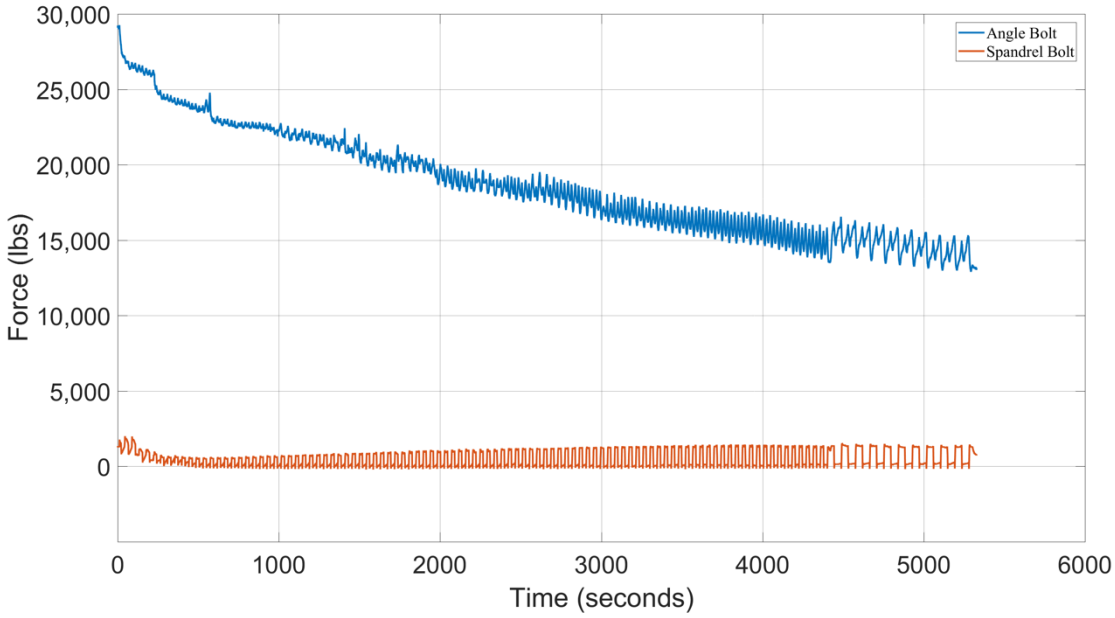

Figure 4-13: Bolt Tension versus Time for High Displacement Testing Protocol

The free rotation force at different points during the testing is shown in Table 4-11. The free rotation force increases throughout the tests for low, medium, and high cycle displacement protocols. The low-displacement protocol had a calculated 34% increase in free rotation force. The medium-displacement protocol had a calculated 104% increase in free rotation force and the high-displacement protocol had a calculated 106% increase in free rotation force. The total energy dissipated in each test is shown in Table 4-12.

Table 4-11: Free Rotation Force at Different Cycle Numbers

	Low	Medium	High
Initial Free Rotation Force (lb)	798	728	635
Cycle 2	715	753	629
Cycle 25	752	977	976
Cycle 50	816	1168	1151
Cycle 75	910	1311	1269
Cycle 100	952	1360	1233
Cycle 101	962	1364	1235
Cycle 110	1077	1484	1308

Table 4-12: Total Energy Dissipated for 100-Cycle Testing Protocols

Test	Hysteretic Energy (kip-in)
Low Displacement	97.5
Medium Displacement	268.7
High Displacement	551.0

A normalized graph of energy dissipated per cycle for the high-displacement protocol is shown in Figure 4-14. The data for Figure 4-14 was normalized by the energy dissipated during the first cycle. Additionally, a graph of the normalized free rotation force for the high-displacement protocol over the course of testing is shown in Figure 4-15. The data for Figure 4-15 was normalized by the free rotation force of the first cycle.

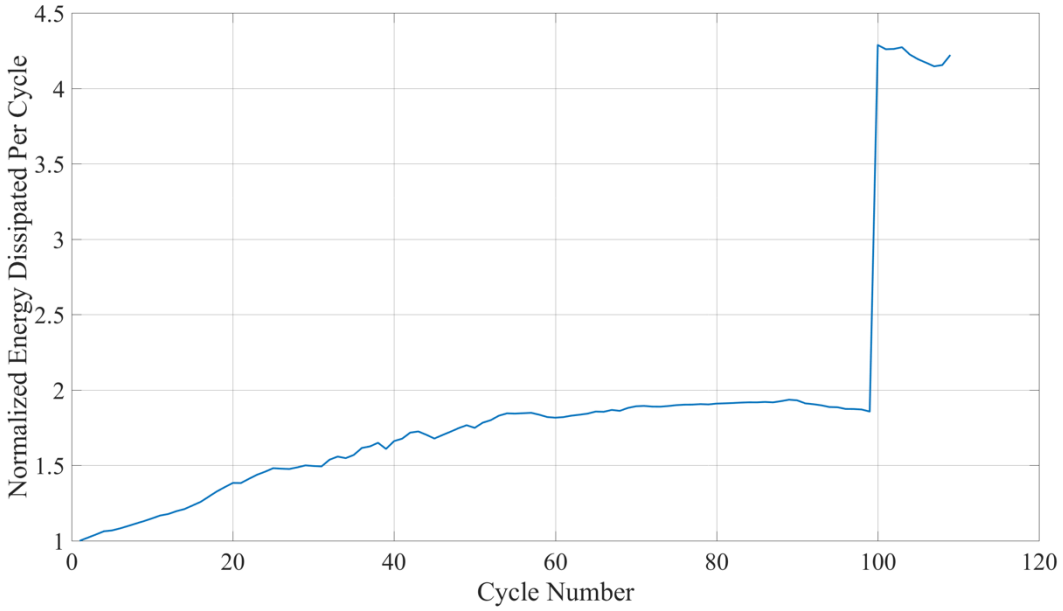

Figure 4-14: Normalized Energy Dissipated per Cycle for High-Displacement Protocol

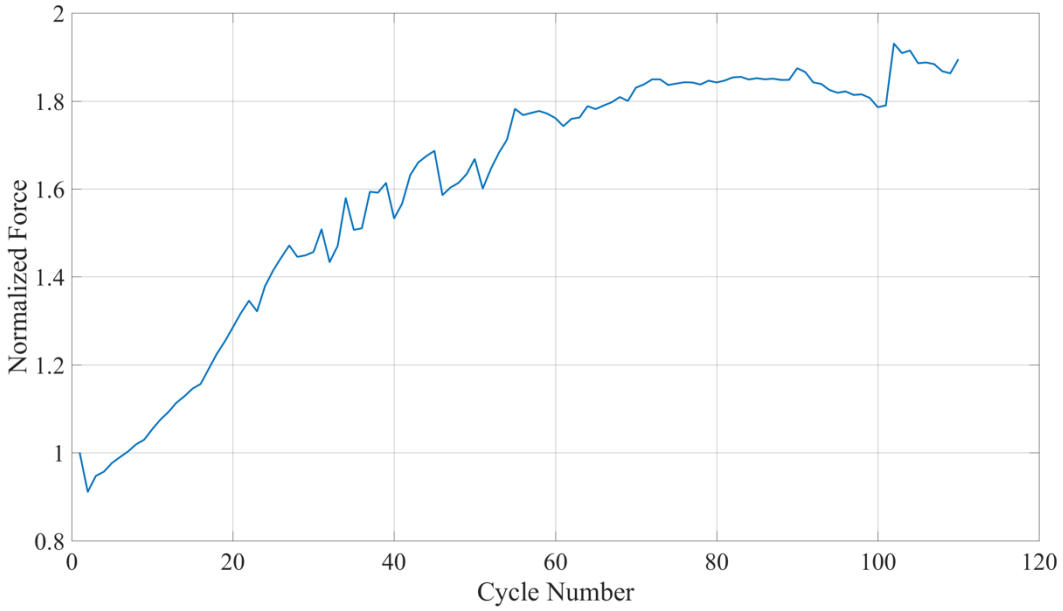

Figure 4-15: Normalized Free Rotation Force for High-Displacement Protocol

The secondary purpose of the 100-Cycle testing was to observe any kind of damage that may be present after a larger number of cycles than the uniaxial testing. Connection location C on Panel

B was selected to undergo all the 100-cycle testing. This was done for consistency as well as to observe the damage of the connection after over 300 cycles of wear. The wearing of the connection is shown in Figure 4-16 and Figure 4-17. After three 100-cycle tests, as well as uniaxial testing, the interior wearing surface of the angle appears to have only minor damage.

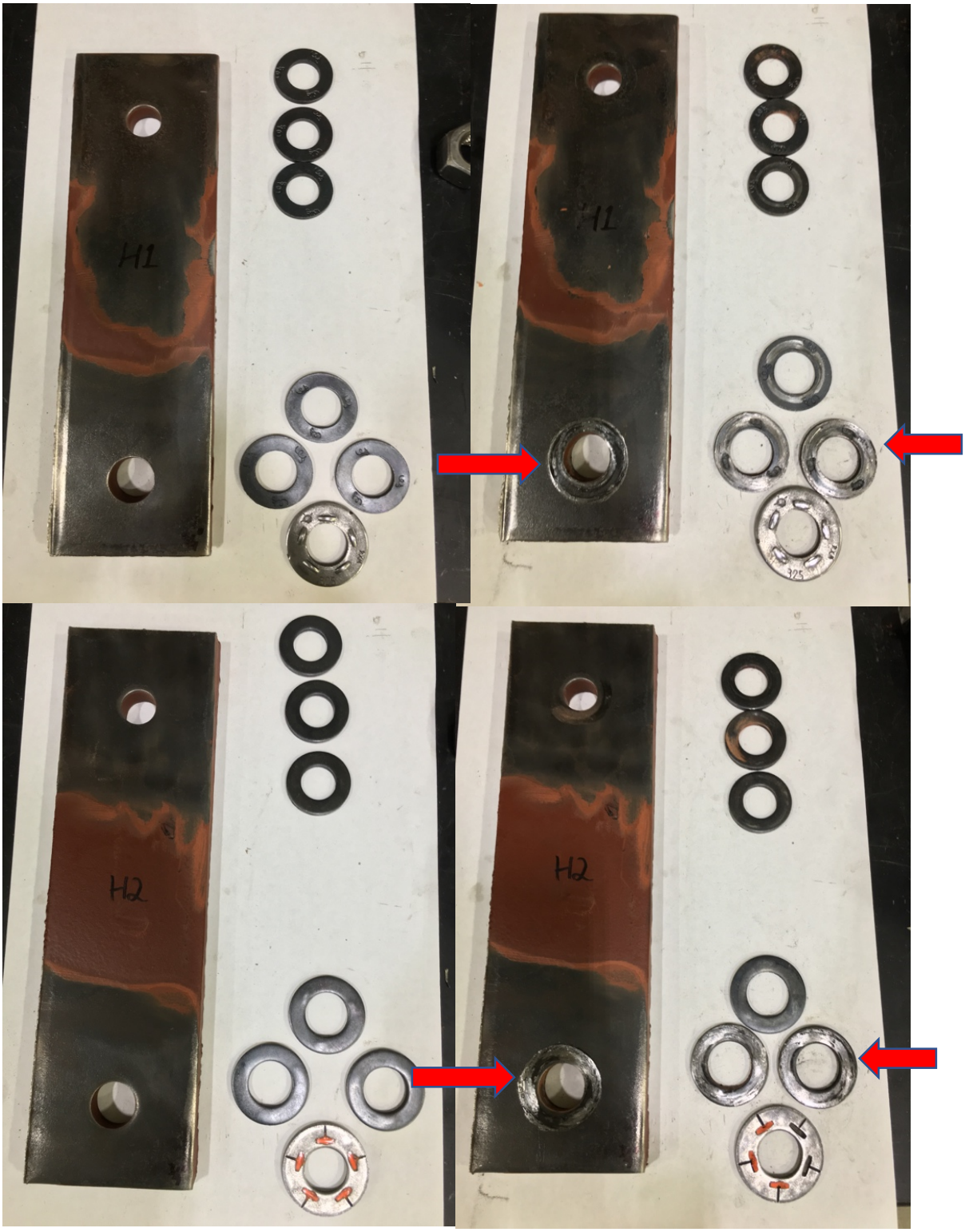

Figure 4-16: Wearing of Connection Before (Left) and After (Right) 100-Cycle Testing

Figure 4-17: Damage on Interior Face of Angle after Three 100-Cycle Tests

4.7 Conclusions

The results of the experiments show that the rotational friction connection is a viable option due to its ability to undergo large displacements while maintaining low damage to the structural system. The monotonic pushover tests provided valuable information such as initial stiffness and free rotation force of the connection. The uniaxial tests revealed the initial flaws in the connection configuration and established the preferred connection configuration. The uniaxial tests also

showed a growing hysteretic behavior of the connection. Through the course of uniaxial testing, no significant damage was observed by the connection. The connection also showed large, growing hysteresis loops in biaxial testing. Pullout testing provided values for out-of-plane stiffness, which will be valuable in future computer models; however, the failure mode was not determined because the wire ropes reached their design capacity before the system failed. The 100-cycle testing proved the effects of surface roughening that were suspected during the uniaxial testing. The 100-cycle testing also proved that the connection displays a growing hysteresis loop over time. Additionally, it showed that the connection could undergo many cycles while remaining minimally damaged and continuing to provide out-of-plane wall support.

Chapter 5. Summary, Conclusions, and Future Work

5.1 Summary

Metal building systems are a popular building option for non-residential low-rise buildings due to their optimized design, causing a large demand for these systems. These systems are also commonly equipped with concrete or masonry hard walls. Due to the optimized design these systems typically have little to no inherent redundancy, making the connections between the frames and the heavy wall critical elements (Thurston 1990).

Previous research in the field of energy dissipation methods has focused on energy dissipation methods such as sliding friction and ductile fuse elements. Although these methods do provide a viable method of energy dissipation, sliding friction methods have shown "ratcheting" effects (Pantoli and Hutchinson 2015) and fuse elements require replacement.

The research presented in this thesis provides results of pushover, uniaxial, biaxial, pullout, and 100-cycle testing on a rotational friction connection between a hard wall and a metal building system. Pushover testing results showed the ability for the connection to slip and remain at a constant force until the final damage limit state of channel bearing to occur at a displacement of 4.5". The uniaxial testing provided results that displayed a rectangular hysteresis that exhibited a growth pattern due to surface roughening of the wearing surface. The biaxial testing results confirmed geometric effects of the connection. The pullout testing results showed the ability of

the connection to withstand out-of-plane loads up to 16 kips with minimal damage. The 100-cycle testing confirmed the effects of surface roughening as well as allowed for the observance of minimal damage to the wearing surface after over 300 cycles of wear. The connection achieved this performance using only standard structural elements and does not require the use of any specialized, customized, or proprietary components.

5.2 Conclusions

The major findings from this research regarding the performance of the rotational friction connection are as follows:

- Testing results proved that the connection can undergo large displacements while maintaining strength without excessive post-slip strength gain.
- The wearing surfaces of the connection exhibited minimal damage and the structural system had no observable damage.
- The connection exhibited surface roughening on the wearing surfaces which caused growing free rotation force through extended testing and resulted in growing hysteresis loops.
- The effects of out-of-plane loading during biaxial testing resulted in large, non-degrading hysteresis loops and no observable damage.
- The rotational friction connection is a viable prototype to resolve compatibility issues between concrete hard walls and metal building systems

5.3 Future Work

The results of the testing performed have shown great promise for the future use of rotational friction connections in hard wall metal building systems. The connection could also be valuable

in other types of construction where the cladding and structural system would benefit from the ability to deform independently. To prove its use as an option the following tasks should be performed:

- Shake table testing of a 3-D system with the rotational friction connection to verify the usefulness of the connection when the connection undergoes earthquake ground motions. Shake table testing will allow a more realistic representation of the out-of-plane pulses that these systems undergo.
- Test the connection with masonry walls to test future applicability with masonry hard walls.
- Full-scale testing of the connection in metal building systems to confirm the usefulness of the connection in its intended environment.
- Complete a full pullout test to determine the full out-of-plane capacity and the sequence of failure for the connection.
- Development of a design methodology to ensure the correct performance for both in-plane and out-of-plane loading.

References

AISC. 2011. *ANSI/AISC 360-10.* Chicago: AISC.

—. 2011. *Steel Construction Manual.* American Institute of Steel Construction.

Applied Technology Council. 2007. *InterimTesting Protocols for Determining the Seismic Performance Characteristics of Structural and Nonstructural Components.* Redwood, City, CA: FEMA.

Baird, A., A. Palermo, and S. Pampanin. 2013. "Controlling Seismic Response Using Passive Energy Dissipating Cladding Connections." *2013 NZSEE Conference.* Christchurch, NZ.

Craig, James I., Ralf Leistikow, and J. Clarence Fennell. 1988. "Experimental Studies of the Performance of Precast Cladding Connections." *Proceedings of Ninth World Conference on Earthquake Engineering.* Tokyo-Kyoto. 201-206.

Grigorian, C.E., T.S. Yang, and E.P. Popov. 1993. "Slotted Bolted Connection Energy Dissipators." *Earthquake Spectra* 9 (3).

Hilti. 2017. "PROFIS Anchor." *PROFIS Anchor Software.* Hilti.

Hong, J.K., and C.M. Uang. 2011. "Cyclic testing of a metal building moment frame system with web-tapered members." *Journal of Constructional Steel Research* 70: 248-255.

Kelly, J. M., R. I. Skinner, and A. J. Heine. 1972. "Mechanisms of Energy Absorption in Special Devices For Use In Earthquake Resistant Structures." *Bulletin of NZ Society for Earthquake Engineering* 5 (3): 67-89.

Marshall, J.D., and N.C. Gould. 2012. *The Performance of Low-Rise Industrial Facilities in the 2010 Haiti and 2011 Christchurch, New Zealand Earthquakes.* Lisbon: 15WCEE.

Mirzabagheri, S., M. Sanati, A.A. Aghakouchak, and S.E. Khadem. 2015. "Experimental and numerical investigation of rotational friction dampers with multi units in steel frames subject to lateral excitation." *Archives of Civil and Mechanical Engineering* 479-491.

Mualla, Imad H., and Borislav Belev. 2002. "Performance of steel frames with a new friction damper device under earthquake excitation." *Engineering Structures* 363-371.

National Concrete Masonry Association. 2011. "Integrating Concrete Masonry Walls With Metal Building Systems." TEK5-5B.

Pantoli, E., and T.C. Hutchinson. 2015. "Experimental and Analytical Study of the Dynamic Characteristics of Architectural Precast Concrete Cladding." *ASCE* 560-574.

Pinelli, Jean-Paul, Christian Moor, James I. Craig, and Barry Goodno. 1996. "Testing of Energy Dissipating Cladding Connections." *Earthquake Engineering and Structural Dynamics* 129-147.

Pinelli, Jean-Paul, James I. Craig, and Barry J. Goodno. 1995. "Energy-Based Seismic Design of Ductile Cladding Systems." *Journal of Structural Engineering* 567-578.

Schultz, A.E., R.A. Magana, M.K. Tadros, and X. Huo. 1994. "Experimental Study of Joint Connections in Precast Concrete Walls." EERI. 579-587.

SketchUp. 2017. "SketchUp." *SketchUp.*

Thurston, Howard. 1990. "Seismic Damage Evaluation of Tilt-Up Buildings." *Journal of Computing in Civil Engineering* 349-369.

Uang, C.M., M.D. Smith, and W.L. Shoemaker. 2011. "Earthquake Simulator Testing of Metal Building Systems." Las Vegas: ASCE Structures Congress. 693-704.

Appendix A. Additional Graphs from Experimentation

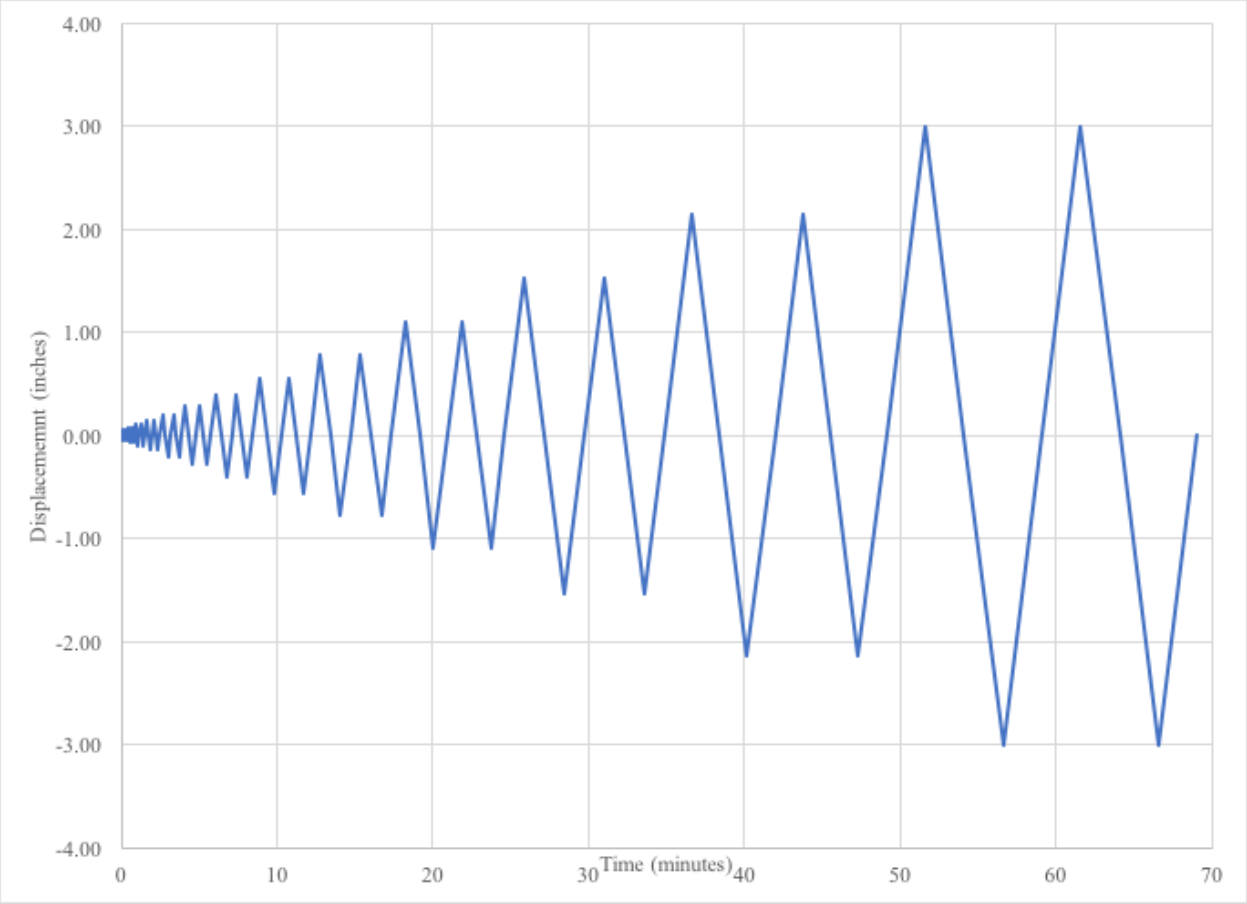

Figure A-1: Displacement Protocol Used for Uniaxial Testing

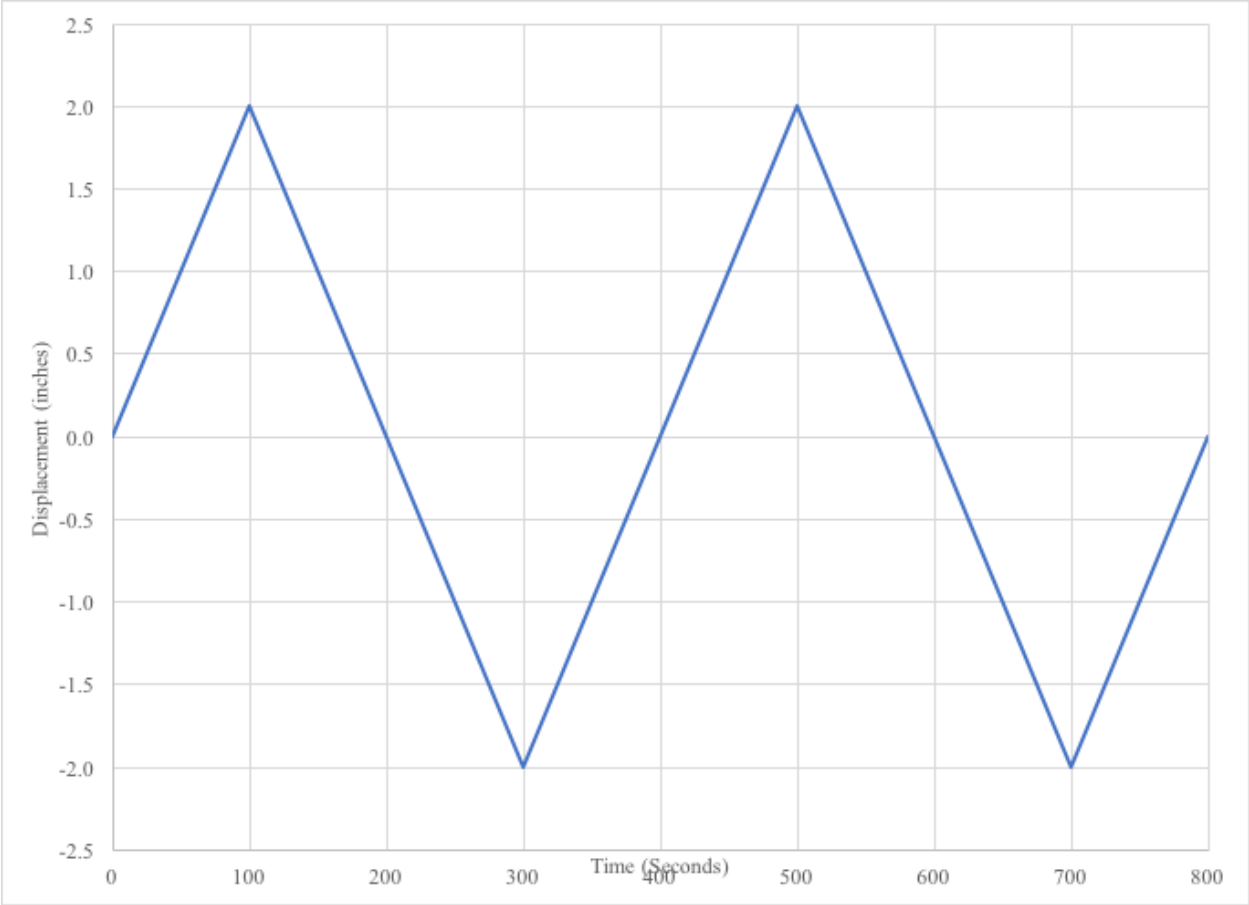

Figure A-2: Displacement Protocol Used for Biaxial Testing

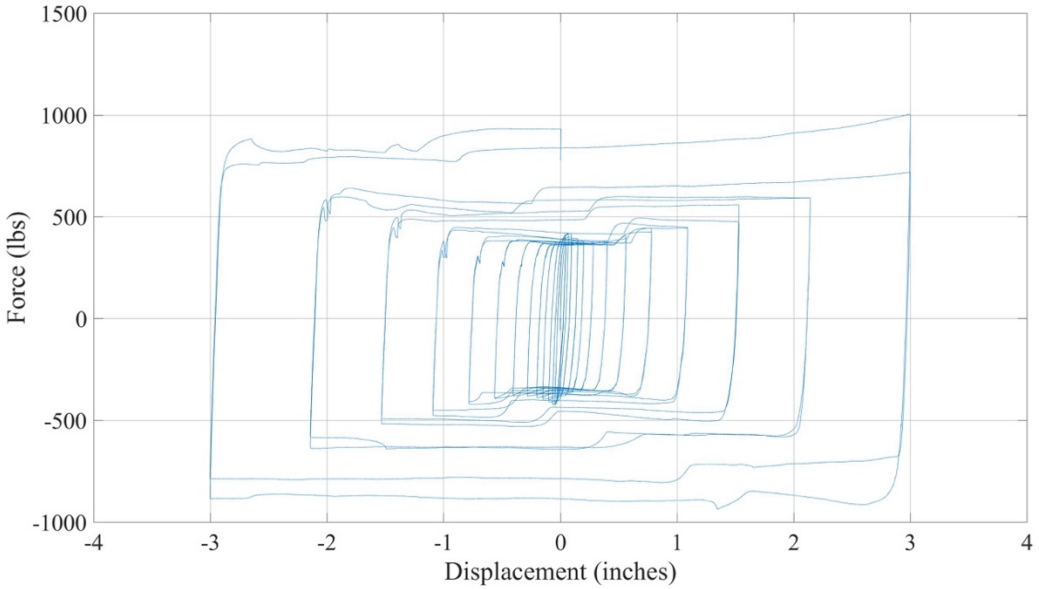

Figure A-3: Hysteresis Loops for Location B on Panel A

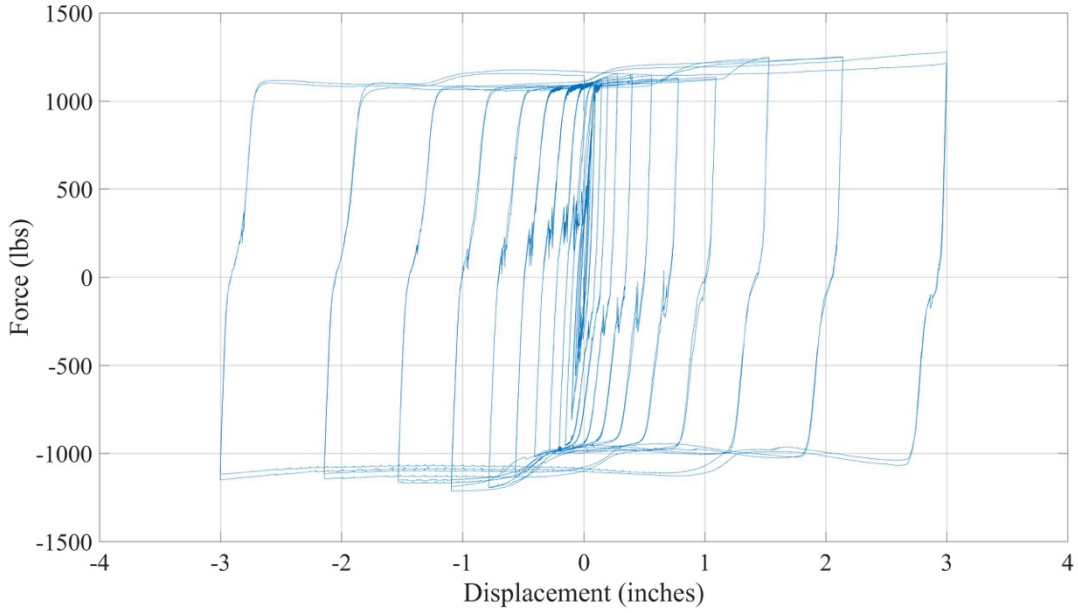

Figure A-4: Hysteresis Loops for Connection C on Panel A

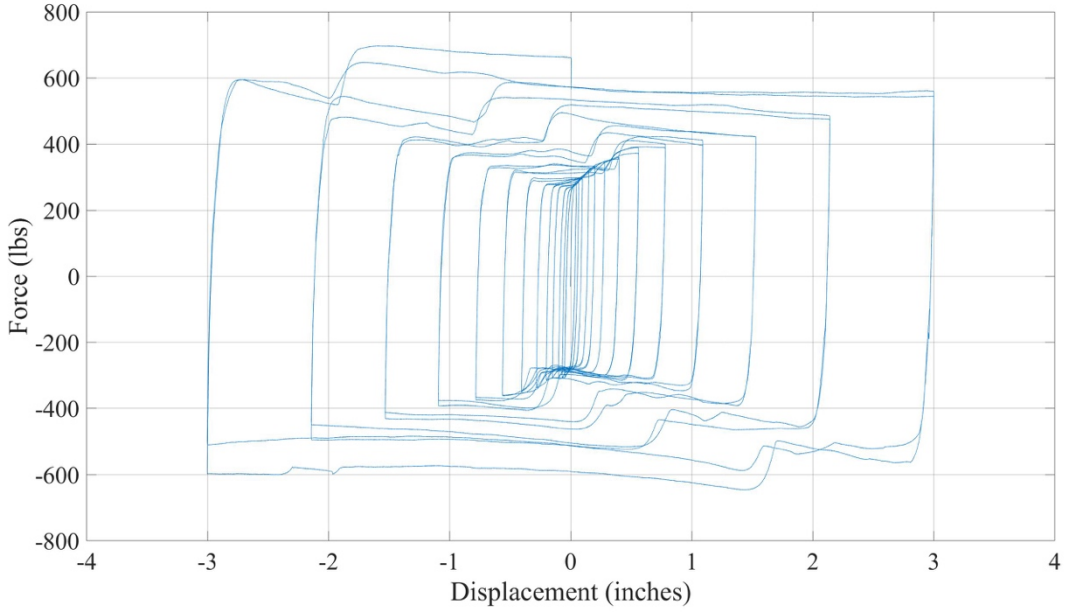

Figure A-5: Hysteresis Loops for Connection D on Panel A

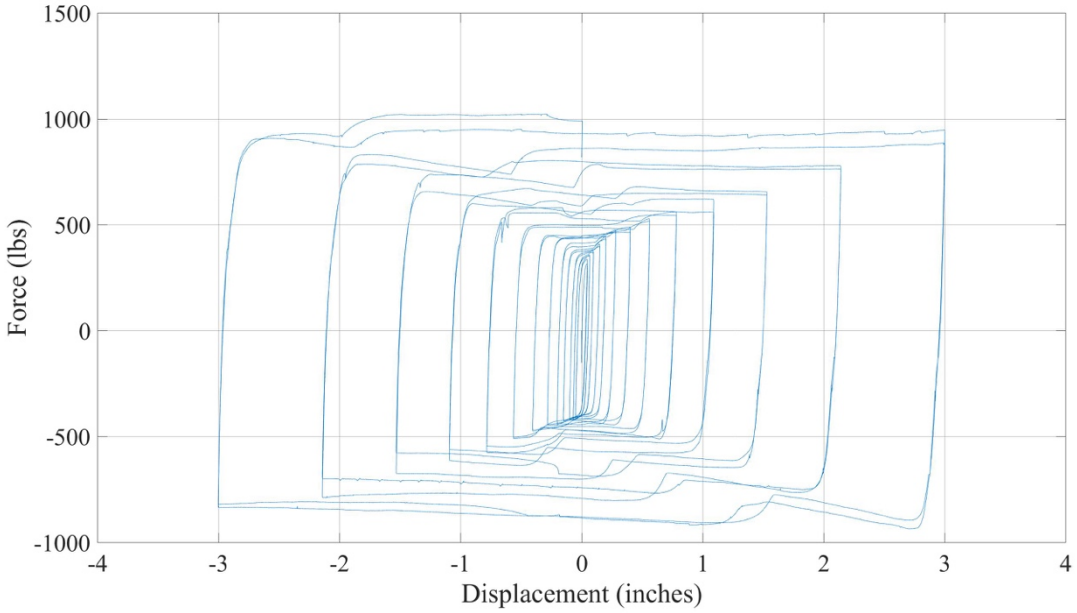

Figure A-6: Hysteresis Loops for Connection E on Panel A

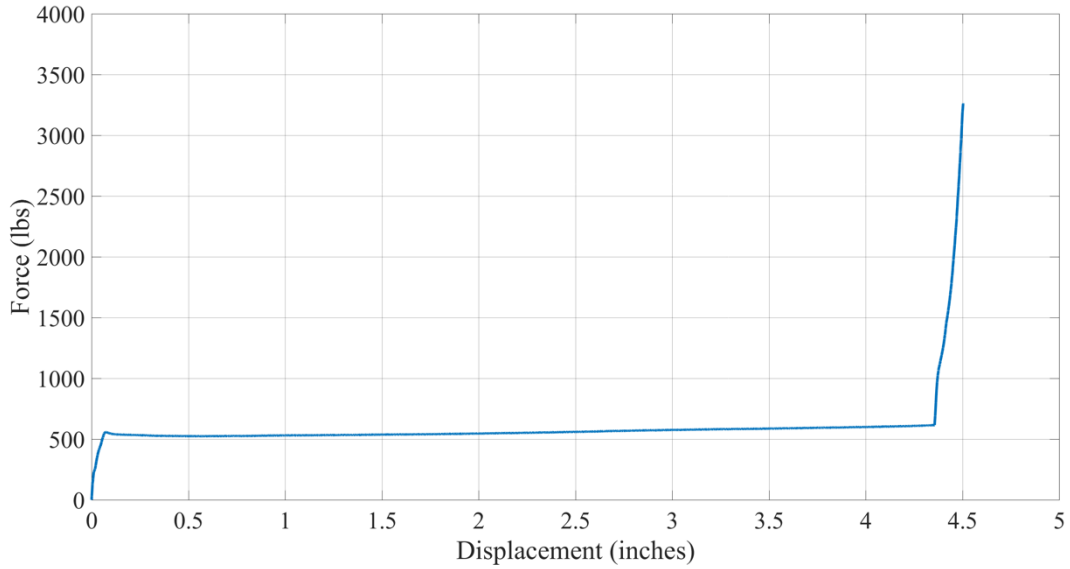

Figure A-7: Pushover Curve for Panel B

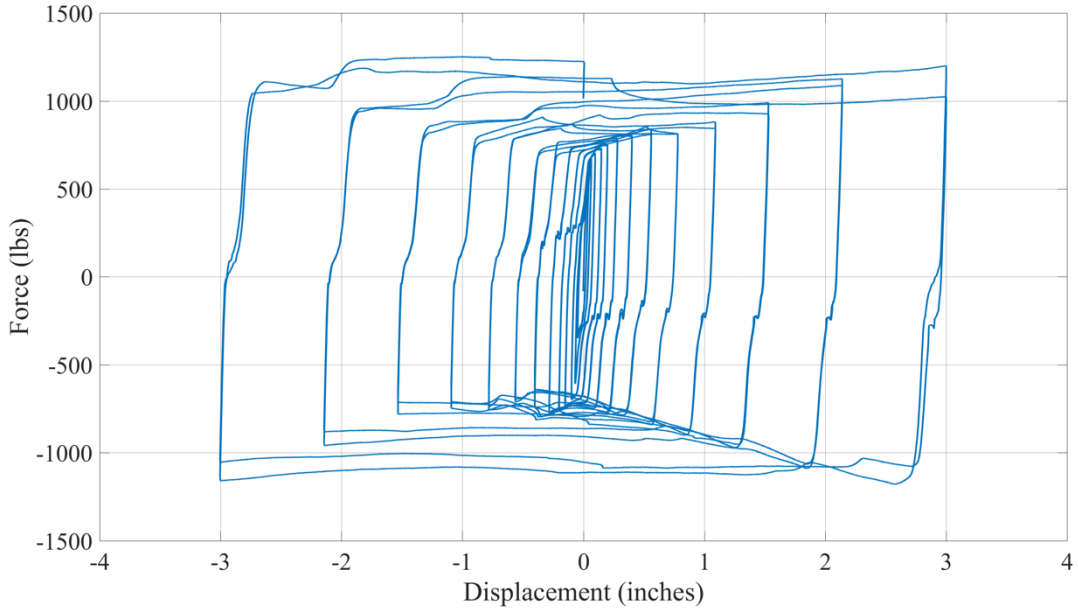

Figure A-8: Hysteresis Loops for Connection A on Panel B, Second Run

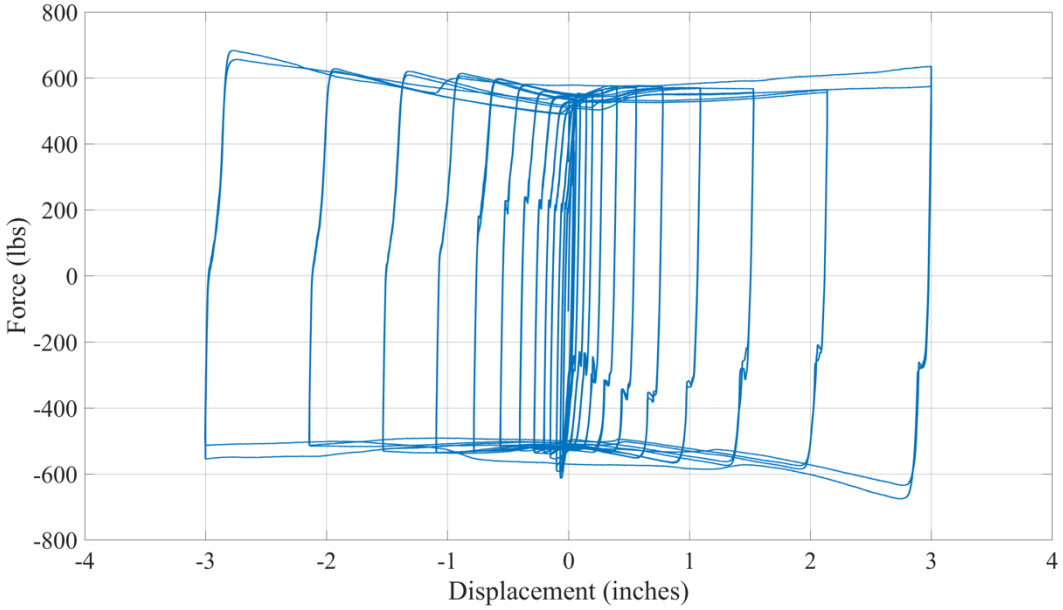

Figure A-9: Hysteresis Loops for Connection B on Panel B, First Run

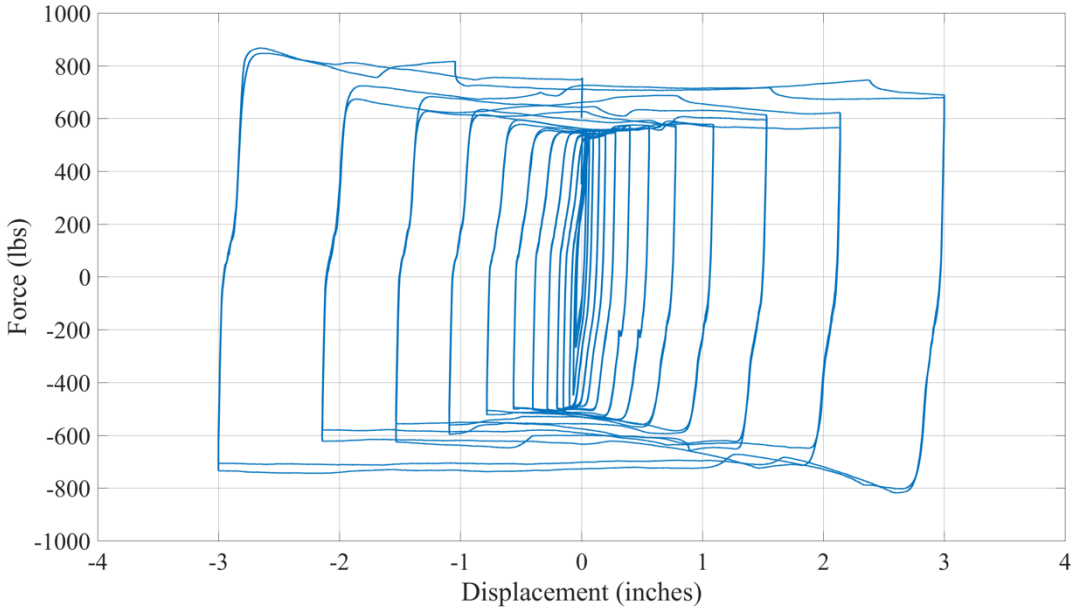

Figure A-10: Hysteresis Loops for Connection B on Panel B, Second Run

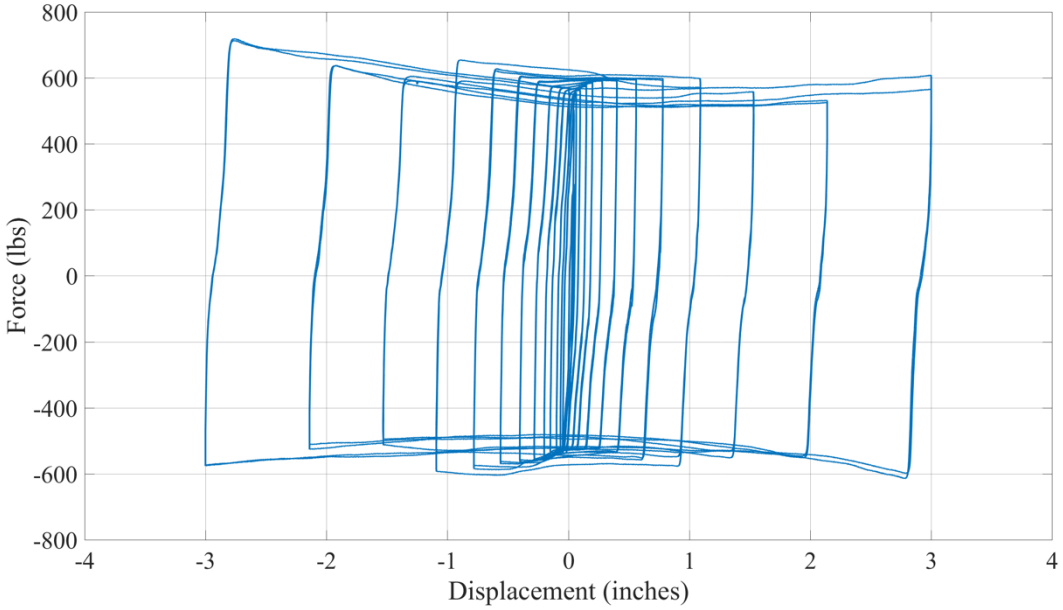

Figure A-11: Hysteresis Loops for Connection C on Panel B, First Run

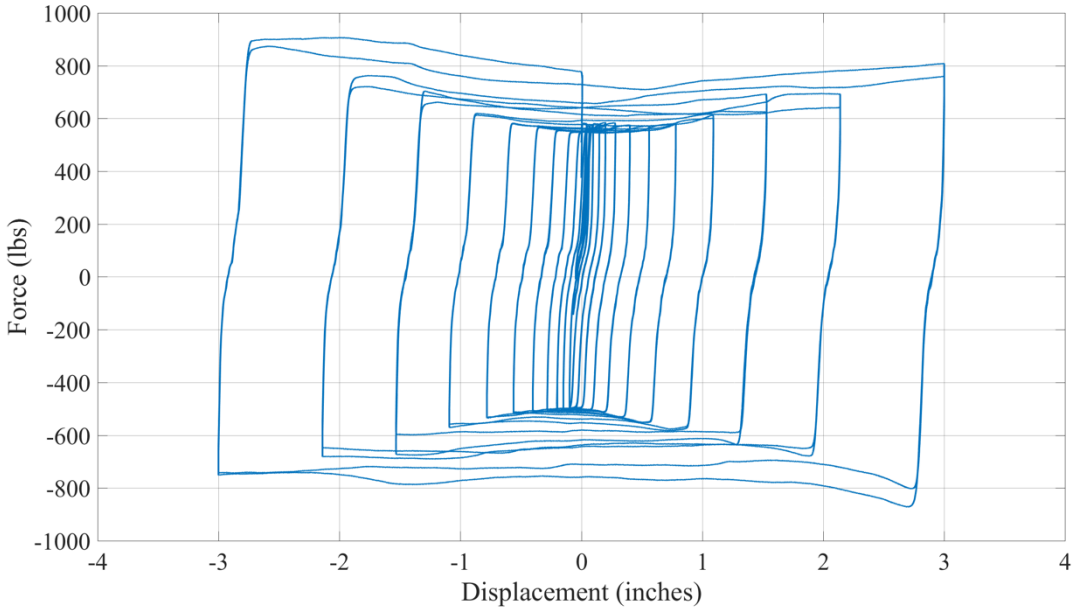

Figure A-12: Hysteresis Loops for Connection C on Panel B, Second Run

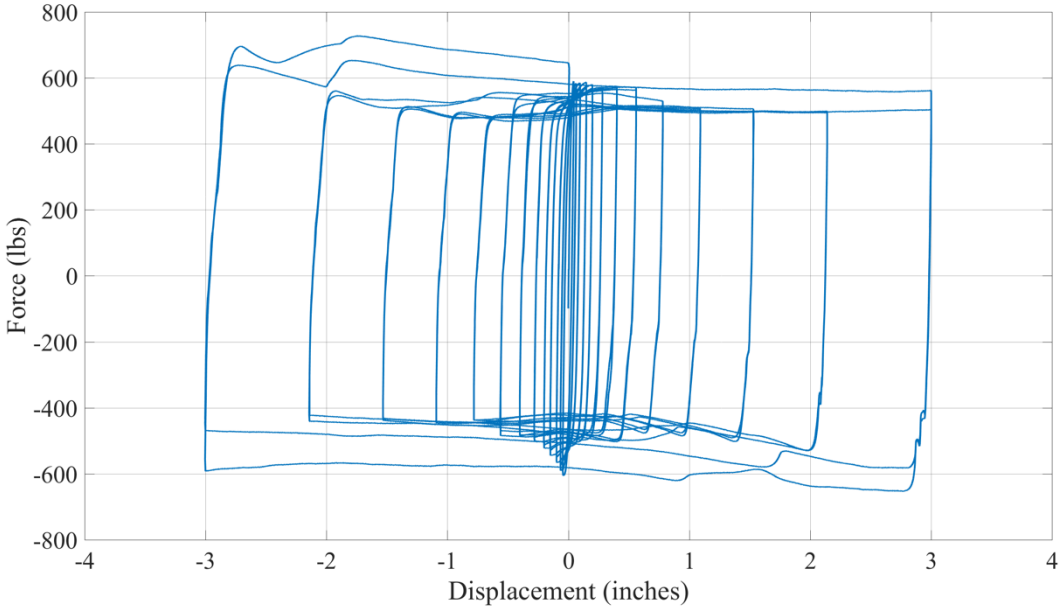

Figure A-13: Hysteresis Loops for Connection D on Panel B, First Run

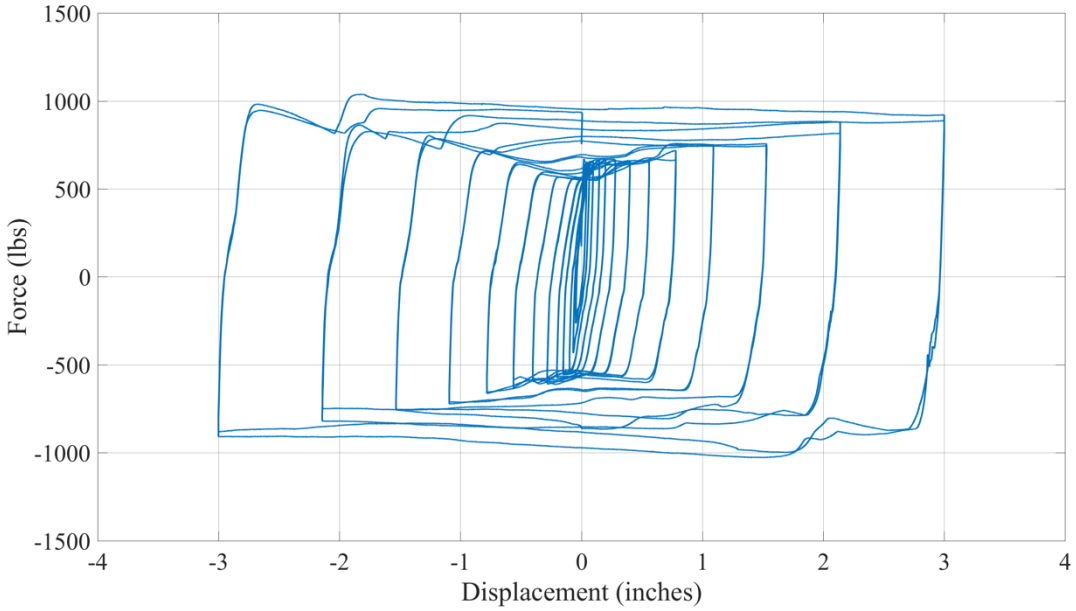

Figure A-14: Hysteresis Loops for Connection D on Panel B, Second Run

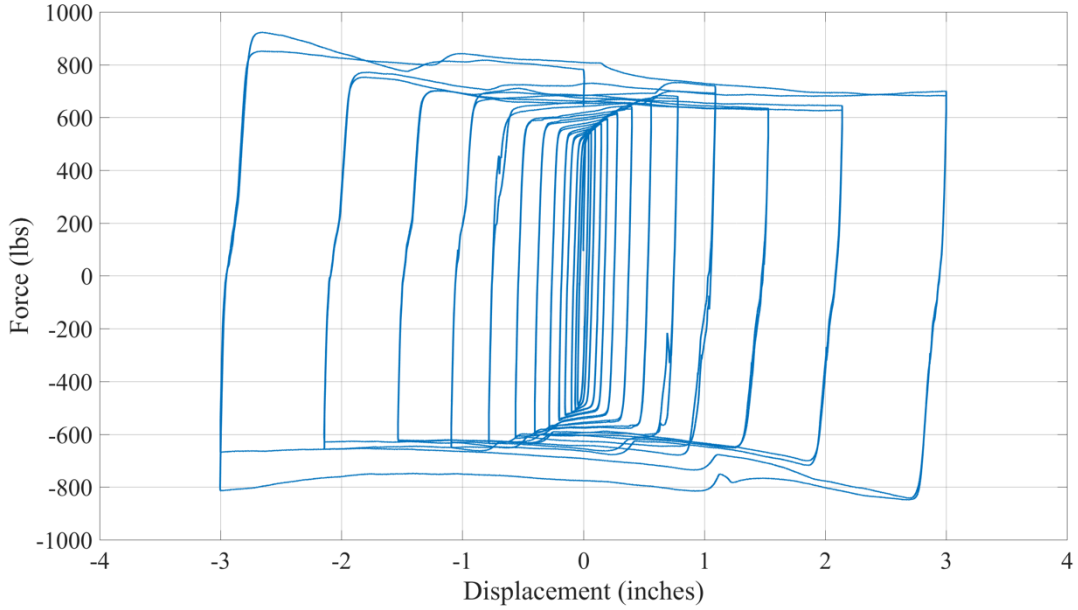

Figure A-15: Hysteresis Loops for Connection E on Panel B, First Run

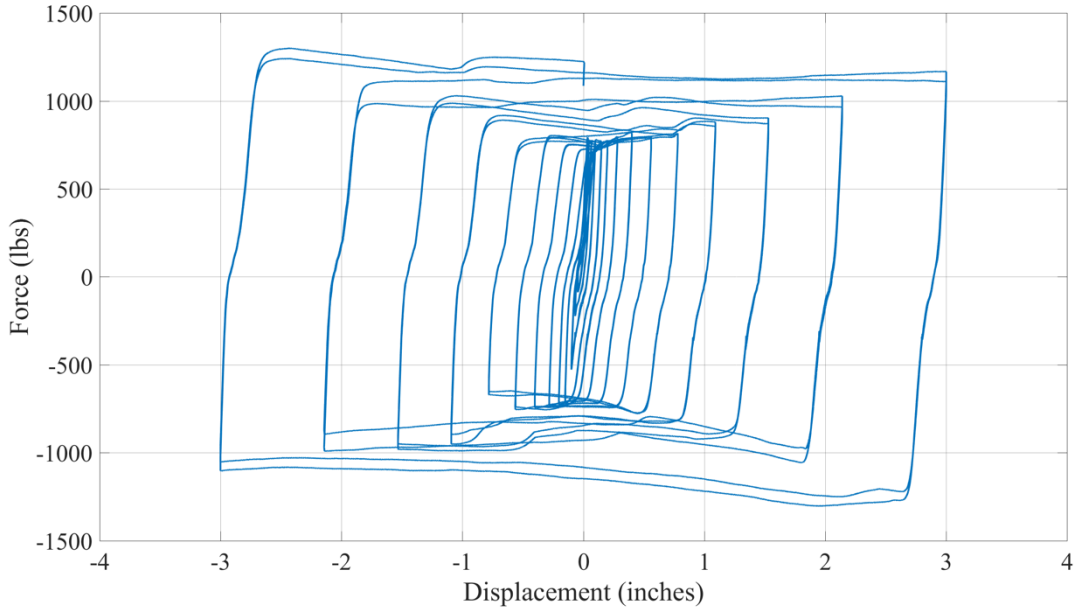

Figure A-16: Hysteresis Loops for Connection E on Panel B, Second Run

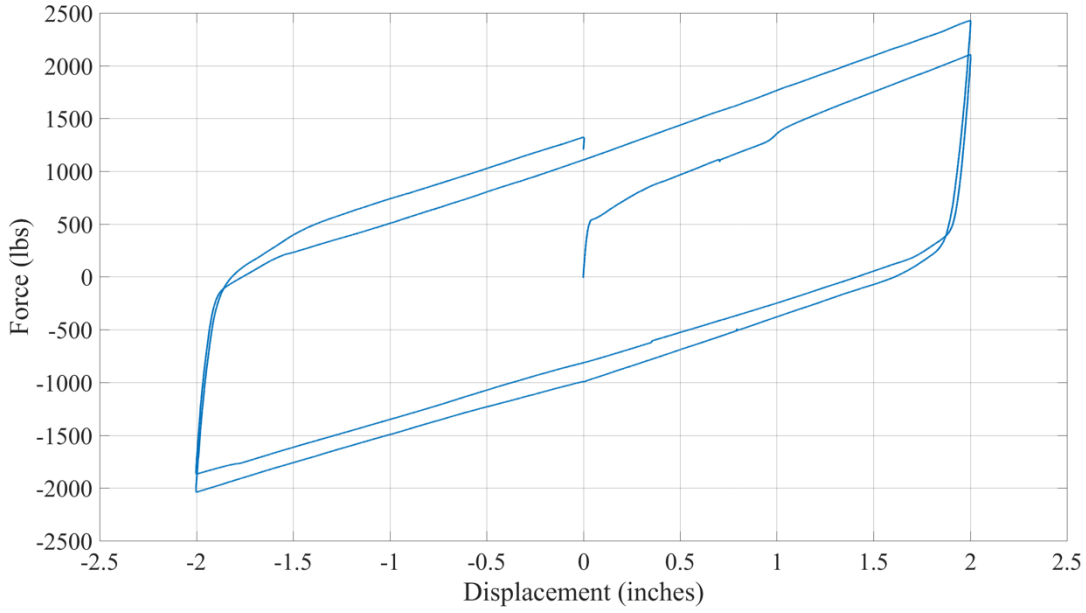

Figure A-17: Biaxial Testing Results for Panel B

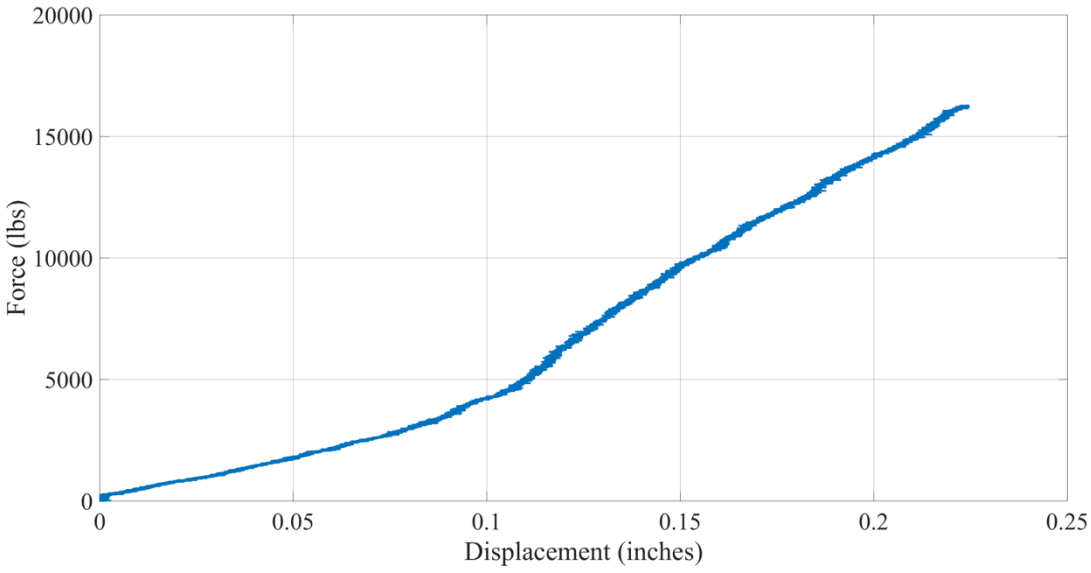

Figure A-18: Pullout Test Results for Panel B

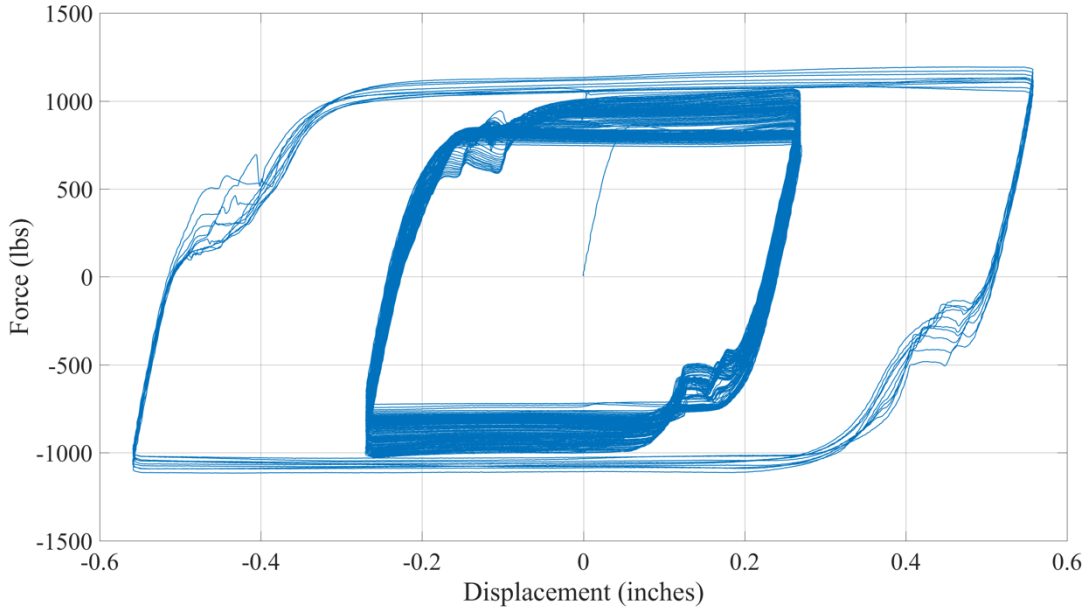

Figure A-19: Hysteresis For 100-Cycle Testing for Low-Displacement Protocol

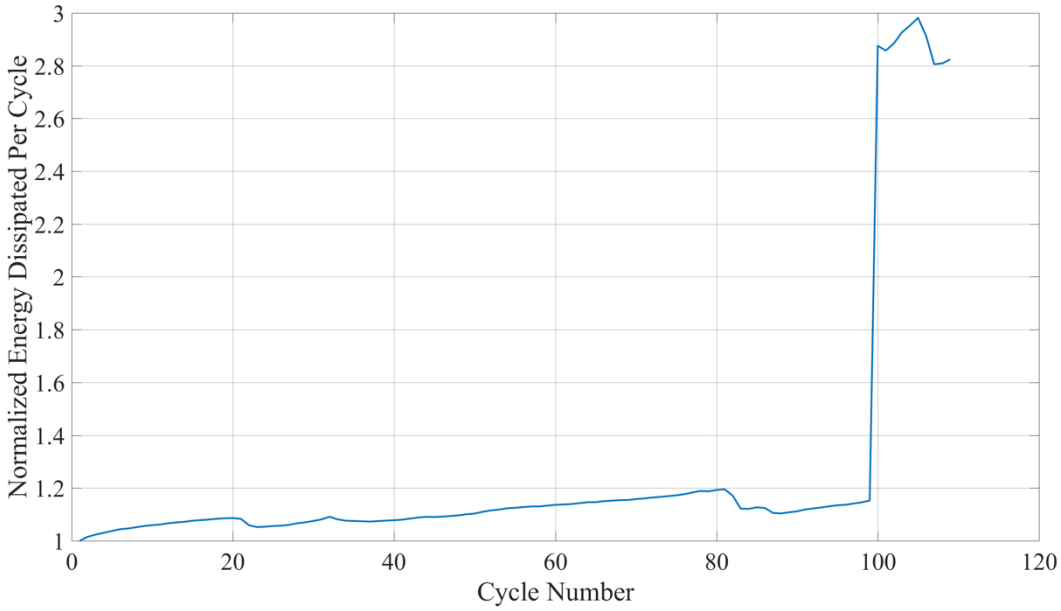

Figure A-20: Normalized Energy Dissipated per Cycle for Low-Displacement Protocol

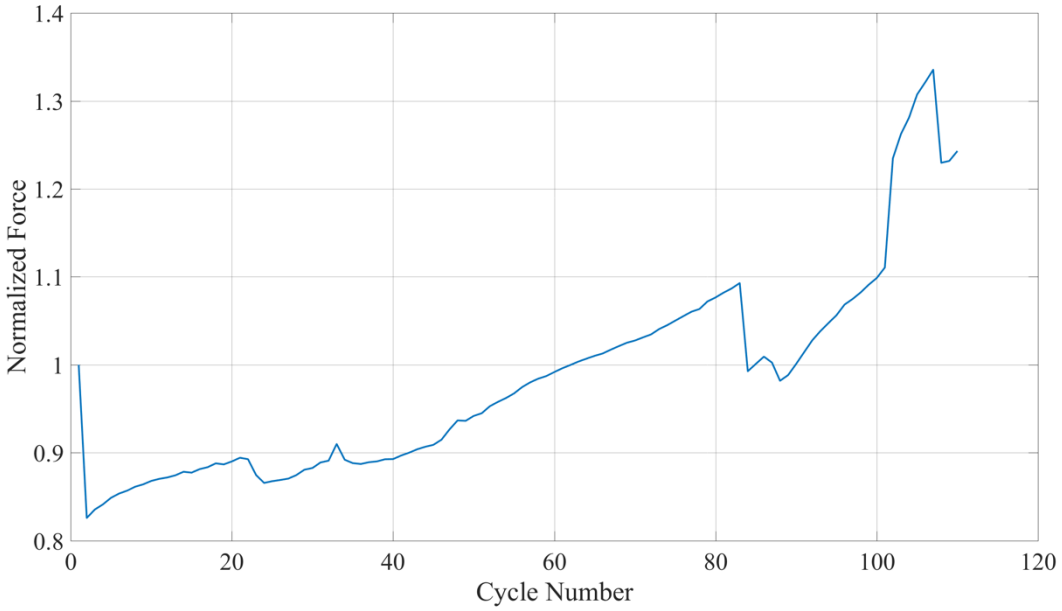

Figure A-21: Normalized Free Rotation Force per Cycle for Low-Displacement Protocol

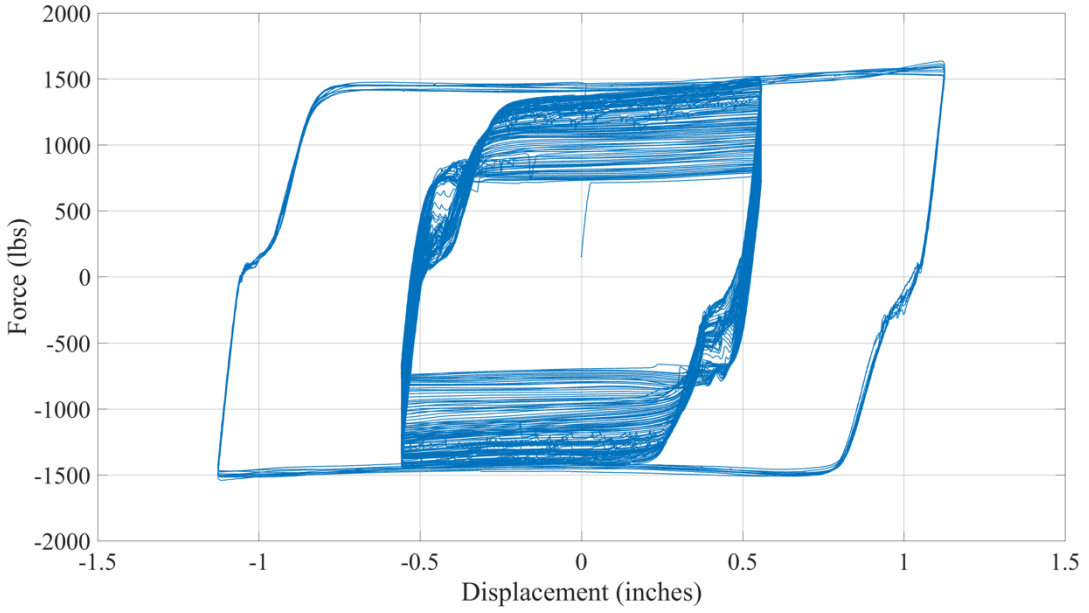

Figure A-22: Hysteresis For 100-Cycle Testing for Medium Displacement Protocol

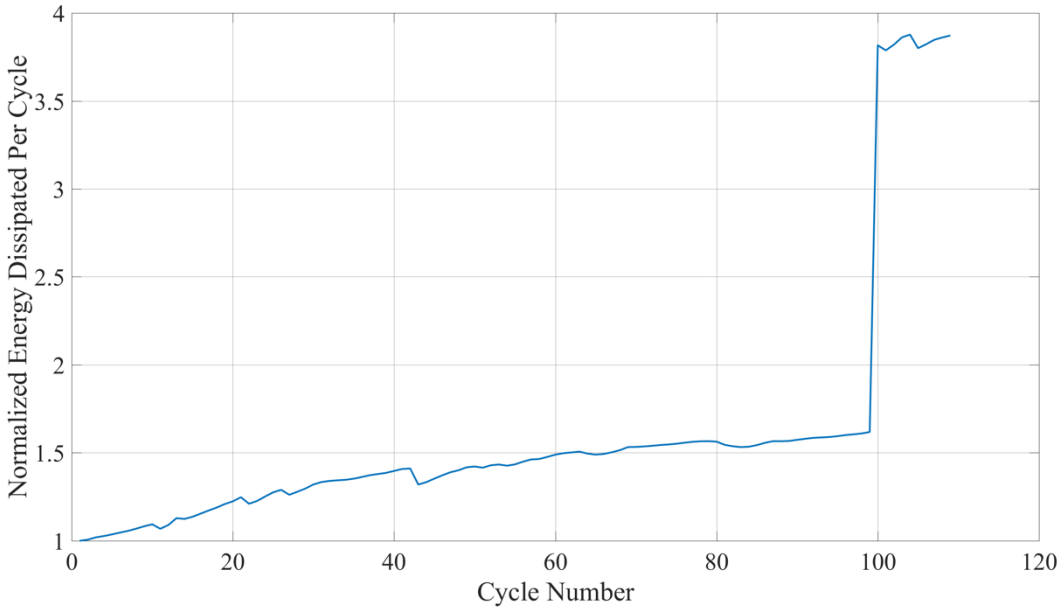

Figure A-23: Normalized Energy Dissipated per Cycle for Medium-Displacement Protocol

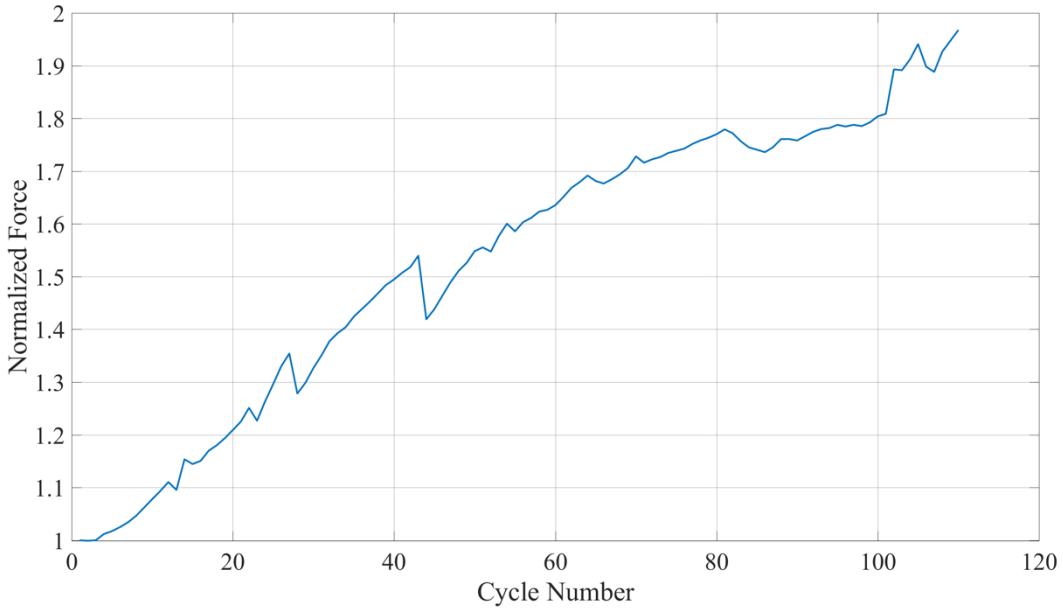

Figure A-24: Normalized Free Rotation Force per Cycle for Low-Displacement Protocol

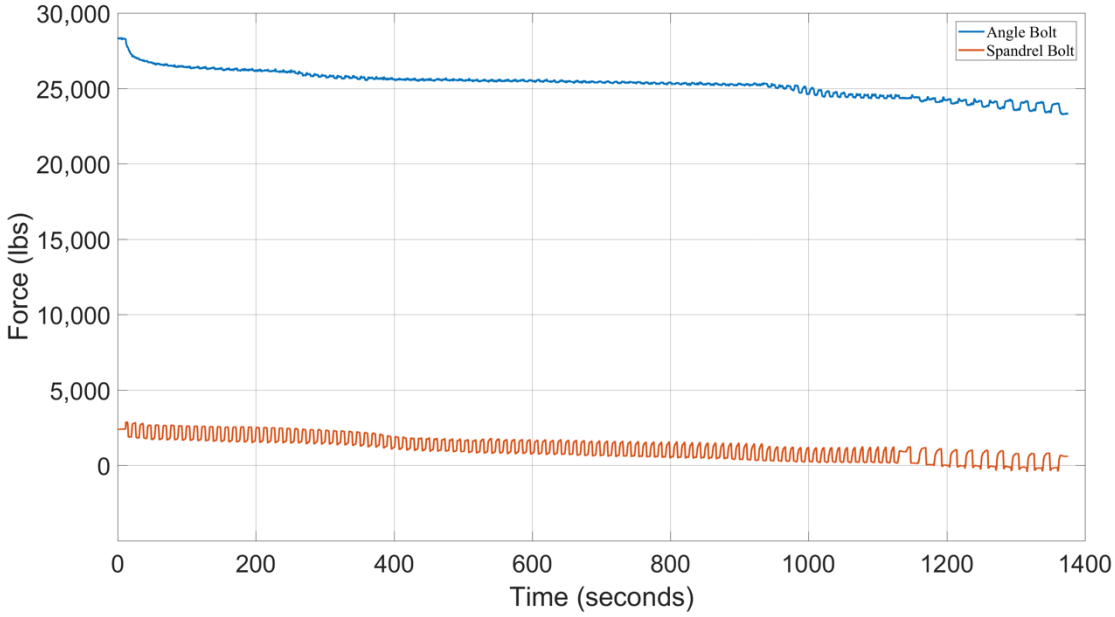

Figure A-25: Bolt Tension versus Time for Low Displacement Testing Protocol

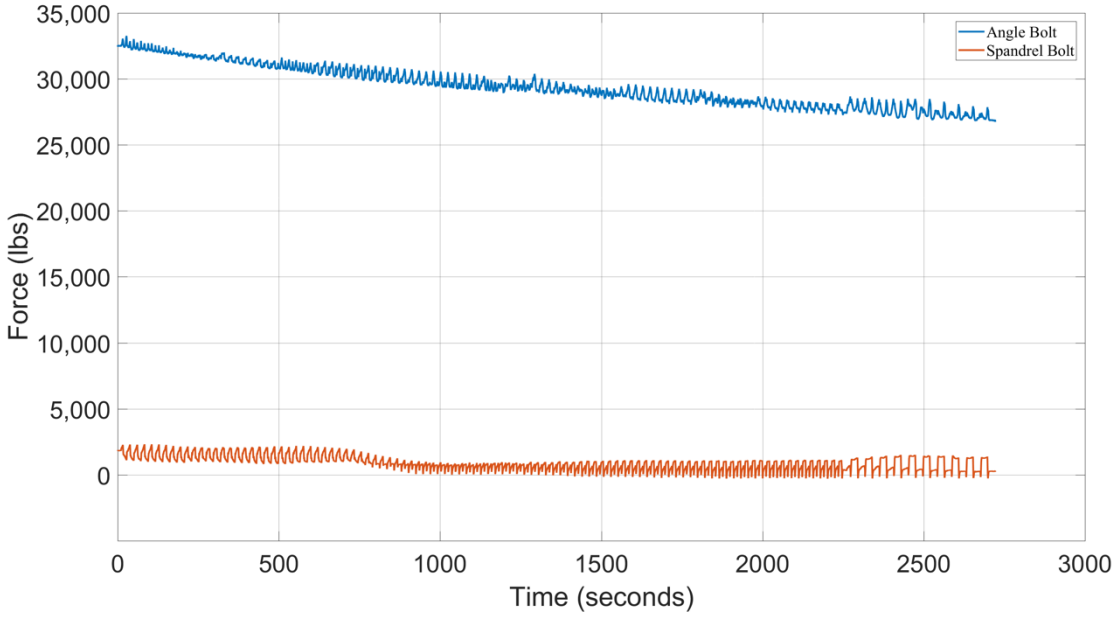

Figure A-26: Bolt Tension versus Time for Medium Displacement Testing Protocol

Appendix B. Component Drawings

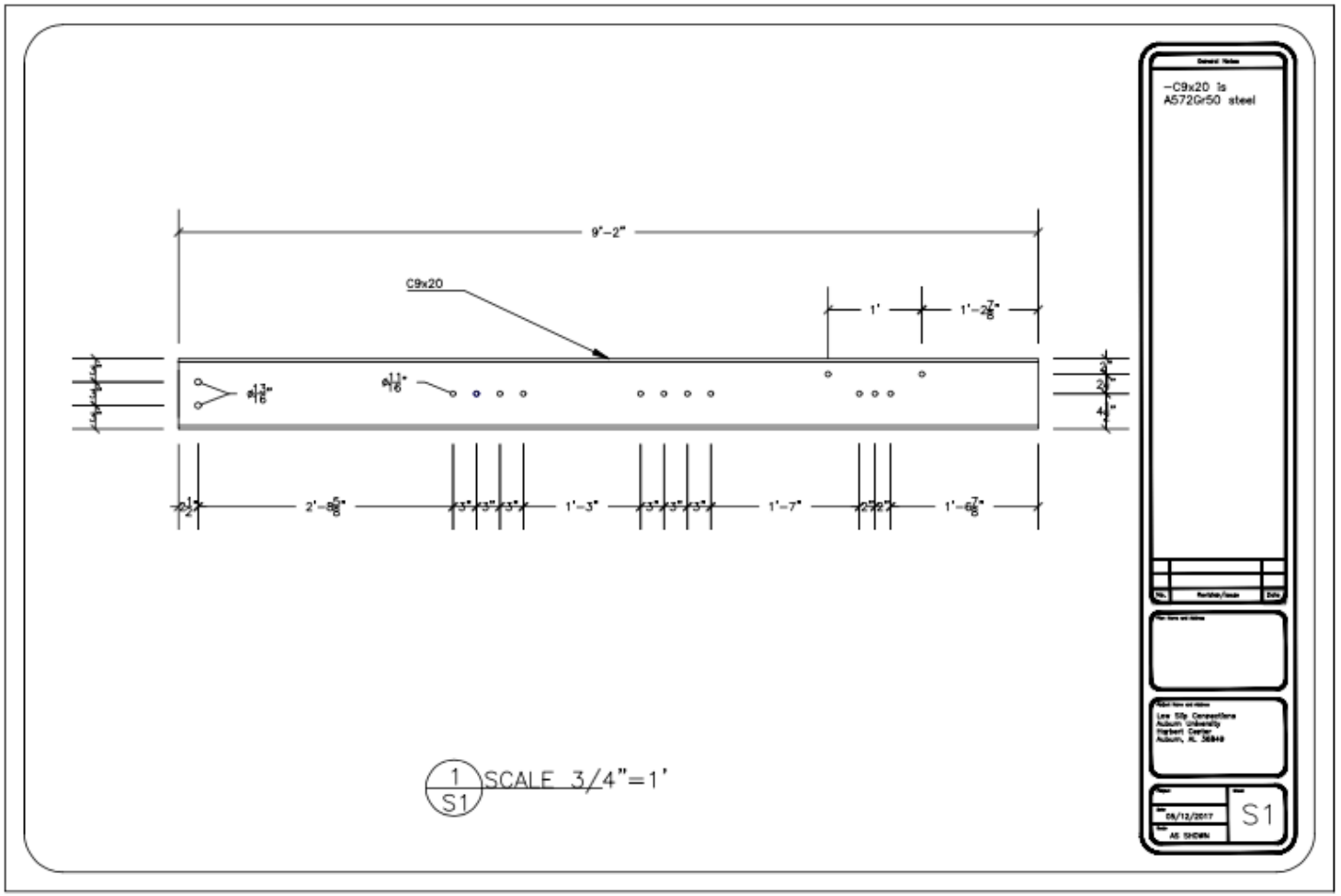

Figure B-1: Spandrel Beam Detail

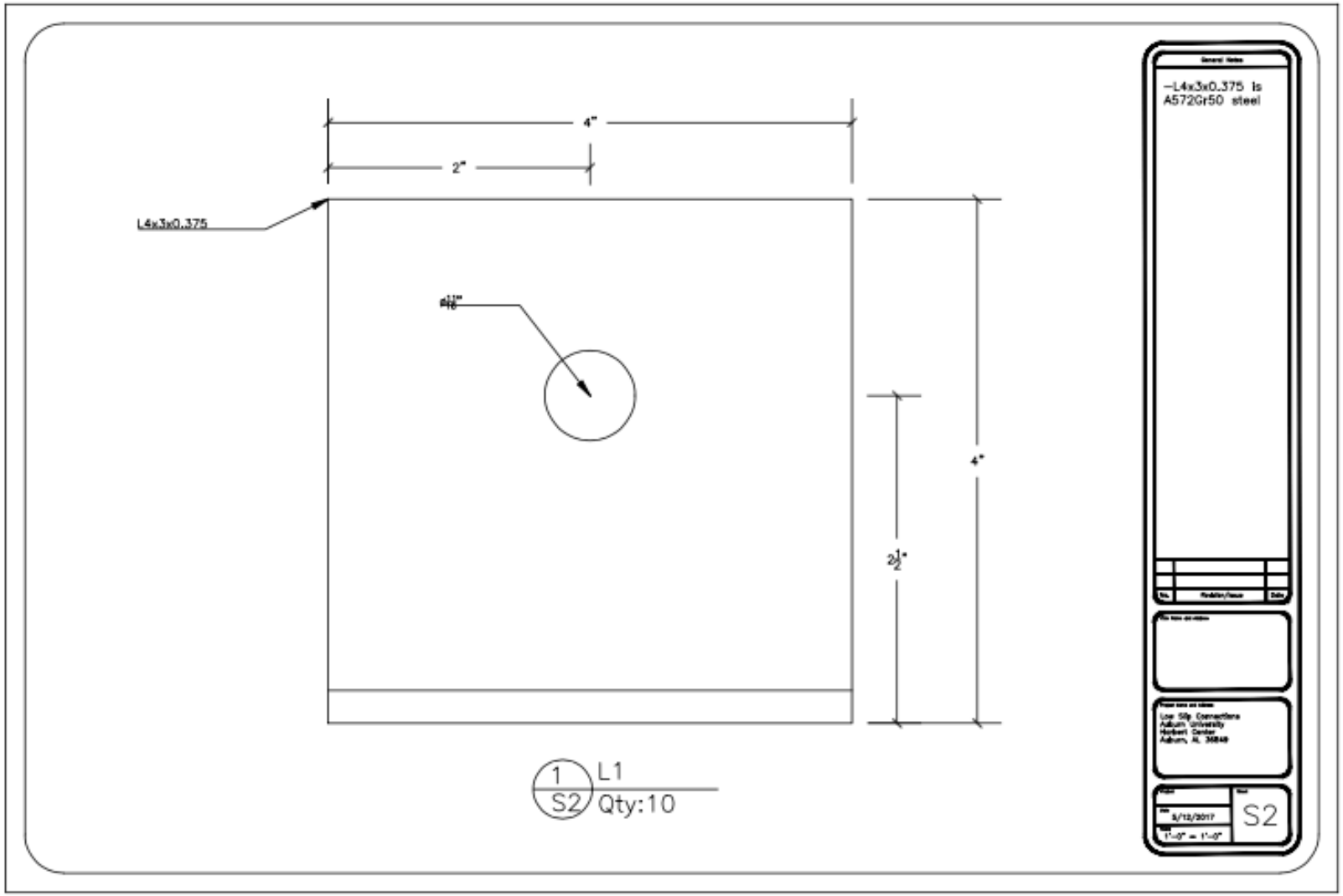

Figure B-2: Angles for Panel A

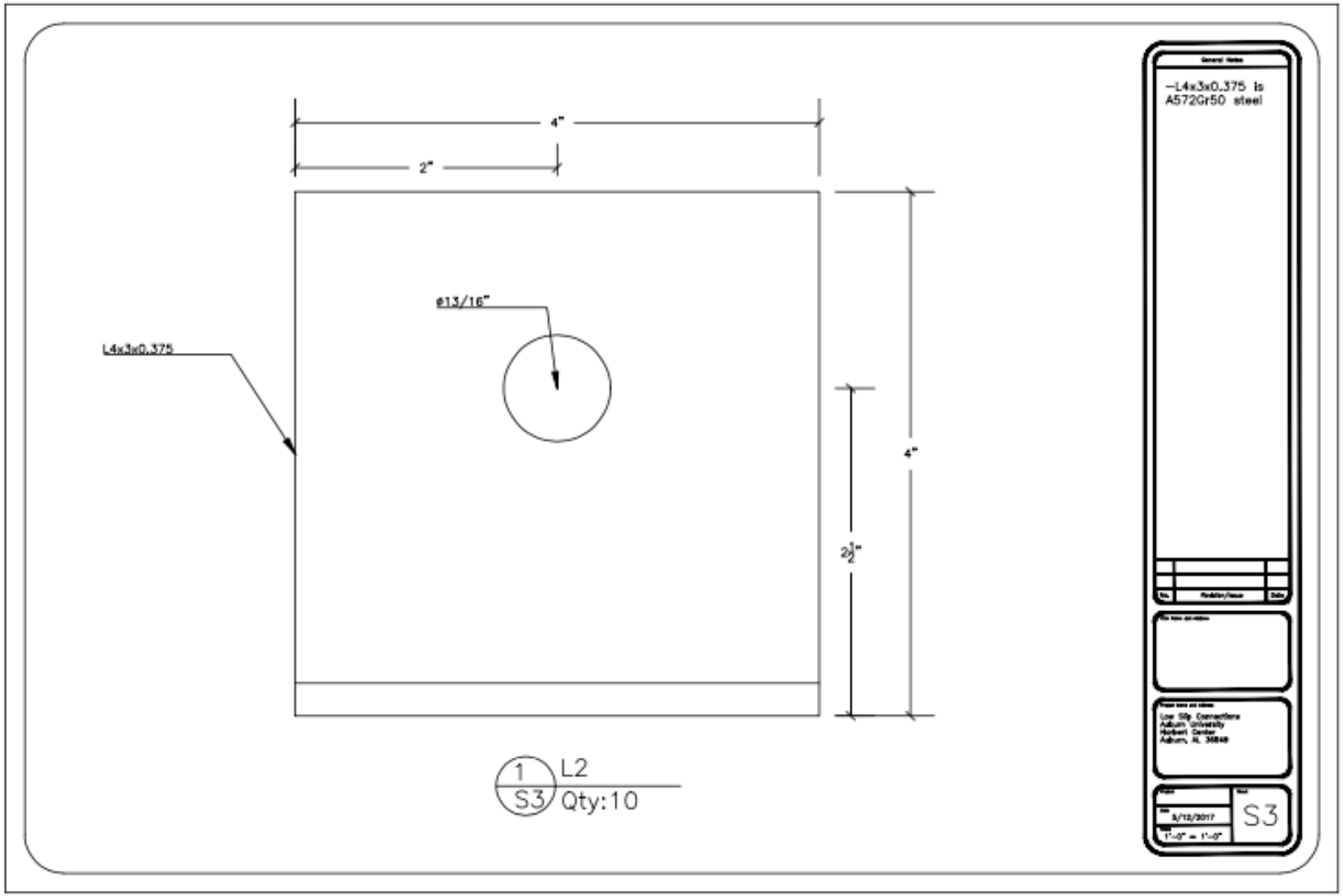

Figure B-3: Angles for Panel B

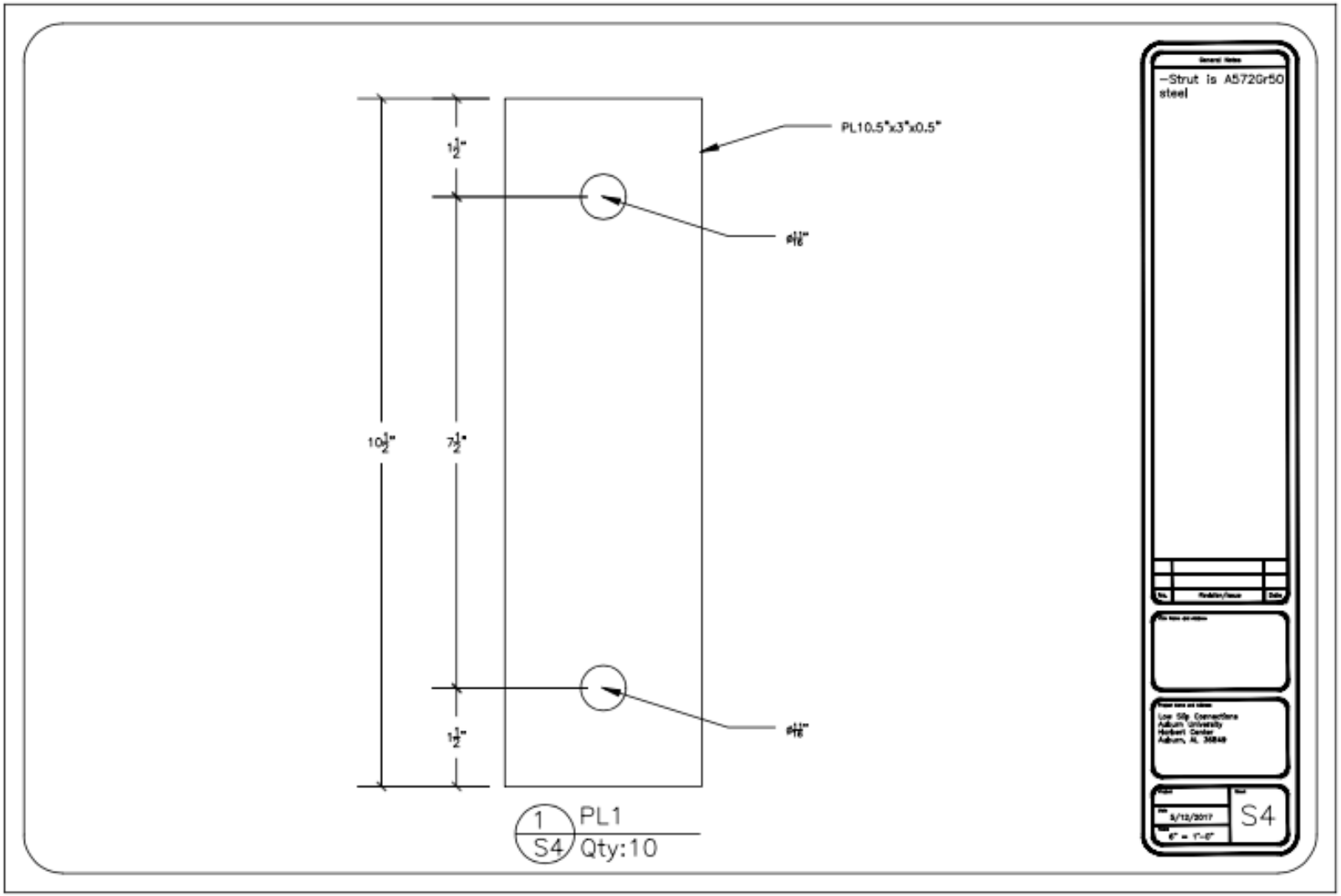

Figure B-4: Struts for Panel A

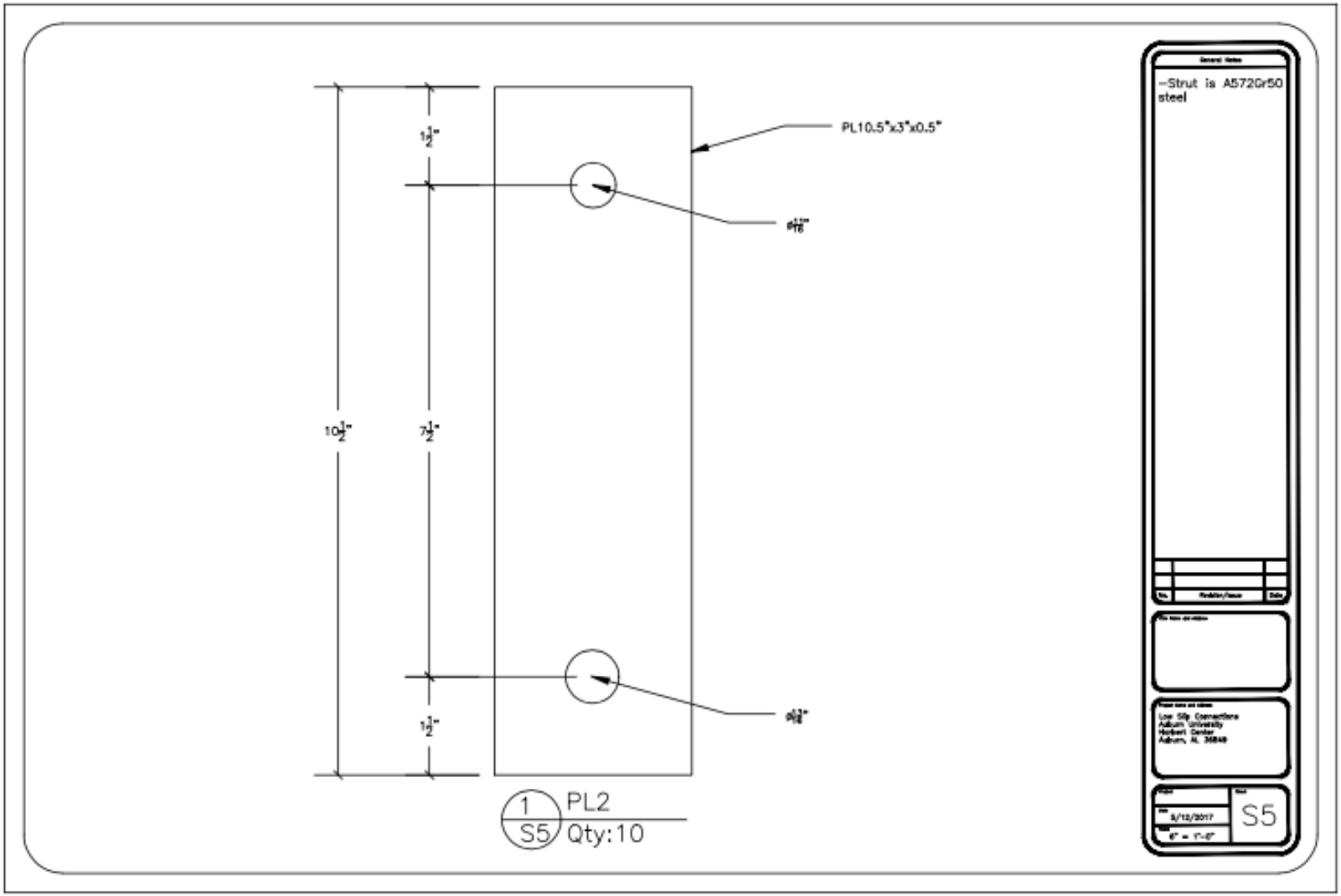

Figure B-5: Struts for Panel B

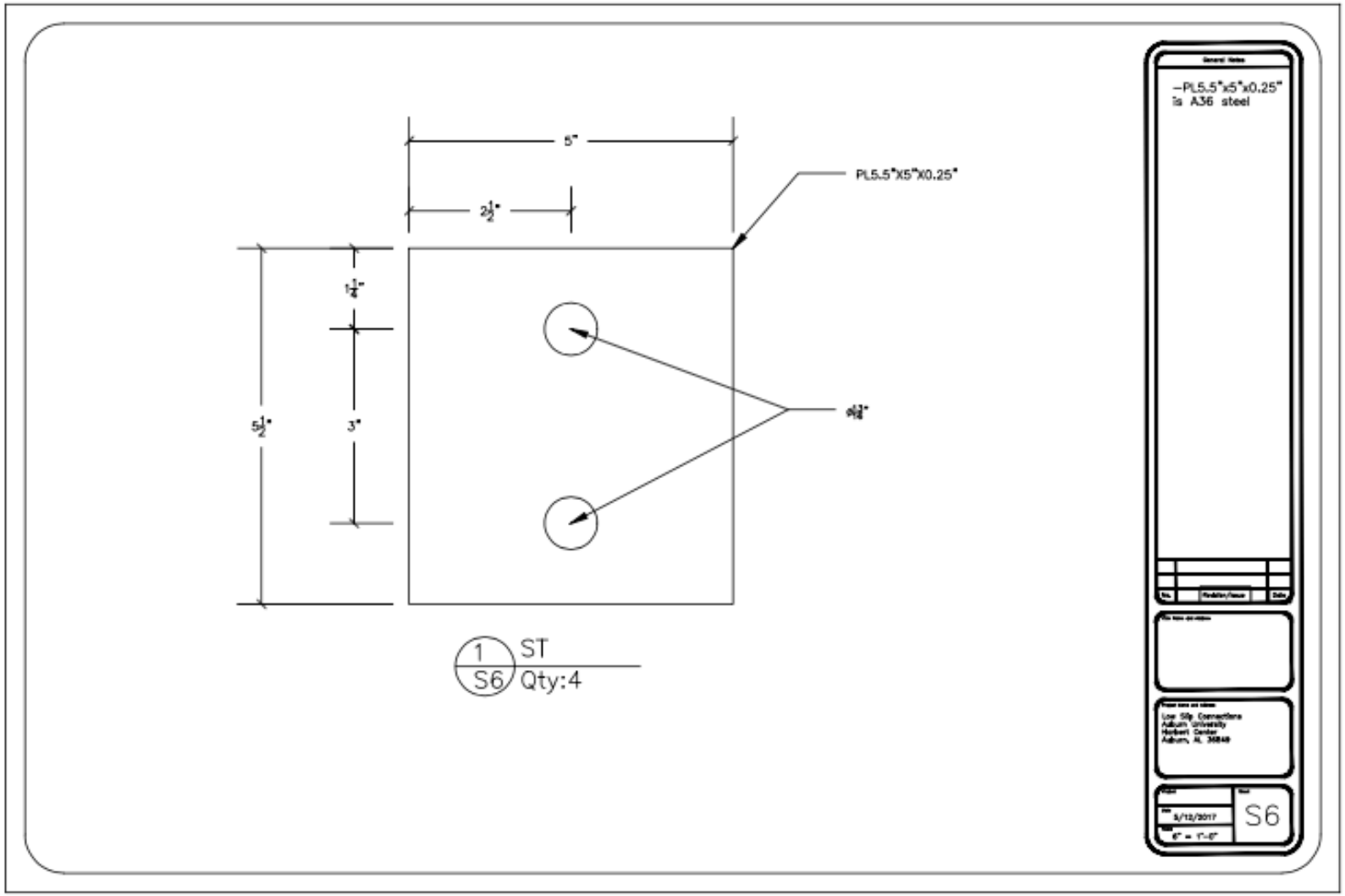

Figure B-6: Tension Tab Detail

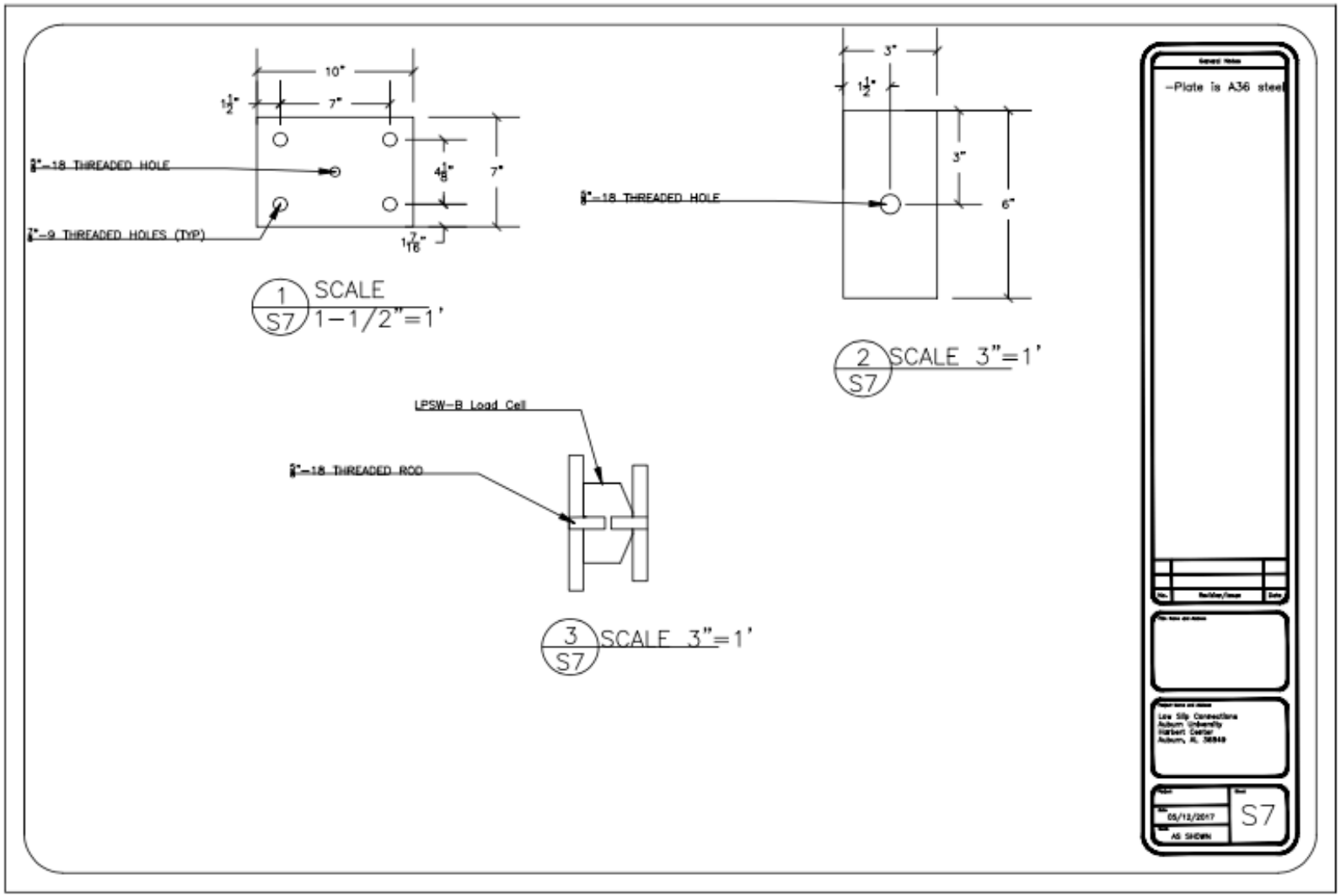

Figure B-7: Load Cell Assembly Component Detail

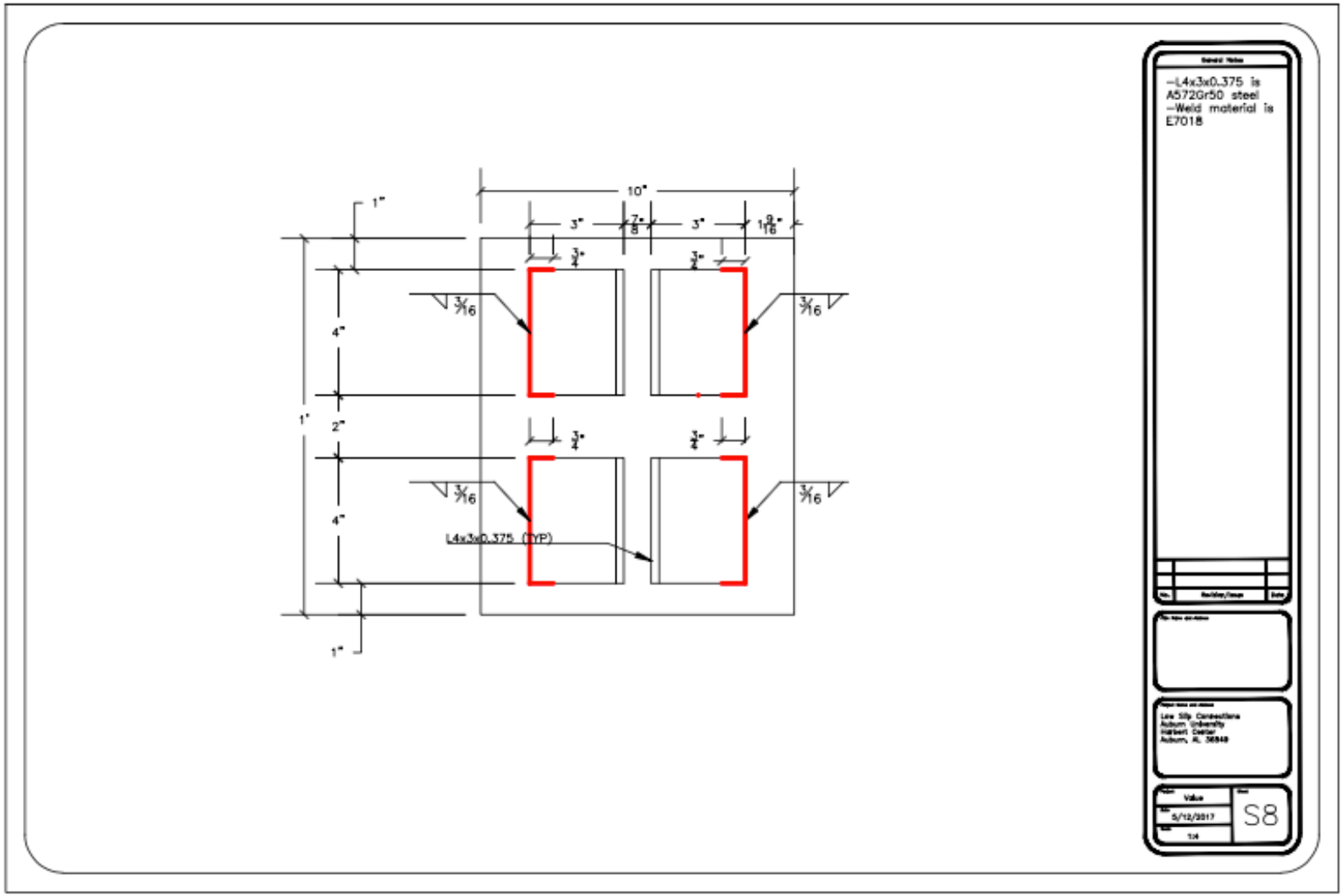

Figure B-8: Embed Plate Detail For Connection Location B,C,D, and E

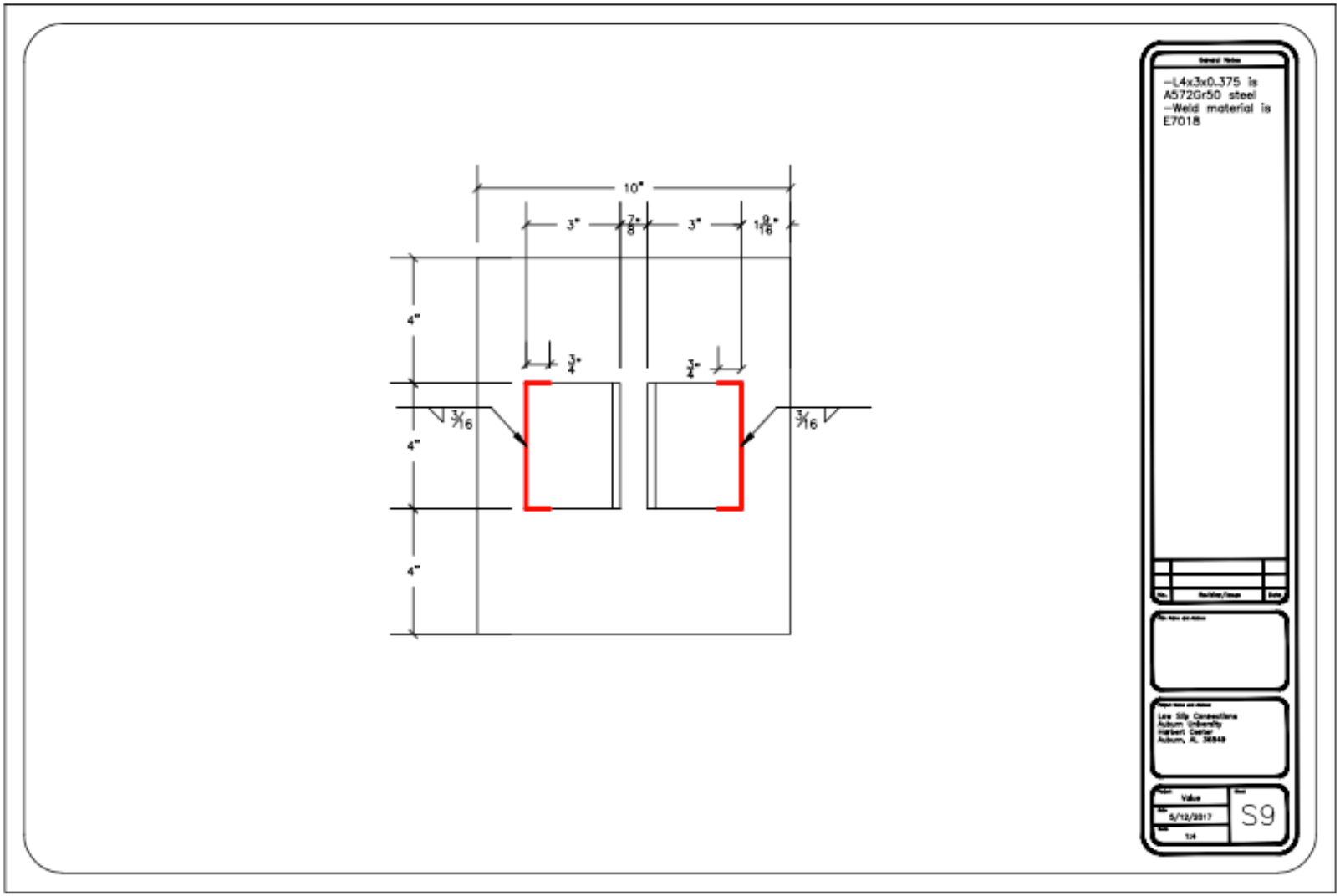

Figure B-9: Embed Plate Detail for Connection Location A